COMPACT SMB CHROMATOGRAPHY FOR BINARY SEPARATION

RUI CLÁUDIO DOS REIS RODRIGUES

Faculdade de Ciências e Tecnologia

Universidade Nova de Lisboa

A thesis submitted for the degree of

Doctor of Philosophy

2009

N° de arquivo _____

Copyright _____

This thesis is dedicated to my loving parents for their endless support and to Fátima who is my source of inspiration.

Some men see things as they are and ask why, I dream things that never were and ask why not.

Robert F. Kennedy

Acknowledgements

Finishing a PhD is truly a marathon event, and I would not have been able to complete this journey without the support and encouragement of a countless number of people over the past four years. I must first express my gratitude towards my advisor, Professor José Paulo Barbosa Mota. His leadership, support, friendship, attention to detail, hard work, scholarship and genius have set an example I hope to match some day.

I would like to acknowledge Fundação para a Ciência e Tecnologia (FCT/MCTES) for the financial aid in the form of a PhD grant, and for my future pos-doctoral position.

I would like to thank Professor Mário Eusébio for his friendship and precious help in the development of the data acquisition and control software.

A special thanks to my colleague João Araújo for his friendship, help and fruitful discussions. To Tiago Canhoto, a very hard-working Master student with a great sense of humor.

I also thank some of my fellow PhD students: João Fernandes and Márcio Temtem, for their effort to help whenever they could. Also to Ricardo Silva, a recent colleague but already a friend.

A special word to Isabel Esteves, not only a colleague but a friend, all your help and friendship is rare to found.

I acknowledge the endless help from D^a Maria José Carapinha and the lab support given by D^a Joaquina Lopes and D^a Palminha.

I thank my parents for instilling in me integrity and a willing to always pursue something more. Their endless support, care and friendship is something immeasurable. Because of them i am a better person.

To you Fátima, my source of inspiration, my light in the dark. This work would not have been possible without your everyday support. For you everything seems worthwhile, thank you for letting me share my life with you.

Resumo

Esta tese consiste essencialmente em desenvolvimentos teóricos e experimentais na área dos processos cromatográficos contínuos usando unidades de pequena escala.

O Leito Móvel Simulado (LMS) é a aplicação prática do processo Leito Móvel Verdadeiro (LMV). O LMS é um processo contínuo de separação cromatográfica multicoluna com inúmeras aplicações. Este foi desenvolvido originalmente como a implementação prática de um sistema de adsorção em contracorrente, mas sem os problemas associados ao movimento de um leito de partículas (LMV). A operação em contracorrente maximiza a força motriz para a transferência de massa, o que aumenta a eficiência com que o adsorvente é utilizado, permitindo um aumento considerável da productividade do sistema e a redução do consumo de eluente.

Algumas tentativas de implementar o LMV na prática (como o processo *Hypersorption*) revelaram-se muito inconvenientes do ponto de vista prático e económico. No início dos anos sessenta a UOP (*Universal Oil Products*) desenvolveu e pantenteou um processo de separação cromatográfica contínuo para a separação de hidrocarbonetos na indústria petroquimica e posteriormente aplicado na separação de açucares: o LMS. O LMS é um processo que usa uma série de colunas cromatográficas conectadas circularmente, o movimento contínuo do sólido é assim simulado através da comutação periódica dos portos de entrada (alimentação e eluente) e de saída (extracto e refinado) na mesma direcção do escoamento do fluido. Por forma a aproximar o movimento discreto do LMS ao movimento contínuo do LMV, cada zona está particionada em várias colunas.

Com a recente expiração do processo UOP, tem-se verificado um crescente interesse no processo LMS, levando ao aparecimento de consideráveis desenvolvimentos no modo de operação do processo. Estes novos modos de operação assentam essencialmente na manipulação das variáveis de operação durante o processo. De entre vários evidenciam-se a comutação assíncrona dos portos de entrada e saída (processo *Varicol*), a modelação periódica dos vários caudais (processo *PowerFeed*) e a modelação da concentração da alimentação (processo *ModiCon*). Como consequência do aumento da eficiência do processo, começou-se a analisar a possibilidade de reduzir a escala do LMS e aplicá-lo em separações nas áreas farmacêutica, biotecnológica e química fina. Actualmente, na indústria farmacêutica o LMS é considerado uma unidade multifuncional que pode ser aplicada em diferentes passos do ciclo de desenvolvimento de uma nova droga.

O emergir destas novas áreas de aplicação do LMS impulsionou o desenvolvimento de novos e mais eficazes esquemas que diferem substancialmente do processo convencional, levando a que a tendência geral seja para unidades com poucas colunas, pois utilizam menos quantidade de adsorvente, são mais compactas e económicas. Para além disso, a mudança entre separações de diferentes misturas processa-se de forma mais simples e rápida do que no caso de unidades com muitas colunas.

No entanto, esta melhoria no desempenho da separação é normalmente obtida à custa de uma complexidade acrescida e de um aumento da sensibilidade do sistema a incertezas processuais e variabilidades operatórias. Esta complexidade acrescida requer a utilização de equipamento altamente versátil, ferramentas eficientes de optimização e procedimentos robustos de controlo automático.

Nesta ordem de ideia, é desenvolvido um processo que se baseia na reprodução do estado estacionário cíclico do LMS utilizando apenas uma coluna cromatográfica. O principal objectivo deste processo monocoluna não é a separação de uma mistura mas sim a reprodução rápida

e expedita do estado estacionário cíclico do LMS sem a necessidade da realização de experiências na unidade multicoluna. Este sistema foi validado experimentalmente para uma separação binária de nucleótidos em fase líquida, tanto para operação LMS clássica como para os diferentes modos de operação *Varicol* e *PowerFeed*. Este provou ser um método simples, compacto e rápido de reprodução do comportamento periódico do LMS com um consumo mínimo de soluto e solvente. O método proposto demonstra assim que poderá ser uma maneira simples e económica de testar experimentalmente as condições de operação, de uma dada separação, para um novo processo cromatográfico multicoluna.

Apesar da configuração LMS com quatro colunas ser a mais utilizada, existem esquemas alternativos que podem ser mais adequados para diversos casos particulares. Um LMS compacto com apenas duas colunas é apresentado. O processo 2-colunas desenvolvido utiliza duas bombas de entrada que fornecem as correntes de alimentação e solvente ao sistema, duas bombas internas de recirculação para manipulação do caudal de efluente que é direccionado de uma coluna para a seguinte e dez válvulas de duas vias para comutação dos portos. O sistema aplica simultaneamente tanto a manipulação assíncrona dos portos como a modelação periódica dos caudais; o sistema 2-colunas proposto foi reproduzido experimentalmente e provou ser um processo mais eficaz que a simples cromatografia *batch* ou que o processo *batch* com reciclo.

Uma evolução do processo 2-colunas é também desenvolvido. Este esquema simplificado assenta no uso de um número mínimo de bombas e num esquema uniforme de caudais. As potencialidades desta unidade são ilustradas comparando-a a esquemas mono- e multi-coluna com a mesma quantidade de fase estacionária. Este processo demonstra poder ser uma alternativa viável ao nível de indústrias de produção e/ou purificação de produtos de alto valor acrescentado, nomeadamente as indústrias farmacêutica e biotecnológica, pois combina as

potencialidades do LMS com a simplicidade da cromatografia *batch*.

Adicionalmente, a problemática do desenvolvimento de uma unidade experimental para reproduzir estes sistemas compactos é abordada. Há vários aspectos a considerar no projecto de um sistema como este. O equipamento que controla a comutação dos portos (as válvulas) tem de ser versátil o suficiente para acomodar diversos tipos de configurações. Isto implica que o sistema tem de possibilitar a operação sem algumas das zonas habituais do LMS. Por outro lado, dado que o sistema proposto se baseia numa manipulação dos caudais, para que este funcione na prática, é necessário adoptar uma configuração de bombas que seja robusta.

Finalmente, o problema da robustez da operação LMS é abordado e um procedimento geral para o projecto e optimização robusta do LMS na presença de incerteza ou variabilidade nos caudais e nos parâmetros da coluna e da isotérmica é apresentado. Estes tipos de incerteza são dos mais difíceis de resolver do ponto de vista processual e dos que ocorrem com mais frequência à escala industrial. O procedimento proposto foi aplicado aos novos esquemas 2-colunas anteriormente desenvolvidos. A operação robusta é particularmente relevante nestes novos processos, pois eles vão proporcionar uma melhoria no desempenho da separação mas à custa de uma complexidade operacional acrescida e de um aumento da sensibilidade às perturbações operatórias.

Abstract

This thesis consists essentially of theoretical and experimental developments in the field of continuous chromatography using small-scale units.

Continuous chromatographic separation processes based on the Simulated Moving Bed (SMB) technology were first patented and applied in 1961 for a large number of separations in the petrochemical industry and later for sugar separation. However, in the last two decades, due to the patent expiration, the process has been gaining great interest in the separation/purification of products in fine chemical and pharmaceutical industries.

The conventional SMB comprises several identical columns which are serially connected in either a closed- or open-loop configuration. In order to simulate the movement of a solid bed in opposite direction to the fluid, the positions of the input and output streams are shifted downstream by one column, at fixed intervals, in the direction of fluid flow. With the development of new and efficient equipment and stationary phases, several new schemes of operating that differ from the conventional one have emerged. These include new concepts such as Varicol, ModiCon and PowerFeed processes, which rely on the periodic modulation of certain process parameters during the switching interval to enhance the efficiency of the separation. These advances are pushing the trend for units with a small number of columns, since the overall setup is more economical.

However, when these newly schemes are applied in practice the process becomes more complex, because of the increased degrees of freedom that must be optimized. It is also less robust and more difficult to

operate because it is more demanding on hardware. This additional complexity requires highly versatile SMB equipment, advanced optimization tools and robust control procedures.

Experimental tools to experimentally reproduce the periodic state of multicolumn countercurrent chromatography with just one column are developed; they are economic and fast methods of experimentally exploring different column configurations and cyclic operation policies, ideally suited for applied research studies but may also be useful in the early stages of development, optimization, and validation of a new chromatographic separation. The feasibility of the proposed single-column system is experimentally demonstrated for several different column configurations, which include both synchronous and asynchronous port switchings and flow modulated schemes.

Following the potentialities of these new operating schemes, a novel SMB system for binary separation that employs only two-columns is developed. The designed two-column process uses both the port switching and the flow rates modulation procedure. The process is very versatile since the cycle itself is optimized and adapted to the difficulty of the separation and process specifications. Furthermore, a simplified extension of the two-column setup which relies on a minimum pump number configuration and on a uniform flowrate scheme is built-up; additionally a further development on these simplified setup is applied which effectively enhances the process with only the cost of a small increase on the setup equipment. Potentialities of this new unit are illustrated comparing it to setups using the same amount of stationary phase.

Moreover, in order to describe all the proposed units, a numerical method to directly compute the cyclic steady behavior of the process is developed and used as modeling procedure.

Additionally, a versatile lab-scale unit is built to evaluate the proposed compact SMB setups. Emphasis is given to the challenges of building up an easy to operate small-scale unit which is more sensible

to contamination and/or extra volume issues relatively to large industrial setups. The developed system is experimentally applied for the separation of two nucleosides by reversed phase chromatography.

Due to the increased complexity of the proposed two-column schemes and because a small number of columns is more dependent on packing reproducibility, the operating cycle becomes more sensitive to process disturbances/fluctuations. To overcome this problem, a general procedure for robust design of simulated moving-bed (SMB) processes under flow rate and isotherm uncertainty is presented. The best solution is chosen only among candidate solutions that are robust feasible, that is, remain feasible for all perturbations from the uncertainty set. This gives rise to a robust approach to optimal SMB design in which the nominal problem is replaced by a worst case problem. The suggested procedure is experimentally implemented and evaluated for the developed two-column chromatographic process.

Resumo Alargado

A cromatografia é uma técnica de separação/análise muito eficiente. Foi inicialmente usada por químicos na extracção/purificação de misturas de tingimentos de origem vegetal, daí o seu nome: do grego *escrever cores*.

De uma maneira simples, cromatografia é um método de separação em que uma mistura de solutos é eluída através de uma fase estacionária (coluna), sendo que cada composto interage com o sólido. A afinidade que cada soluto tem com a fase estacionária é diferente, logo as espécies irão ter diferentes velocidades de migração, o que faz com que seja possível recolher, à saída da coluna, cada um em separado.

Numa tentativa de tornar o processo contínuo e consequentemente mais eficiente, desenvolveu-se um processo designado Leito Móvel Verdadeiro (LMV). A ideia é simples: em vez de se manter a fase sólida imóvel, esta passa a ter um movimento contínuo, contrário ao escoamento do fluido e com uma velocidade intermédia em relação à de

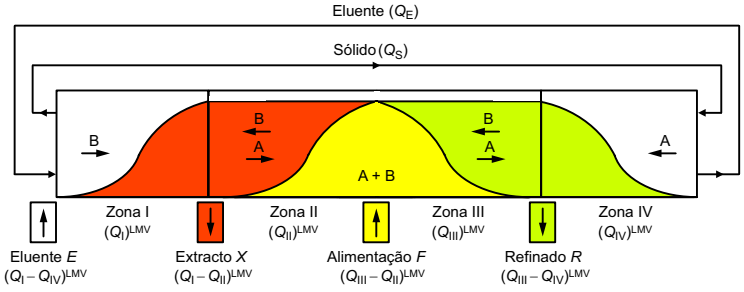

Figura 1: Diagrama esquemático do processo Leito Móvel Verdadeiro com quatro zonas.

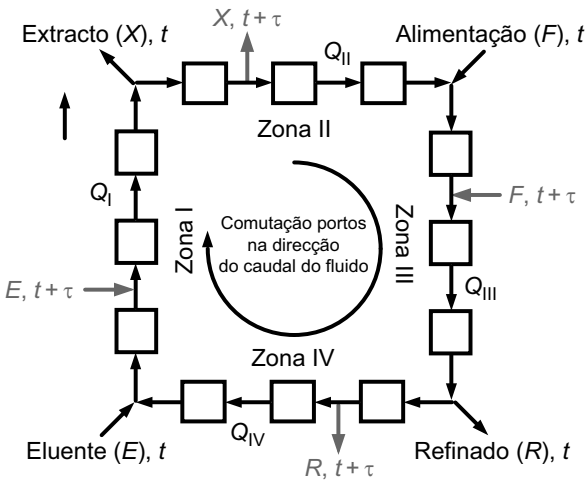

Figura 2: Diagrama esquemático do Leito Móvel Simulado. O movimento contínuo do sólido é simulado através da comutação periódica das linhas de entrada e saída na direção dos escoamento do fluido. A alimentação, Eluente, Extracto e Refinado são representados pelas letras F, E, X, R respectivamente; Q_j é o caudal de fluido na zona j (j =I,...,IV) e τ é o intervalo de comutação.

migração dos dois solutos a separar; o composto que interage mais fortemente com fase (extracto) vai então ser arrastado pelo sólido e o outro (refinado) continua a migrar com o fluido mas a uma velocidade mais baixa. É assim possível recolher cada composto puro em cada um dos extremos da coluna, possibilitando uma contínua adição da mistura a separar.

Algumas tentativas de implementar na prática o processo LMV (processo *Hypersorption*) foram desenvolvidas, no entanto, este revelou muitos problemas operacionais (atrito das partículas do leito), sendo pouco viável do ponto de vista económico.

De forma a ultrapassar os problemas inerentes do processo LMV, foi desenvolvido o processo Leito Móvel Simulado (LMS). O LMS (ver Figura 2) é um processo contínuo de separação cromatográfica multicoluna com numerosas aplicações. Este foi desenvolvido originalmente como a implementação prática de um sistema de adsorção em contra-

corrente, mas sem os problemas associados ao movimento de um leito de partículas. Trata-se essencialmente da discretização do LMV em várias colunas; quanto maior o número de colunas mais o LMS se aproxima da eficiência do LMV.

No início dos anos sessenta a UOP (*Universal Oil Products*) desenvolveu e pantenteou o processo LMS para a separação de hidrocarbonetos na indústria petroquímica e posteriormente para a separação de açúcares. O LMS é um processo que usa uma série de colunas cromatográficas conectadas circularmente, o movimento contínuo do sólido é simulado através da comutação periódica dos portos de entrada (alimentação e eluente) e de saída (extracto e refinado) na direcção do escoamento do fluido. Esta operação em contracorrente maximiza a força motriz para a transferência de massa, o que vai aumentar a eficiência com que o adsorvente é utilizado, permitindo um aumento considerável da productividade do sistema e a redução do consumo de eluente.

Desde o início dos anos noventa, desenvolveu-se um crescente interesse à volta do processo LMS, levando ao aparecimento de consideráveis desenvolvimentos no modo de operação deste processo. Estes novos modos de operação assentam essencialmente na manipulação das variáveis de operação durante o ciclo do processo. De entre vários, destacam-se a comutação assíncrona dos portos de entrada e saída (processo *VariCol*), a modelação periódica dos vários caudais (processo *PowerFeed*) e a modelação da concentração da alimentação (processo *ModiCon*). Devido a estes desenvolvimentos, o processo tornou-se mais eficiente, levando à possibilidade de usar cada vez menores unidades LMS, sendo a tendência geral para unidades com poucas colunas, pois utilizam menos quantidade de fase estacionária, são mais compactas e económicas.

No entanto, esta melhoria no desempenho é normalmente obtida à custa de uma complexidade acrescida e de um aumento da sensibilidade a incertezas processuais e variabilidades operatórias. Este facto

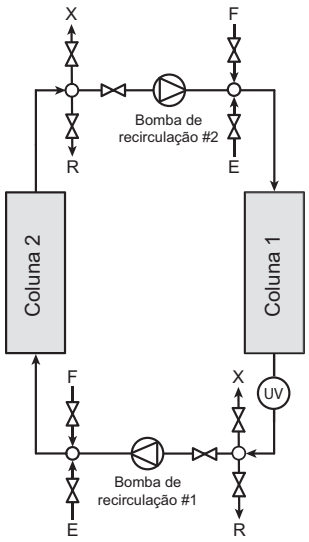

Figura 3: Diagrama esquemático da unidade LMS de apenas duas colunas.

requer a utilização de equipamento altamente versátil, ferramentas de optimização avançadas, e procedimentos robustos de controlo automático.

Com o objectivo de criar uma ferramenta prática de desenvolvimento processual, um processo monocoluna que se baseia na reprodução do estado estacionário cíclico do LMS foi desenvolvido. A principal função deste esquema não é a separação de uma mistura mas sim a reprodução rápida e expedita do estado estacionário cíclico do LMS sem a necessidade da realização de experiências na unidade multicoluna.

Este sistema foi validado experimentalmente para uma separação de dois nucleosídeos em fase líquida, tanto para a operação LMS clássica como para os diferentes modos de operação *Varicol* e *PowerFeed*, bem como para um sistema híbrido com combina esses dois. Provou ser um método simples, compacto, e rápido de experimentalmente reproduzir o comportamento periódico do LMS com um consumo mínimo de soluto e solvente. O método proposto demonstrou ser uma maneira simples e económica de testar experimentalmente as condições de operação para um novo processo cromatográfico multicoluna.

Apesar do LMS clássico necessitar de no mínimo quatro colunas, através da manipulação dos portos torna-se possivel operar com menos colunas. Um sistema LMS compacto com apenas duas colunas é apresentado.

A problemática do desenvolvimento de uma unidade experimental para reproduzir sistemas compactos é abordada. Há vários aspectos a considerar no design de um sistema como este. Por um lado, o equipamento que controla a comutação dos portos (as válvulas) tem de ser versátil o suficiente para acomodar os diversos tipos de configurações possíveis. Por outro lado, devido à modelação dos caudais, a configuração das bombas tem que ser suficientemente robusta. Na unidade desenvolvida optou-se por uma configuração de válvulas distribuídas, baseada em válvulas on-off, e por um conjunto de bombas de deslocamento positivo (duplo-pistão). Uma fotografia da unidade experimental pode ser vista na Figura 4.

Um processo LMS que usa apenas 2-colunas para separação binária foi desenvolvido. Este utiliza duas bombas de entrada para fornecer ali-

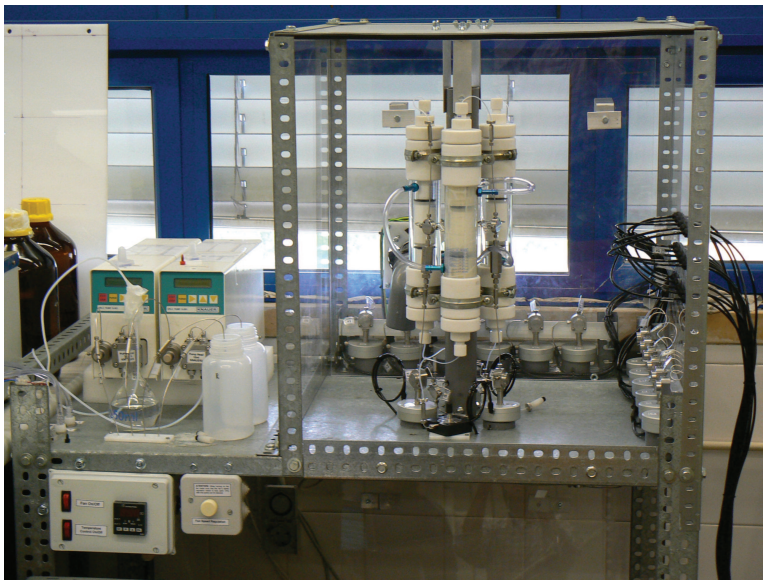

Figura 4: Fotografia da unidade experimental.

mentação e solvente ao sistema, duas bombas internas de recirculação para manipulação do caudal de efluente que é direccionado de uma coluna para a seguinte e dez válvulas de para manipulação dos portos (ver Figura 3). O sistema aplica simultâneamente a modelação periódica dos portos e dos caudais; o processo foi reproduzido experimentalmente e provou ser bastante eficiente quando comparado com cromatografia *batch* ou *batch* com reciclo. Este facto demonstra que o processo poderá ser uma alternativa viável ao nível de indústrias de produtos de alto valor acrescentado, nomeadamente farmacêutica e biotecnológica.

Apesar das potecialidades deste novo processo, este continua a apresentar alguma complexidade quando comparado com processos cromatográficos monocoluna. De forma a simplificar o processo, um novo ciclo foi desenvolvido. Este novo ciclo assenta num esquema de loop-aberto ao mesmo tempo que mantem os caudais o mais uniforme possivel; assim, como não existe recolha parcial da corrente de produto, as duas bombas de recirculação podem ser retiradas do processo, fazendo com que se torne numa unidade mais económica e simples de operar. O diagrama de um ciclo de operação do processo está representado na Figura 5.

Este esquema foi testado experimentalmente para a separação binária dos nucleosídios uridina e guanosina em cromatografia de fase reversa. A concordâcia entre resultados experimentais e design teórico foi total. O processo demontra assim ser uma mais valia do ponto de vista operacional pois apresenta uma simplicidade idêntica ao de um processo monocoluna mas aplica as características de um processo cromatográfico contracorrente, resultando num esquema simples mas de alta *performance*.

Foi também estudada a hipótese de adicionar ao esquema um passo de reciclo. Esta possibilidade foi validada experimentalmente com sucesso, revelando ser uma boa opção para a redução do consumo de eluente. No entanto, a adição do passo de reciclo implica que a

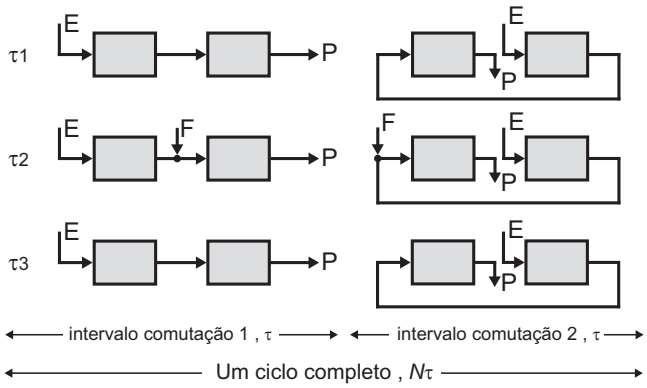

Figura 5: Diagrama esquemático do ciclo completo do processo simplificado LMS de duas colunas. Cada intervalo de comutação está dividido em 3 passos de duração variável que representam dois passos de eluição e um de alimentação. No segundo intervalo de comutação, o esquema repete-se mas com uma coluna de desfasamento (como no LMS clássico). De notar que P representa a saída de produto que pode representar tanto o extracto como o refinado.

unidade necessita de uma terceira bomba (para efectuar o reciclo), pelo que esta opção deverá será mais viável no caso de separações que apresentem baixa selectividade.

Finalmente, o problema de robustez da operação LMS é abordado. Um procedimento geral para o design e optimização robusta na presença de incerteza ou variabilidade nos caudais e nos parâmetros da isotérmica é proposto. Estes tipos de incerteza são dos mais difíceis de resolver do ponto de vista operacional e dos que ocorrem com mais frequência à escala industrial. A operação robusta é particularmente relevante nestes novos processos, pois estes proporcionam melhorias no desempenho da unidade mas á custa do aumento da complexidade operacional, tornando-se num process mais sensivel a perturbações.

O design robusto desenvolvido assenta na pré-avaliação dos piores casos, isto é, aqueles que mais afectam a variável de controlo: as purezas do extracto e do refinado. O problema é então resolvido de forma a que, na situação correspondente às piores perturbações, o

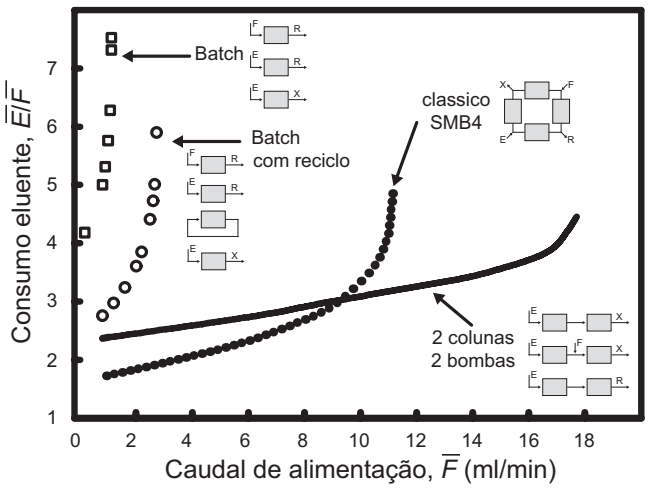

Figura 6: Curvas de operação óptima para o processo LMS com 2 colunas para a separação binária de dois nucleosídeos. Comparação entre este e os processos batch, batch com reciclo e o LMS clássico de 4 colunas. Para todos os processos a quantidade de fase estacionária é mantida constante.

processo mantém os níveis mínimos de pureza.

Foram reproduzidas um conjunto de três experiências de optimizações robustas para o processo descrito na Figura 5. Em duas delas foram infligidas perturbações, nos caudais e nos parâmetros da isotérmica. No entanto, o processo conseguiu manter níveis de pureza dentro de valores admissiveis.

Resumindo, os processos desenvolvidos provaram que podem ser instrumentos poderosos ao nível de indústrias de produtos de alto valor acrescentado, pois o volume de material processado é muito baixo quando comparadas com as indústrias petroquímica ou do açucar. Um procedimento geral para o design de processos robustos que antecipam as perturbações e fluctuações experimentais dos parâmetros do processo foi desenvolvido.

Contents

List of Figures

List of Tables

Nomenclature

Roman Symbols

a_p	surface of the adsorbent particles (cm^2)
D_L	lumped axial dispersion coefficient (cm^2/min)
h	dimensionless plate height
k	LDF mass transfer coefficient (min^{-1})
Pe	Péclet number
q	solute concentration in the adsorbed phase (g/l)
x	dimensionless axial position, z/L
z	axial position in column (cm)
A	column cross-section area (cm^2)
c	solute concentration in the liquid phase (g/l)
c_F	Feed concentration (g/l)
E	Eluent
F	Feed
f_{obj}	Objective function
G	guanosine
K	Henry constant
L	column length (cm)

m	flowrate ratios
N	number of columns
N_p	number of chromatographic plates
n_{Q}	number of piecewise constant subintervals of the SMB cycle
P	Purity
Q	flowrate (ml/min)
R	Raffinate
t	time coordinate (min)
U	uridine
V	column volume (cm^3)
X	Extract

Greek Symbols

υ	interstitial velocity of the mobile phase (cm/min)
β	phase ratio, $(1-\epsilon)/\epsilon$
δ	relative deviation
ϵ	interparticle porosity
ϵ_p	particle porosity
λ	wavelength (nm)
ρ	density (g/cm^3)
θ	dimensionless time, t/τ
τ	switching interval (min)

ϵ^*	overall porosity, $\epsilon^* = \epsilon + \epsilon_p(1-\epsilon)$

Subscripts and superscripts

*	value for equilibrium
exp	experimental value
I, . . . , IV	SMB zones, I, . . . , IV
i	solute index
in	column inlet
j	column index
max	maximum admissible value
min	minimal admissible value
out	column outlet
sim	simulated value

Acronyms

CSS	Cyclic Steady State
HETP	height equivalent to a theoretical plate
MCSGP	Multi-column Solvent Gradient Process
NLP	Non-linear programm
NPLC	Normal phase liquid chromatography
RPLC	Reversed phase liquid chromatography
SEC	Size exclusion chromatography
SF-SMB	SuperCritical Fluid Simulated Moving Bed

SMBR	Simulated Moving Bed Reaction Process
SMB	Simulated Moving Bed
TMB	True Moving Bed

1 Introduction

1.1 Relevance and Motivation

Chromatographic processes for separation at preparative and production scales have experienced a great deal of development over the last decades. An efficient way to implement countercurrent chromatography in a continuous mode was developed in the early 1960s as a process called simulated moving bed (SMB). It consists of an extremely ingenious way of simulating the countercurrent movement of the solid and the liquid phase by means of a periodic movement of the inlet and outlet lines. This process presents the big advantages of providing good separation even when the resolution is low, and at the same time increasing the productivity and reducing solvent consumption relatively to conventional batch chromatography.

The increasing demands of the pharmaceutical and biotechnology industries are clearly moving the need towards better separation and purification technologies. Continuous countercurrent chromatography has been increasing its importance as a separation and purification tool in the aforementioned areas since it is a flexible and efficient technique with high purity performance. Nowadays, the SMB technology is used in these industries for a broad class of applications, such

as enantiomeric separation and bio-separations. Following this increasing interest, several recent developments have emerged through the variation of selected control parameters during the operation of the cycle, leading to an improvement of the setup efficiency and consequentially to SMB units with smaller number of columns and more economical systems.

These smaller units provide further gains, but usually at the expense of additional complexity. This additional complexity requires the development of highly versatile SMB equipment, advanced optimization tools, and robust control procedures.

Although the SMB process increases throughput, purity and yield relative to batch chromatography, the batch process still presents the obvious advantages of being easy to operate, requiring a low capital investment, and being easily prone to the application of solvent gradients or center-cut separations. Those facts present challenges to anyone who is developing simple chromatographic processes with the enhanced properties of simulated countercurrent behavior, but still maintaining the simplicity of the batch system.

1.2 Objectives and Thesis Structure

The main objective of this work is to develop and experimentally validate compact SMB units with only two columns, which incorporate the simplicity and versatility of bath chromatography and the countercurrent behavior of the continuous SMB process.

Furthermore, a robust strategy under uncertainty, based on a worst-case approach, for process design was developed as well as a broad class of numerical and experimental tools for optimization and validation of new chromatographic processes and separations.

This thesis comprises 8 chapters. The first chapter describes the relevance and motivation of this work as well as the structure of the thesis. The second chapter introduces some basic notions and a brief history of the chromatographic separation, followed by a discussion of the principles of the true moving bed (TMB) and the simulated moving bed chromatography. Moreover, a brief review of the state of the art on the SMB process is included. In chapter 3 we discuss

the SMB modeling strategies and all the possible different approaches. Part of this chapter is based on the following published papers:

- J.M.M. Araújo, R.C.R. Rodrigues, J.P.B. Mota, Use of Single-Column Models for Efficient Computation of the Periodic State of a Simulated Moving-Bed Process, Ind. Eng. Chem. Res. 45 (2006) 5314-5325;
- J.M.M. Araújo, R.C.R. Rodrigues, J.P.B. Mota, Optimal Design and Operation of a Certain Class of Asynchronous Simulated Moving Bed Process, J. Chromatography A 1132 (2006) 76-89.

In chapter 4 a novel single-column setup for experimentally reproducing the steady periodic behavior of simulated countercurrent multicolumn chromatography is presented. This chapter describes the work published in two recent papers:

- R.C.R. Rodrigues, J.M.M. Araújo, M.F.J. Eusébio, J.P.B. Mota, Experimental Assessment of Simulated Moving Bed and Varicol Processes Using a Single-Column Setup, J. Chromatography A 1142 (2007) 69-80;
- R.C.R. Rodrigues, J.M.M. Araújo, J.P.B. Mota, Optimal Design and Experimental Validation of Synchronous, Asynchronous and Flow-modulated, Simulated Moving-Bed Processes using a Single-column Setup, J. Chromatography A 1162 (2007) 14-23.

Chapter 5 describes extensively the developed experimental unit for chromatographic separation, which can operate with up to three chromatographic columns. The report is done from the process engineering point of view. It focus on the issues that must be dealt with when creating a versatile and compact small-scale system.

In chapter 6 a simulated-moving-bed setup using only two columns is proposed. The system exploits the potentialities of the simulated countercurrent movement between mobile and stationary phase combined with a periodic modulation of the flowrates to design a whole class of practical high-performance chromatographic unit schemes. This chapter is based on a work published in:

- R.C.R. Rodrigues, T.J.S.B. Canhoto, J.M.M. Araújo, J.P.B. Mota, Two-column simulated moving-bed process for binary separation, J. Chromatography A 1180 (2008) 42-52.

Chapter 7 reports some further developments to simplify the previously developed two-column SMB process. These developments create a simplified two-column scheme which couples the advantages of the simple batch chromatography process and still maintains the high performance behavior of the countercurrent SMB system.

In chapter 8, a general procedure for robust design of SMB processes under flowrate, packing, and isotherm uncertainty is presented. The approach relies on a worst-case scenario to create an enlarged optimization solution which fulfils the purity requirements for all considered possible perturbation. This chapter can be viewed as an extension of the work published in:

- J.P.B. Mota, J.M.M. Araújo, R.C.R. Rodrigues, Optimal design of simulated moving-bed processes under flow rate uncertainty, AIChE Journal 53 (2007) 2630-2642.

Finally, a few remarks and ideas for future work are presented, before summarizing the work and drawing final conclusions.

2

Chromatographic Separation

2.1 History and development

Chromatography is a very effective separation and/or analysis technique. It was first used by chemists for the extraction/purification of dye mixtures by dipping strings or pieces of cloth or filter paper into a dye vessel. The dye solution migrated up the inserted material by capillary action, and the dye components produced bands of different colour.

However, the discovery of chromatography is generally attributed to the russian botanist Mikhail S. Tsvet who, in the first decade of the 20th century, was the first to recognize the physicochemical basis of the separation and applied it in a rational and organized way to the separation of plant pigments. Basically, what he did was to pack a vertical glass column with an adsorptive material, such as alumina or silica, add a solution of plant pigments to the top of the column and wash the pigments through the column with an organic solvent. The result was a series of separated colour bands on the column, divided by regions entirely free of pigments.

Because Tsvet worked with coloured substances, he called the method chromatography (from the Greek *colour writing*).

Later on, chromatography began to take its modern form in the 1940s and 1950s. The principles and basic techniques of partition chromatography appeared from the work of Archer Martin and Richard Synge and lead to the rapid development of several lines of chromatography methods: paper chromatography, gas-solid and gas-liquid chromatography and several techniques of column liquid chromatography. Subsequent advances continually improved the performance of chromatography, allowing the separation and/or purification of an extensive variety of molecules.

2.2 Elution batch Chromatography

Modern, conventional liquid or elution batch chromatography consists of a cylindrical column packed with a porous media, usually called stationary phase, which is subjected to a pulse injection of a mixture followed by a continuous flow of fluid phase (mobile phase). Each of the species present in the mixture (analytes) may interact with the stationary phase, the stronger they interact with the porous media the slower they will elute along the column. Therefore, each species will have a concentration band profile of distinct velocity along the column making it possible, with a long enough column, to collect at the output pure fractions

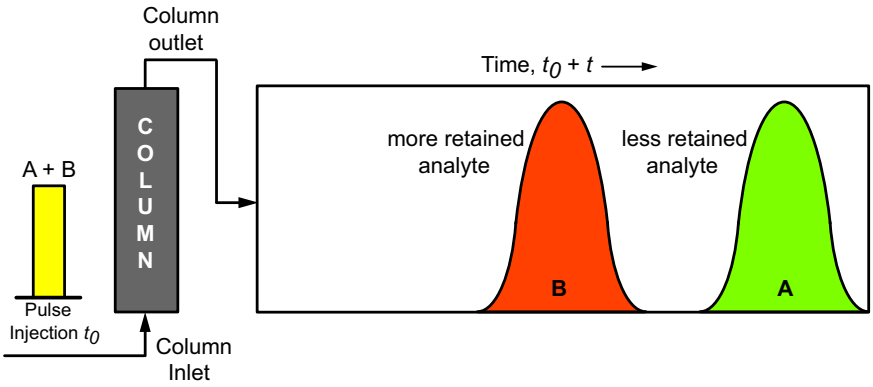

Figure 2.1: **Elution Batch chromatography** - Schematic representation of the elution batch chromatography process for a binary separation (A+B). Note that A represents the less retained specie and B the more retained.

of each component at different elution times. When all species have eluted from the column a fresh injection of mixture takes place and a new separation cycle is initiated. A simplified scheme of the elution batch chromatography process for a binary mixture can be viewed in Figure 2.1.

It is worth mentioning that because this is a discontinuous process where each product is collected at different times, one cannot continuously feed the column.

2.3 Theory of Linear Chromatography

Generalizing, liquid chromatography is, in essence, a batch process that uses one or more columns (operating in parallel) that provide a semi-continuous flow of products. Each analyte flows axially along the column and interacts with the stationary phase in different ways. Based on the way the species interacts with the solid phase, one can divide column chromatography into five major subclasses:

- Affinity chromatography, where selective non-covalent interactions occur between each analyte and specific molecules present in the porous medium. It is very specific and often used in biochemistry for the purification of proteins.

- Ion exchange chromatography utilizes an ion exchange mechanism to separate analytes. It uses a charged stationary phase to separate charged compounds. In conventional methods the stationary phase is an ion exchange resin that carries charged functional groups which interact with oppositely charged groups of the compound to be retained.

- Size exclusion chromatography (SEC) separates molecules according to their size (or more accurately according to their hydrodynamic diameter or hydrodynamic volume). Smaller molecules are able to enter the pores of the media and, therefore, take longer to elute, whereas larger molecules are excluded from the pores and elute faster.

- Normal phase liquid chromatography (NPLC), where the stationary phase is more polar than the mobile phase and the elution of substances from the column is in the order of decreasing polarity.

- Reversed phase liquid chromatography (RPLC), in contrast with NPLC the stationary phase is less polar than the mobile phase and the elution of substances from the column is in the order of increasing polarity. Ironically the "normal phase" has fewer applications and RPLC is therefore used considerably more.

The adsorption equilibrium behavior that occurs between the liquid solute and the surface of the solid is usually described mathematically by an equilibrium isotherm, which describes the concentration of adsorbate in the adsorbent as a function of its concentration in the bulk solution at constant temperature. There is no single characteristic shape for an isotherm. Brunauer et al. classified it into five different classes: type I,. . .,V [1]. A typical type I isotherm is represented in Fig. 2.2.

For sufficient low concentrations the equilibrium relationship between the two phases has a linear behavior. This linear relation is commonly referred to as the

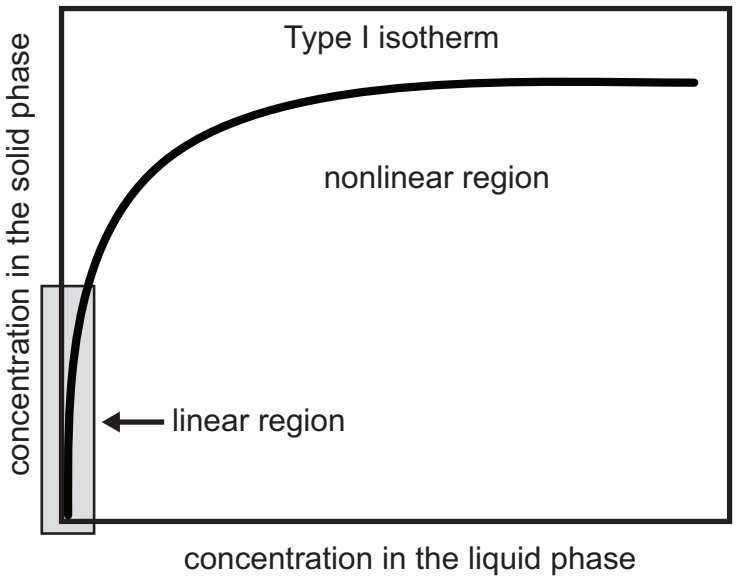

Figure 2.2: Type I adsorption isotherm. An adsorption isotherm describes the phase equilibrium between the fluid and the solid phase. Notice that for low concentrations zones (shaded area) this equilibrium can be approximated by a linear relation.

Henry's law:

$$q = K\ c \tag{2.1}$$

where q and c are the concentrations in the adsorbed and fluid phases, and K is called the Henry constant.

Linear and nonlinear chromatography have experienced an enormous progress over the last 50 years, mainly because of the evolution of computers making it possible to easily solve the inherent complex numerical calculations typical of a chromatographic model [2].

The modeling of chromatography, and the linear case in particular, developed mainly along three different classes of models that describe and predict elution profiles (see Fig. 2.3):

- "Tank in series" model, also known as plate model (lumped models).

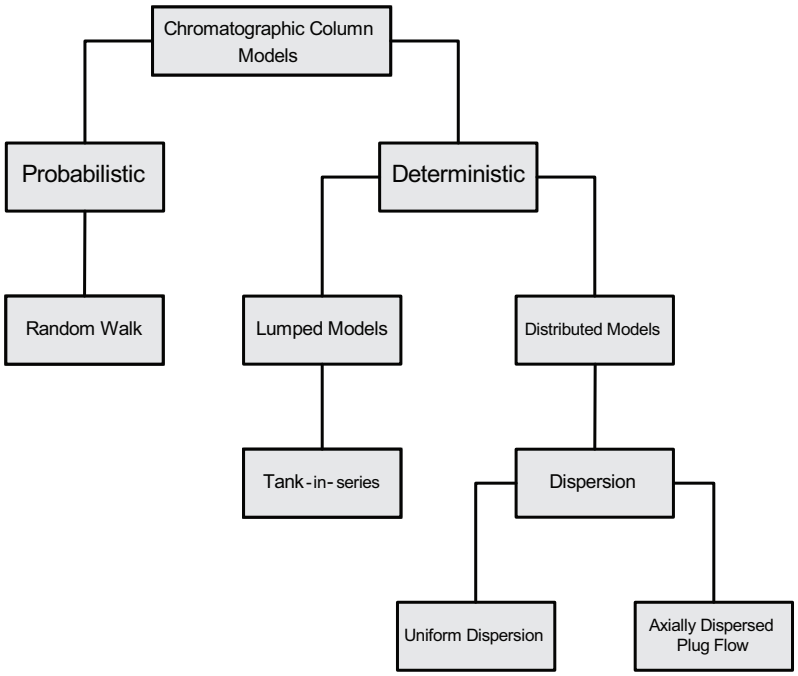

Figure 2.3: Flowchart of the several mathematical approaches to model a chromatographic column.

- Probabilistic models.
- Systems of differential equations that describe the mass balance and the mass transfer kinetics (distributed models).

2.3.1 The Plate Theory

The plate theory of chromatography was introduced by Martin and Synge in 1941 and later by Craig offering the first description of the development of quasi-Gaussian bands in linear elution chromatography. It states that a column can be represented by a series of well-mixed stirred tanks or equilibrium stages, and the mobile phase percolates from one tank to the next after equilibrium is achieved between the mobile and the stationary phases. It was an attempt to work out in detail the theory of chromatography using the previously known concepts developed in distillation and extraction.

This theory assumes that the solute, during its passage through the column, is always in equilibrium with the mobile and stationary phases. However, equilibrium between the phases never actually occurs, consequently to deal with this non-equilibrium condition, the column is considered to be divided into a finite number of plates. Each plate is allotted a specific length and, thus, the solute

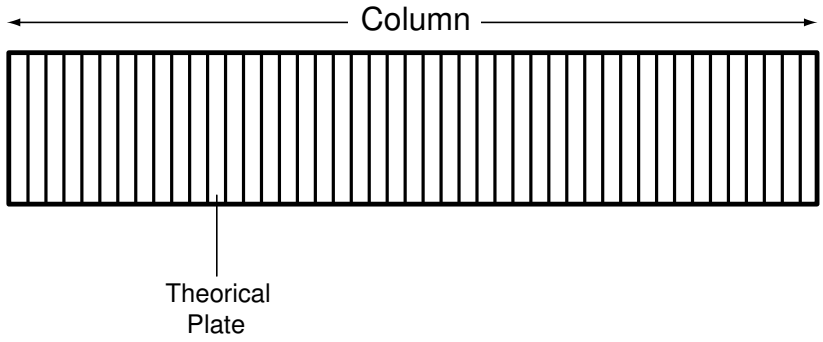

Figure 2.4: Chromatography plate theory - In this chromatography model the column is divided into a discrete number of equilibrium stages. It is important to remember that the plates do not really exist, they are a figment of the imagination that helps to describe the process that occurs in the column.

will spend a finite time in each plate. Hence, the smaller the plate, the faster the equilibrium is obtained and the more plates there will be in the column. Consequently, the number of theoretical plates contained in a column will be directly related to the equilibrium rate and, for this reason, has been termed the column efficiency. If we consider the column length L and the total number of theoretical plates N_p, then the *Height Equivalent to a Theoretical Plate* (HETP) is:

$$HETP = \frac{L}{N_p} \tag{2.2}$$

This division of the column into a series of plates can be empirically correlated, after the facts, with the column parameters, however the model completely neglects mixing mechanisms, have no predictive value and do not allow a reliable theory of linear chromatography.

A more realistic description of the processes at work inside a column takes into account the time taken for the solute to equilibrate between the stationary and mobile phase (unlike the plate model). The resulting band shape of a chromatographic peak is therefore affected by the rate of elution. It is also affected by the different paths available to solute molecules as they travel between particles of stationary phase. If we consider the various mechanisms which contribute to band broadening, we arrive at the Van Deemter equation for plate height:

$$HETP = A + \frac{B}{\upsilon} + C\upsilon \tag{2.3}$$

where υ is the linear velocity of the mobile phase, A is known as the Eddy diffusion which accounts for the different paths and lengths of the solute molecules passing through the column, B is the longitudinal diffusion coefficient for a concentration peak and C is the resistance to mass transfer component which describe the amount of time a solute takes to equilibrate between the stationary and mobile phase. A, B and C together are factors which contribute to describe the band broadening that occurs in a chromatographic column. Provided that N_p is large enough (> 10), the discrete stage model becomes numerically equivalent to the continuous linear rate model.

In practice, a plot like the one showed in figure 2.5 can be drawn to determine the optimum flow rate for a chromatographic process.

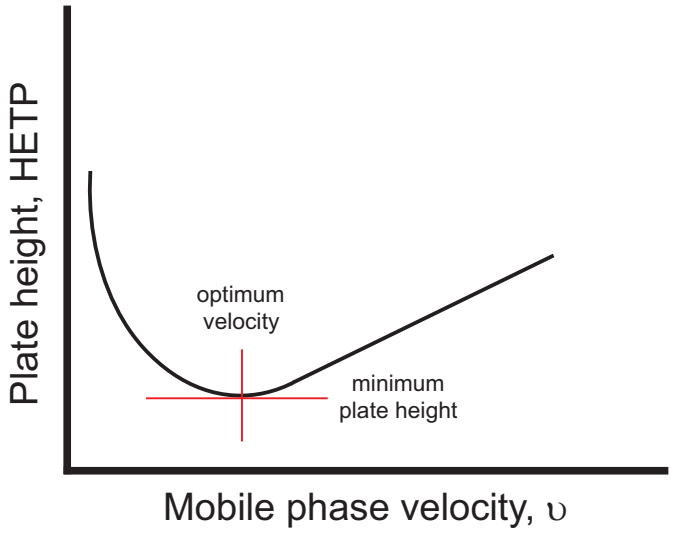

Figure 2.5: Typical Van Deemter plot - By representing the column HETPs dependence of the linear mobile phase velocity υ, the optimum flow rate for a chromatographic process can be obtained.

2.3.2 The Stochastic Theory

In 1955, Giddings and Eyring employed probability (stochastic) concepts to describe the molecular migration process in chromatography. They developed a rigorous probability theory that gave a precise description of the influence of simple adsorption-desorption processes on the zone profile. These authors considered the random migration of a single solute molecule along a chromatographic column. They derived an expression for the elution profile of the molecules of the sample in the column, assuming random adsorption-desorption processes, with a single type of site or two different sites on the stationary phase and pulse injection. They ignored the axial dispersion and approximated the mass transfer kinetics in the mobile phase by what is now referred by the random walk theory of chromatography or theory of zone dispersion for the situation when the time spent by the solutes inside the column is large enough to allow each molecule to undergo a large number of individual sorption and desorption steps.

Later, McQuarrie extended the stochastic theory to the case of multiple adsorption sites and to a column with a single type of site, but with various input

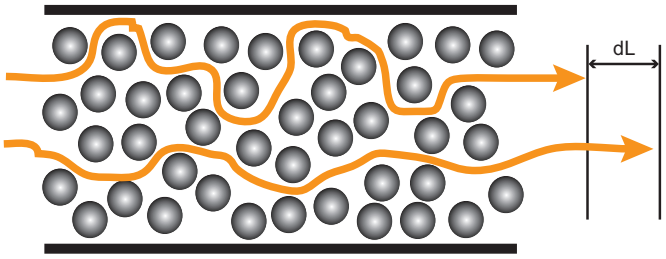

Figure 2.6: Random Walk Model - In a packed column the solute molecules will describe a tortuous path through the interstices between the particles and obviously some will travel shorter paths than the average and some longer paths. Consequently, some molecules will move ahead of the average and some will lag behind thus causing band dispersion.

distribution functions, by means of the theory of the Laplace transform.

2.3.3 The Solid-Diffusion Model

As clear shown by Giddings, chromatography is a separation method combining a chemical potential discontinuity in a direction perpendicular to that of a convective transport. This naturally introduces the mass balance approach to calculate the chromatographic response to a given input injection or profile. This approach is based on the use of an equation of motion. In this method, one search for the mathematical solution of the set of partial differential equations describing the chromatographic process, or more precisely, the differential mass balance of the solute in a slice of column and its kinetics of mass transfer in the column. Various mathematical models have been developed to describe the chromatographic process with great predictive value, the most important of these models are:

- Ideal model.
- Equilibrium-dispersive model.
- Lumped kinetic models.
- Pore model.

- General rate model.

The use of these several different models to describe the dynamic behavior of a chromatographic column has been extensively reported in literature. This work will focus on a lumped solid-diffusion model with linear driving-force approximation for mass transfer. Despite its simplicity, this model is usually a precise tool to describe the chromatographic band profiles in most circumstances [1]. The mass balance equation comes:

$$\epsilon\frac{\partial c_i}{\partial t} + (1-\epsilon)\frac{\partial q_i}{\partial t} + \epsilon\upsilon\frac{\partial c_i}{\partial z} = \epsilon D_i\frac{\partial^2 c_i}{\partial z^2} \tag{2.4}$$

where subscript i is the solute index, z is the axial coordinate, D_i is the dispersion coefficient, υ is the linear velocity of the mobile phase, t is the time coordinate, c and q is the concentration in the fluid and solid phases.

The equation for adsorption kinetics is:

$$\frac{\partial q_i}{\partial t} = k_i\ a_p\ (q_i^* - q_i) \tag{2.5}$$

where k_i is the mass-transfer coefficient, a_p the surface of the adsorbent particles and q_i^* is the adsorbed concentration in equilibrium with the bulk concentration $(c_1, \ldots, c_n)$.

With the proper initial and boundary conditions, the lumped solid-diffusion model (Equations 2.4 and 2.5) is equivalent to the equilibrium dispersive model (Eq. 2.6) [1, 3, 4]. An equilibrium-dispersive model still assumes that mass transfer across the column is infinitely fast (like in the plate theory) but it accounts for band broadening by axial dispersion. Further, it treats the finite rate of the mass transfer kinetics as another contribution to axial dispersion. Thus, it relates apparent axial dispersion and column HETP. This approach is valid when the column efficiency is high, as it is in the reversed-phase liquid chromatography (RPLC) of small molecules of moderate polarity. Because this model considers the influence of a finite column efficiency, as a small correction it should not be applied when this efficiency is poor. The lumped model for the overall mass balance is

$$\epsilon\frac{\partial c_i}{\partial t} + (1-\epsilon)\frac{\partial q_i^*}{\partial t} + \epsilon\upsilon\frac{\partial c_i}{\partial z} = \epsilon D_{i\mathrm{L}}\frac{\partial^2 c_i}{\partial z^2} \tag{2.6}$$

where $D_{i\mathrm{L}}$ is a lumped axial dispersion coefficient.

For the case of linear adsorption conditions, i.e. $q_i^* = K_i\ c_i$, the lumped solid-diffusion model is given by the following relationship:

$$\frac{1}{N_p} = \frac{2D_i\ \epsilon}{\upsilon\ L} + \frac{2\upsilon}{(1-\epsilon)L\ K_i\ k_i\ a_p}\left(\frac{(1-\epsilon)K_i}{\epsilon+(1-\epsilon)K_i}\right)^2 \tag{2.7}$$

where N_p is the number of theoretical stages that contribute to the axial dispersion.

The simplified equilibrium axial dispersive is equivalent to the solid-diffusion model provided that $D_{i\mathrm{L}}$ is chosen so that the number of theoretical plates in the two models are the same. Moreover, with the introduction of additional auxiliary dimensionless scales the equilibrium axial dispersive model (Eq. 2.6) can be simplified to:

$$(1+\beta K_i)\frac{\partial c_i}{\partial \theta} = \frac{\tau\upsilon}{L}\left(\frac{h_i}{2}\frac{\partial^2 c_i}{\partial x^2} - \frac{\partial c_i}{\partial x}\right) \quad (0<x<1), \tag{2.8}$$

where $\theta = t/\tau$ and $x = z/L$ are the dimensionless temporal and axial coordinates, respectively, $\beta = (1-\epsilon)/\epsilon$ is the phase ratio, L is the column length, $\mathrm{Pe}_i = \upsilon L/D_{i\mathrm{L}}$ is the individual Péclet number, q_i^* is the adsorption isotherm for solute i and k_i is the LDF mass-transfer coefficient. Moreover,

$$h_i = \frac{H_i}{L} = \frac{2}{\mathrm{Pe}_i'} = \frac{2}{\mathrm{Pe}_i} + \frac{\beta K_i}{(1+\beta K_i)^2}\frac{2\upsilon}{k_i L} \tag{2.9}$$

is the dimensionless plate height. The usual boundary conditions are:

$$c_i - \frac{1}{\mathrm{Pe}_i'}\frac{\partial c_i}{\partial x} = c_i^{\mathrm{in}} \quad \text{for} \quad x = 0, \tag{2.10}$$

$$\frac{\partial c_i}{\partial x} = 0 \quad \text{for} \quad x = 1. \tag{2.11}$$

In the working range of fluid velocity used in preparative chromatography, the contribution of axial molecular diffusion is negligible [5] and one can consider the Péclet number as being approximately independent of v. Furthermore, adsorption kinetics is usually governed by intraparticle diffusion rather than by external film resistance, which means that k_i is also usually independent of v. Under these assumptions, the influence of v on column efficiency simplifies into a linear relationship:

$$\frac{h_i}{2} = \frac{1}{\mathrm{Pe}_i} + \alpha_i v, \quad \alpha_i = \frac{\beta K_i}{k_i L (1+\beta K_i)^2}. \tag{2.12}$$

2.4 Batch Chromatography with Recycle Closed-loop

Closed-loop recycling is a chromatography process with a single-column that increases productivity and efficiency relatively to elution batch chromatography. The basic idea of the process is simple; because in batch chromatography the feed pulse is limited by the resolution of the peaks in the column, i.e. the column has to be sufficient long enough to allow complete separation of the peaks as one can see in Fig. 2.7, by means of recycling the traveling mixture several times through the column one can achieve higher peak resolution without the need of a longer column.

In closed-loop chromatography, like in batch mode, a feed pulse is injected into the column however at the end of the column there is the possibility of collecting the pure products fractions or recycling again to the top of the column. Through this recycling behavior, in practice one are increasing the column number of theoretical plates available for the separation because we are simulating the use of a longer column [6]. As showed in Fig. 2.7, the system setup is similar to a typical batch unit with the simple addition of a 4-way valve.

Recycling chromatography is characterized by the fact that the mixture to be separated is transported several times through the column. Thus, a longer column is simulated leading to an improvement of separation until a situation is reached when the sample is spread over the whole column and subsequent cycles begin to overlap [7]. Furthermore, there is the additional possibility of collecting

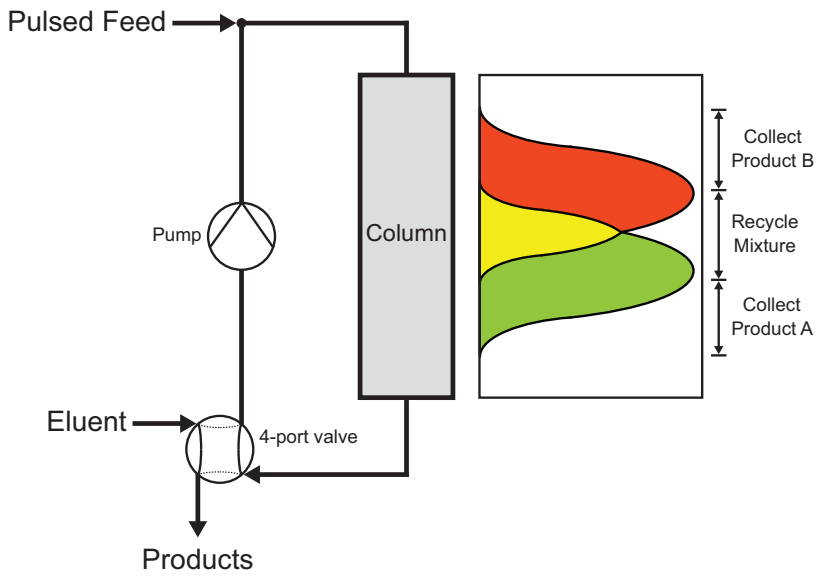

Figure 2.7: Closed-Loop Recycling Chromatography.

purified product fractions in each cycle to substantially decrease the cycle time and increase the overload of the column [8].

This process have been applied mainly in small-scale units as in the case of enantiomer separation [9] and have proved to produce fractions of high purity with higher load capacity and less solvent consumption relatively to elution batch chromatography.

2.5 Simulated Moving Bed Chromatography

The Simulated Moving Bed (SMB) process has acquired considerable importance in the recent years due to its economic benefits specially in the separation/purification of high valued products in the pharmaceutical, fine chemistry, and biotechnology industries. Because elution batch chromatography is an inherently discontinuous process, it presents the disadvantages of poor adsorbent usage and high product dilution. Furthermore, to achieve an efficient separation the peak resolution has to be high which usually implies longer columns (high number of theoretical plates) generating pressure drop issues. To overcome the

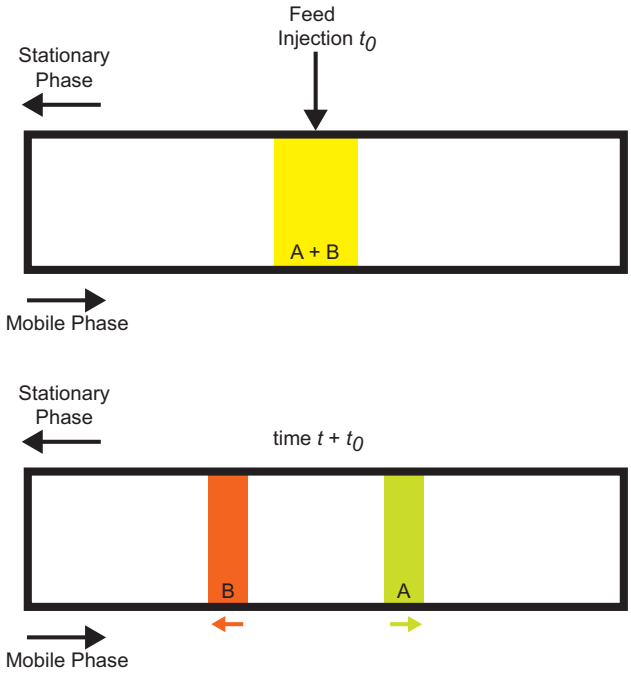

Figure 2.8: Moving Bed Pulse Injection - schematic of the true moving bed principle. If one imagine a moving solid phase with a velocity between the elution rates of the two components, after a injection of a binary mixture the more retained solute (B) accompanies the solid flow and the less retained (A) follows the opposite direction.

disadvantages of the batch process a new process called True Moving Bed (TMB) was developed. With regard to column batch chromatography, let us imagine that we can somehow feed a pulse of a binary mixture in the middle of the column. If we are eluting with fresh desorbent (eluent) then both solutes will migrate at different speeds in the direction of the eluent flow. However, if we move the stationary phase in the opposite direction of the fluid flow at a speed halfway between the migration velocity of the two compounds, then the more retained solute will be dragged with the solid and the less retained analyte will still move with the eluent but at a lower speed. This makes it possible to individually collect both products, one at each end of the column. A schematic figure of this principle is shown in Figure 2.8.

Using this concept one can continuously feed the column, creating two bands of pure material, each one moving to opposite ends of the column. This is the basic idea behind the TMB process. As one can see in Figure 2.9, this process is divided into four different zones, each one with a specific function:

- Zone I - The function of this zone is to regenerate the stationary phase, preventing that only clean solid passes to zone IV in the other end of the unit. It comprises the area between the addition of eluent (E) and the withdrawal of the more retained component, i.e. the extract (X).

- Zone II - This zone, together with zone III, are called *separation zones* because it is where the separation of the two products is actually made. The main function here is to enrich the solid phase with the more retained component in a way that the fluid phase passing to zone III only drags the less retained component. It is defined between the lines of withdrawal of extract and the inlet of feed (F).

- Zone III - This is the other *separation zone*, where is adsorbed the more retained component that moves with the mobile phase so that the less retained product is carried by the fluid to the raffinate withdrawal (R). This zone is located between the feed and the raffinate ports.

- Zone IV - The role of this zone is to regenerate the solvent, preventing that the eluent that is recycled to zone I is not contaminated with products. It is the zone within the raffinate and the eluent lines.

Each zone corresponds to a column section between an inlet (Feed or Eluent) and an outlet (Extract or Raffinate) line. The moving bed operation, due to its countercurrent movement between the liquid and solid phases, allows for the obtainment of high purity products even when the selectivity of the two solutes in the mobile phase is very poor (i.e. the difference between the migration velocities is very low). Because it is not necessary to have a complete separation, as in batch chromatography, only a small band profile of pure component is needed to make the separation. Therefore, we have a much more efficient process because the stationary phase is used more effectively allowing for much higher productivity.

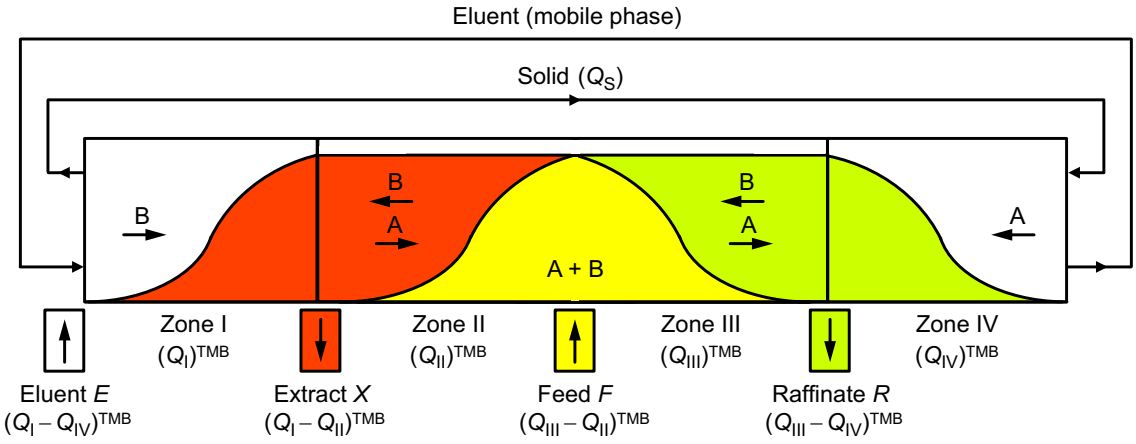

Figure 2.9: Schematic diagram of the countercurrent chromatography process (true moving bed) with four zones.

The first practical implementation of the true moving bed concept was the Hypersorption process [10]. It was invented in 1919 by Soddy and developed by the Union Oil Company of California in 1946. They used a bed of activated carbon moving countercurrently to a gas flow to separate light hydrocarbons from each other and from hydrogen in refinery operations. However, the process was abandoned because attrition of the bed particles proved uneconomic. In practice, TMB has several built-in issues such as the difficulty to promote an homogeneous motion of the solid and the consequent mechanical erosion as well as back-mixing problems. As a consequence, true moving bed chromatography is nowadays only a theoretical concept, barely used in some liquid-liquid chromatography applications.

To overcome the inherent practical problems of the TMB process, continuous chromatographic processes were achieved by simulating in a discrete manner the continuous countercurrent movement of the solid. The result is a process known as simulated moving bed (SMB) chromatography. As shown in Figure 2.10, SMB is achieved by fixing the stationary phase in a series of columns and with a complex valve arrangement, the inlet and outlet lines are switched periodically and simultaneously in the direction of the fluid flow. In practise, SMB is a discrete way of simulating the continuous TMB process.

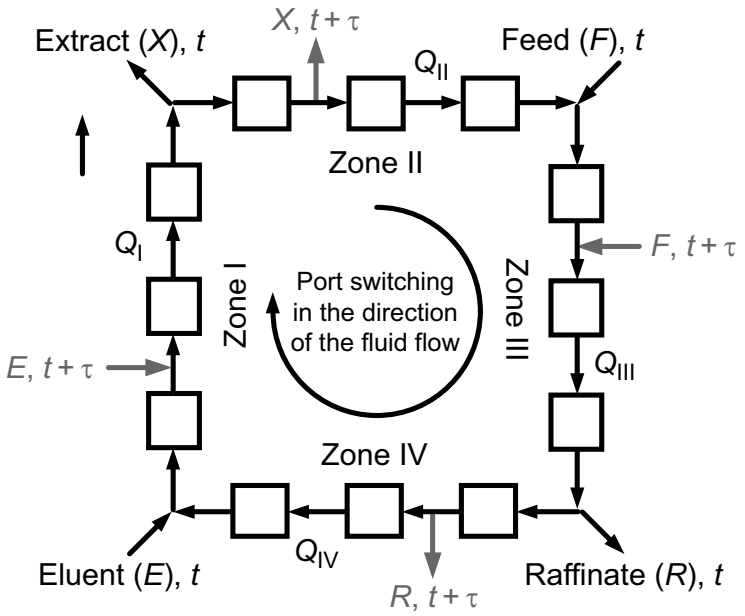

Figure 2.10: Schematic diagram of the Simulated Moving Bed process. The continuous movement of the solid is simulated through the periodic switch of the inlet and outlet ports in the direction of the fluid flow. The Feed, Eluent, Extract and Raffinate are represented by the letters F, E, X, R respectively; Q_j is the fluid flowrate in zone j (j =I,...,IV) and τ is the switching interval.

The simulated moving bed process was first patented in 1961 by the company UOP LLC (Universal Oil Products) as the SORBEX process. This process has been applied for a large number of separations in the petrochemical and sugar industry under various tradenames, related to the specific separation in use. As showed in Fig. 2.11, the process relies on a single rotary valve to impose the switching scheme.

With the recent expiration of the first SMB patents and the development of new and efficient stationary phases, many companies have gained interest in the process, leading to an exponential increase on process research and development, thus resulting in the appearance of new schemes of operating that differ from the conventional one.

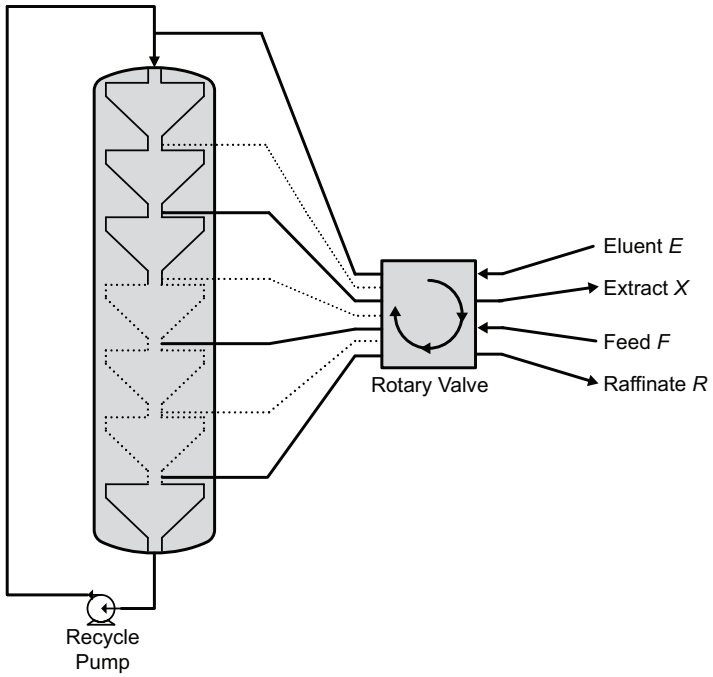

Figure 2.11: Schematic diagram of the SORBEX process. A single rotary valve controls the switching of the inlet and outlet lines through a single column separated by various adsorbent beds. This process was firstly applied in large-scale for the petrochemical industry.

2.6 Unconventional Simulated Moving Bed

Due to the cyclic arrangement and the periodic nature of the SMB process, after an initial transient state, the system reaches a cyclic steady state (CSS) in which the process exhibits the same dynamic behavior during each switching interval. Thanks to recent developments in cyclic operation schemes, a number of possibilities for improving SMB performance have merged through variation of parameters during a switching interval.

2.6.1 The VARICOL process

As discussed above, the SMB is a practical way of implementing a countercurrent chromatographic process characterized by periodically advancing both the inlet

(Eluent and Feed) and outlet (Extract and Raffinate) lines simultaneously. As a consequence of this synchronous switching of lines, the number of columns in each zone stays the same in every moment, regardless of the location of the inlet/outlet ports, making it possible to describe an SMB process in terms of how the columns are distributed among zones: $N_{\mathrm{I}}/N_{\mathrm{II}}/N_{\mathrm{III}}/N_{\mathrm{IV}}$, being $\sum N_j = N$. Obviously, in a conventional SMB process N_j is an integer number, however if one allow the ports to have an asynchronous shift then we have a column zone distribution that represents the average zone length during a complete process cycle, expanding N_j to the rational domain (provided that $\sum N_j$ is still an integer). This means that the process is no longer equivalent to a TMB but now has some extra parameters, i.e. the switching times of the single inlet and outlet lines.

A simplified scheme of the Varicol process is showed in Fig. 2.12. The Varicol can be viewed as a subdivision of the switching interval into one or more steps of different port configurations; in the case of the SMB all ports remain in the same position for the all interval and then they shift together one column ahead in the direction of the fluid flow. However, in the Varicol case there is one or more subdivisions of the switching interval where the ports do not shift together but in the end of the interval they all have advanced by one column. Fig. 2.12 represents an example of a Varicol scheme with one simple subdivision α ($\alpha < 1$) of the switching interval τ where only the raffinate port is moved forward expanding zone III to 2 columns and eliminating zone IV. For this example, the SMB is a process with 4 columns with a column zone configuration of 1/1/1/1, but the Varicol can be described with a average zone length of $1/1/(2-\alpha)/\alpha$ and still maintain $\sum N_j = 4$.

In Figure 2.13 one can see the example of a more complex Varicol port switch scheme applied to a 4-column process. Notice that in Varicol mode all lines are allowed to coexist in the ports; in this example the average zone length is 1.0/1.2/1.4/0.4. Obviously some restrictions arise with this mode of operation: one cannot withdraw extract and raffinate nor add feed and eluent in the same node and the process design has to be prepared to accommodate these extra features, but this simple approach gives rise to a all new class of operating schemes that proved to enhance the process productivity and reduce solvent consumption for a broad class of applications.

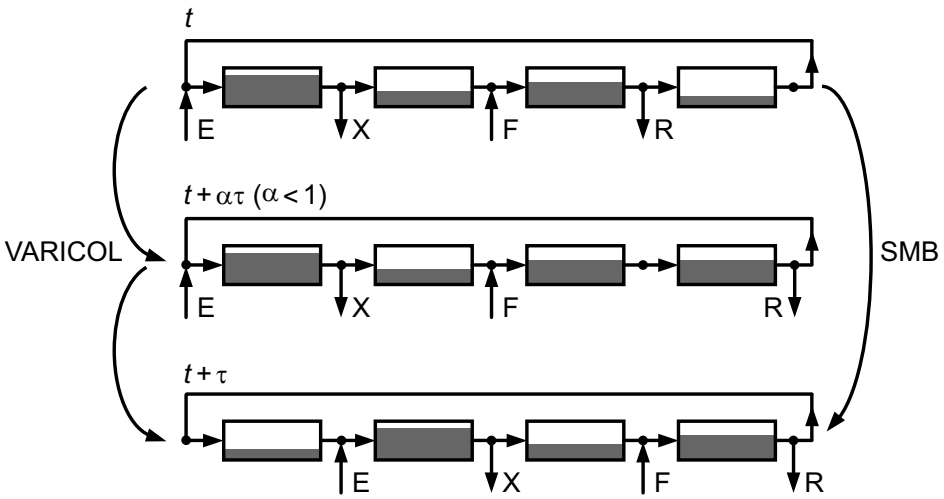

Figure 2.12: Simplified scheme of the Varicol process. The position of eluent (E), feed (F), extract (X), and raffinate (R) ports are identified by arrows. The height of each shaded area is proportional to the flowrate through the corresponding column. The standard SMB scheme keeps the topmost configuration constant over the whole switching interval τ; all ports are then switched forward by one column in the direction of fluid flow. In Varicol mode the ports are switched asynchronously. For example, after a fraction $\alpha < 1$ of the switching interval the position of the raffinate port is moved forward by one column, giving rise to the middle configuration, which has increased zone III by one column and removed zone IV but still maintaining the same zone I, II and III flowrates; at the end of the switching interval all ports have moved forward by one column like in the SMB scheme.

This process was patented in 2000 [11, 12], it has been commercialized since then by the company Novasep mainly for enantiomer separations. The big advantage of this process relies on the fact that one can now achieve a more effective and flexible allocation of the stationary phase to each of the four zones accordingly to the needs of the separation task, making the process more efficient and leading to the possibility of operating with small number of columns setups and still maintain or even improve the productivity of the process relatively to larger classical SMB units [13, 14, 15, 16].

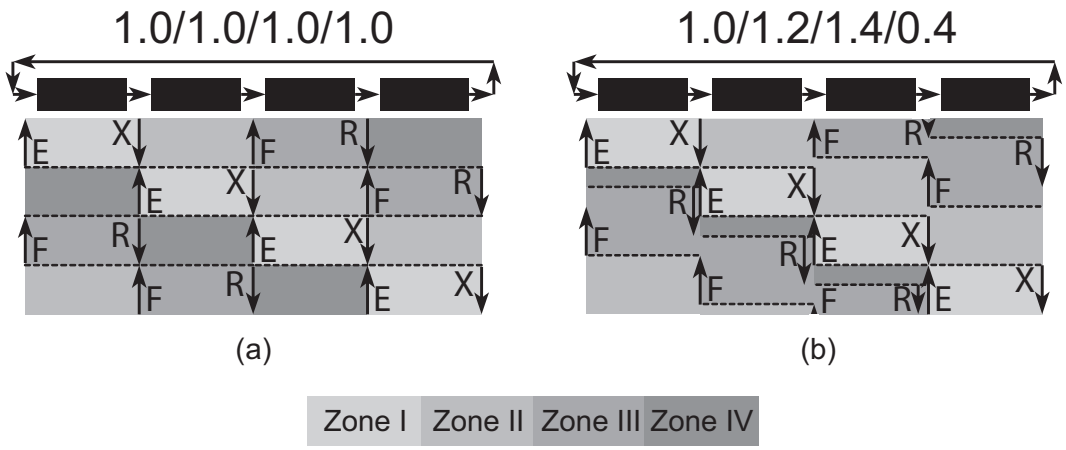

Figure 2.13: Chronograms of port switch over a complete cycle for the (a) SMB and (b) VARICOL processes. Notice that in the case of the SMB all ports shift simultaneously at the same time, for the VARICOL process the switch is made asynchronously. In the beginning of the next process cycle in both cases all ports have moved N columns ahead.

2.6.2 The PowerFeed process

Other parameters that can be manipulated during a switching interval of the SMB process are the zone flowrates. This mode of operation was first patented in 1992 [17] and was named as a "Time Variable Simulated Moving Bed" where the internal flowrates are manipulated for each switching interval in a way that the characteristic steady state waveform is modified to favor the separation process, and demonstrated for a simple sugar separation. More recently, this operation was analyzed for various classes of τ-periodic modulations that extend from a simple discontinuous pulsed feed and product withdrawal [18, 19] to a simultaneous piecewise-constant change of all internal flowrates in a theoretical study of the separation of xylenes [20] and chiral separations [21, 22].

This operation was termed PowerFeed [21], a name that have been positively accepted by the academic community. All the studies on flowrate modulation are theoretical or numerical, the exception is a simple PowerFeed scheme [23] for enantiomer separation based on a simple 3-step feed variation policy. These additional degrees of freedom available with a time-variable flowrate operation

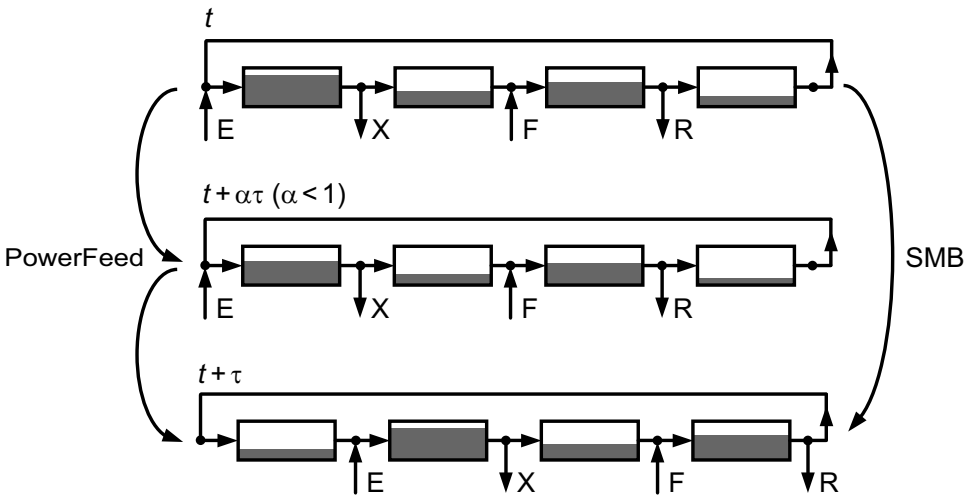

Figure 2.14: Simplified scheme of the PowerFeed process. The position of eluent (E), feed (F), extract (X), and raffinate (R) ports are identified by arrows. The height of each shaded area is proportional to the flowrate through the corresponding column. The standard SMB scheme keeps the topmost configuration constant over the whole switching interval τ; all ports are then switched forward by one column in the direction of fluid flow. In PowerFeed operation, which is illustrated by the intermediate step, the flowrates are varied over a fraction of the switching interval but the ports are only moved forward by one column at the end of the step like in the SMB mode.

have shown to either increase the productivity or reduce the specific solvent consumption.

2.6.3 Other nonclassical modes to operate an SMB

Extending the concept of new operating schemes that introduce periodic modulations of selected control parameters into the operating cycle, one can also introduce a modulation of the feed concentration [24] to improve the typical SMB unit, this process was named ModiCon [25]. The ModiCon process was patented in 2004 [26] and is commercialized by Knauer (Berlin, Germany). Again, the main idea is to modulate an SMB parameter during the switching interval, in this case the feed concentration. As showed in Fig. 2.15, essentially the ModiCon

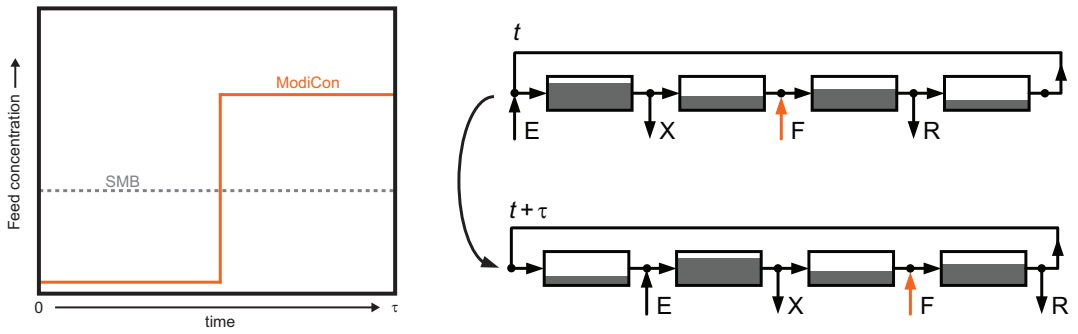

Figure 2.15: Simplified scheme of the ModiCon process. In the right one can see the port switch scheme for the switching interval which is exactly like in the classical SMB process, i.e. at the end of the switch all ports move simultaneously one column ahead in the direction of the fluid flow. The left graphic shows the evolution of the feed concentration over the switch; in the case of the SMB it is constant over time but for the ModiCon process the feed concentration profile is defined by various steps. In the exemplified case there is a part of the interval where the feed is pure eluent ($cF = 0$) then one create a step wave where cF is two times the feed concentration of the equivalent SMB process, this means that one are adding the same amount of feeding mixture to the process.

process consists of dividing the switching interval into several piecewise constant steps of different feed concentration. This scheme has proved to both increase productivity and product concentration and at the same time reduce the specific solvent consumption [25]. However it presents the drawback that can only be a valid approach in separations where the feed concentration is limited by technical reasons and not by the solubility of the components in the used solvent [24].

Probably the most simple unconventional SMB scheme is the 3-zone SMB [27]. This configuration relies on the removal of zone IV, letting all fluid coming from zone III to be collected as raffinate, in this way preventing any contamination of the extract coming from the recirculation line. In Figure 2.16 (a) one can see a schematic diagram of the 3-zone process. It can comprise several chromatographic columns per zone and has the same periodic switch behavior of the classical SMB. Compared to a classical 4-zone SMB, the 3-zone configuration is usually more robust and easier to control process, having the advantage of cutting the total

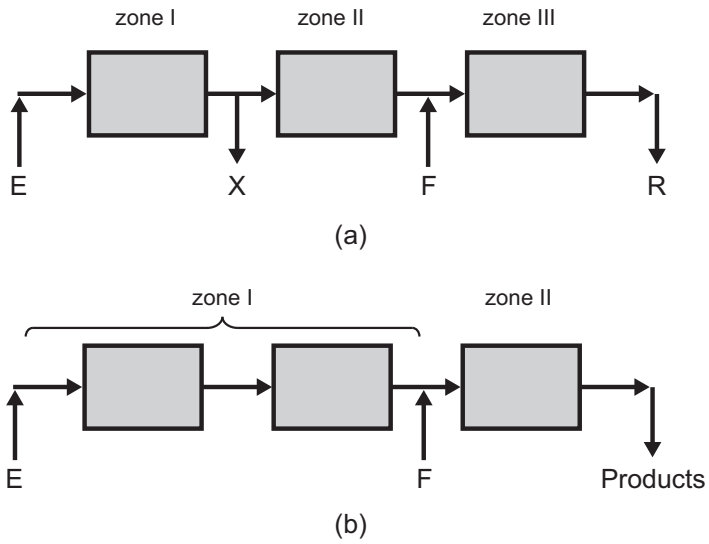

Figure 2.16: Schematic diagram of a (b) two- and (a) three-zone SMB process. The 3-zone process is the simple elimination of zone IV from the standard SMB, collecting the stream coming from zone III as the raffinate. For the 2-zone scheme there is an additional removal of the extract port and both products are collected in the same line at different times. The switching scheme in both cases is made synchronously like in the classical SMB. Notice that all zones can comprise several chromatographic columns, the representation of only one column per zone (2 columns in the case of zone I of the 2-zone process) is for simplicity of the representation.

number of columns (stationary phase), pumps and valves. However, it normally leads to an increase of solvent consumption and a consequent higher dilution of the raffinate stream [28]. Nevertheless, because the residence time of the solute collected in the raffinate is reduced, this could be a very important factor in some separations/purifications such as in the case of proteins where one has to avoid aggregation and denaturation. Another interesting theoretical approach is the application of a "partial withdrawal" strategy, that only opens the SMB ring in a part of the cycle, and a "partial feed" scheme which is nothing more than a modulation of the feed flow (PowerFeed), in order to improve the performance of a 3-zone configuration [19].

One can also cut one additional zone and operate with only a 2-zone process. As described in Figure 2.16 (b), Lee [29] used 12 columns equally divided in a 2-zone SMB with a continuous feeding and partial withdrawal policies for a high concentration fructose-glucose separation. In this case the extract line is eliminated and both products are sequentially collected in what used to be the raffinate line, however this operating strategy, although quite simple, proved to have difficulties to achieve high purity products, nonetheless could be a handy solution in a product enriching process [28]. More recently, Jin and Wankat [30] theoretically derived a 2-zone SMB for binary separation in which they incorporate a storage tank to temporarily hold the solvent for later use. This strategy has the main objective of surpassing the inherent increase on solvent consumption that results from the less then 4-zone processes. This scheme numerically proved to have good performance but still with the need of more solvent than the equivalent 4-zone SMB.

One-column processes that reproduce the cyclic behavior of the multicolumn SMB chromatography by means of a recycle lag (Fig. 2.17) have also been proposed [31, 32]; this setup exploits the cyclic behavior of the SMB where all columns are subjected to the same inlet/outlet concentration waveform every $N\tau$ time units. Recently, a mechanical solution employing a 4-zone SMB into one column axially divided in 4 inlet/outlet sections was suggested [33] but still need an efficiency/economic validation.

The original SMB process is only suitable for binary separations, partitioning one or more less retained components (raffinate) from more retained ones (extract), however in most separation cases our mixture is composed of more then three components and the goal is to isolate one that is intermediately retained in the columns. The first logical step to achieve a "center-cut" separation is to implement two SMB units [34, 35] or even more [36] in cascade, making a series of partitions to isolate the desired product. Although this is a very straightforward solution, it has an economical drawback since the need of several SMB units implies the use of much more equipment, as for example in a theoretical unit with 60-zones discussed by Kim and Wankat [36]. The cascade SMB solution is no more than the simple extension of the total number of zones of the process by multiples of four, however one can compact the several units into a single

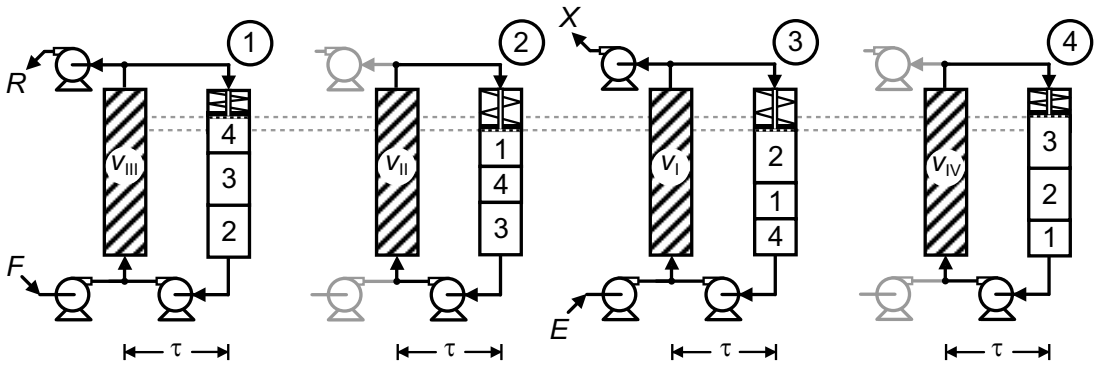

Figure 2.17: Schematic of a single-column with recycle lag analogous to an 4 zone SMB process. The single chromatographic column is connected to a plug-flow tube which incorporates a moving piston. The tube implements a recycle lag of $(N-1)\tau$ time units. The piston compensates the difference between the inlet and outlet flowrates. The complete cycle is equivalent to a 4-column SMB (with one column per zone 1/1/1/1). F, E, R and X denote the feed, eluent, raffinate and extract currents.

setup that holds multiples zones. A 5-zone SMB with two raffinate or two extract lines [37] have proved to be efficient in a ternary separation; 9-zone systems for quaternary separations [38] and a 5-zone setup where the regeneration and re-equilibration zones are disconnected and the separation zones are open-looped [39] are also worth mentioning. Another interesting process for ternary separation is based on a novel operation technique wherein the feed is discontinuously added during a part of the total cycle time while operating in open-loop mode; for the remaining cycle time the system is switched to SMB mode of operation but with no feed addition. This process is commercialized by the Japan Organo Company [40, 41] and is named as "JO Chromatographic Separation System". Mata and Rodrigues [42] developed a simulated model of the JO process and described it as "Pseudo SMB" since its operation mode is semi-SMB type.

Solvent strength is another variable that can suffer modulation to improve the SMB process. A conventional SMB, as in classical bach elution chromatography, is based in an isocratic operation, which means that all the solvent used in the process has the same composition. In batch elution chromatography, solvent gra-

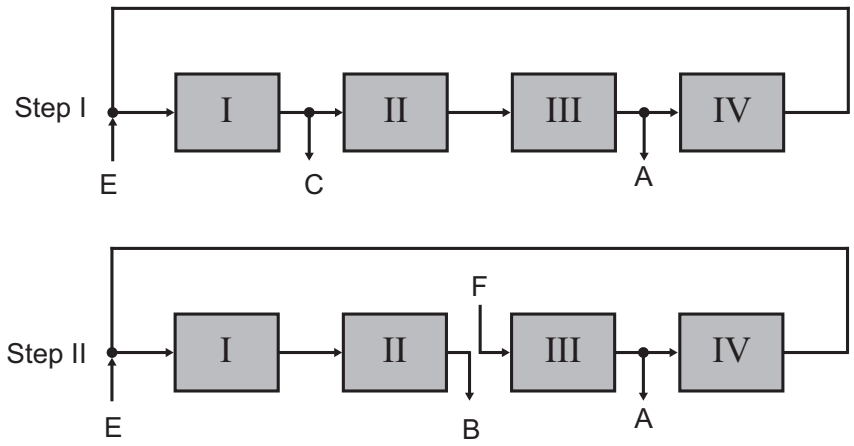

Figure 2.18: JO Chromatographic Separation System. The process is divided into 2 main steps; if one consider a feeding mixture of A+B+C (being A the less and C the more retained component), in step 1 the scheme is in the same way as in the simulated moving-bed mode excepted with no adding of feed mixture, i.e. the the eluent and withdrawal lines A, and C are periodically moved. At a certain point the scheme passes to step 2 mode where in the middle of the column loop the circulation flow is stopped, feed mixture is fed in, and the component having an intermediate affinity to the adsorbent B is withdrawn.

dient as been routinely used for more than 40 years, it consists in increasing the solvent strength during the separation either gradually or stepwise to enhance the resolution of the early eluted components and decrease the retention time of the latest eluted components, resulting in a reduced solvent consumption and less diluted products [4]. However, solvent gradient in SMB is not so straightforward due to its inherent recycling nature. The first attempts to implement gradients in a classical SMB [43, 44, 45, 46] proposed a two-step gradient SMB process using a weaker solvent in the feed stream than in the eluent line, which showed to effectively reduce solvent consumption and decrease product dilution but proved to be a difficult process to modulate and very sensitive to input parameters changes. An attempt to also create a thermodynamic gradient in an SMB process has also been theoretically exploited through a thermal operation [47, 48] although due to its practical difficulties it was never implemented in practice.

More recently, an SMB based chromatography process which incorporates the principle of counter-current operation with solvent gradients has been developed and applied in biochemical and pharmaceutical separations/purifications [49, 50]. It was named MCSGP which stands for Multi-Column Solvent Gradient Process, and originally consisted in a fully continuous process of at least 6 chromatographic columns [51]. As described in the scheme of Fig. 2.19, the continuous 6-column MCSGP process consists of a group of 3 columns that are interconnected and another 3 columns that operate in batch mode; the interconnected columns perform the separation gradient like in column batch chromatography, the batch columns perform the loading, the elution of the target product and the elution of strongly adsorbed species from column plus washing, cleaning-in-place and re-equilibration. In between the interconnected columns additional inlet streams are used to adjust the modifier concentrations required in order to reproduce the desired eluent gradient. Later, a semicontinuous mode with only 3 chromatographic columns has been developed [52].

Simulated moving bed applied to gas separations [53, 54] and using supercritical fluids as the eluent (SF-SMB) [55] also showed promising developments and

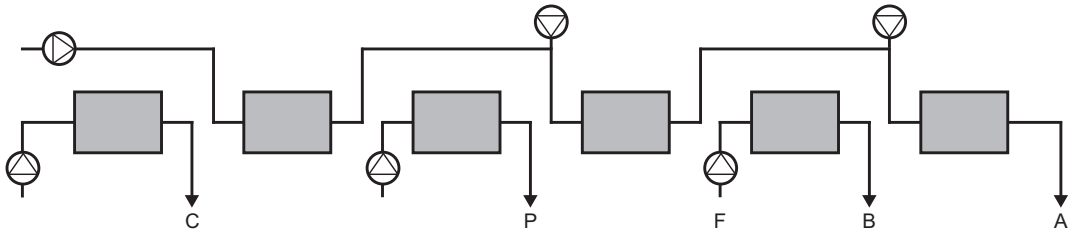

Figure 2.19: A schematic diagram of the Multi-Column Solvent Gradient Process (MCSGP). It is a fully continuous system comprising of 6 chromatographic columns using solvent gradient for a three-fraction separation/purifications. Like in the SMB process, the system moves one column ahead every switching interval. C is the strongly adsorbing impurities, P is the target product, B is the weakly adsorbing impurities, A the very weakly adsorbing impurities and F the feeding mixture. The system comprises a group of 3-columns that function on open-loop and 3 other that operate in batch mode. Like in the SMB unit, the scheme moves periodically ahead one column.

applications. Another auspicious process is the so called SMBR which couples the SMB operation with simultaneous chemical reaction within the columns [56].

The possibility of combining several operating modes into a single hybrid system has also been considered. For instance, combining the Varicol and PowerFeed [57, 19, 22, 58] operating modes, 2- and 3-zones setups with partial-feed and selective withdrawal [19], the possibility of mixing ternary separation schemes with gradient elution [59] and an interesting proposal of coupling SMB and crystallization [60] have been proposed. Another different scheme that uses 2 feed lines is also worth mentioning [61].

These newly cyclic operation schemes are pushing the trend towards the use of units with a small number of columns, since less stationary phase is used, the setup is more economic, and the overall pressure drop can be reduced. However, when these schemes are applied in practice the process becomes more complex, because of the increased degrees of freedom that must be optimized. It is also less robust and more difficult to operate because it is more demanding on hardware, particularly in regard to the flowrate profiles imposed on the pumps. This additional complexity requires the development of highly versatile SMB equipment [28], advanced optimization tools [58, 62, 63], and robust control procedures [64, 65, 66, 67].

References

[1] D. Ruthven, Principles of Adsorption and Adsorption Processes, Wiley, 1984. 8, 14

[2] G. Guiochon, Preparative liquid chromatography, Journal of Chromatography A 965 (2002) 129–161. 9

[3] H. Haynes, P. Sarma, A model for the application of gas chromatography to measurements of diffusion in bidisperse structured catalysts, AIChE Journal 19 (1973) 1043–1046. 14

[4] G. Guiochon, S. Golshan-Shirazi, A. Katti, Fundamentals of Preparative and Nonlinear Chromatography, Academic Press, 1994. 14, 31

[5] O. Ludemann-Hombourger, M. Bailly, R. Nicoud, Design of a simulated moving bed: Optimal particle size of the stationary phase, Separation Science and Technology 35 (2000) 1285–1305. 16

[6] C. M. Grill, Closed-loop recycling with periodic intra-profile injection: a new binary preparative chromatographic technique, Journal of Chromatography A 796 (1998) 101–113. 16

[7] C. Heuer, A. Seidel-Morgenstern, P. Hugo, Experimental investigation and modelling of closed-loop recycling in preparative chromatography, Chemical Engineering Science 50 (1995) 1115–1127. 16

[8] A. Seidel-Morgenstern, Optimization and comparison of different modes of preparative chromatography, Analusis Magazine 26 (1998) 46–55. 17

[9] C. M. Grill, L. Miller, Separation of a racemic pharmaceutical intermediate using closed-loop steady state recycling, Journal of Chromatography A 827 (1998) 359371. 17

[10] C. Berg, Hypersorption process for separation of light gases, Trans. Am. Inst. Chem. Eng. 42 (1946) 665–680. 20

[11] P. Adam, R. Nicoud, M. Bailly, O. Ludemann-Hombourger, Process and device for separation with variable-length, US Patent 6 136 198 (2000). 24

[12] O. Ludemann-Hombourger, R. Nicoud, M. Bailly, The varicol process - a new multicolumn continuous chromatographic process, Separation Science and Technology 35 (2000) 1829–1862. 24

[13] O. Ludemann-Hombourger, G. Pigorini, R. Nicoud, D. Ross, G. Terfloth, Application of the "varicol" process to the separation of the isomers of the sb-553261 racemate, Journal of Chromatography A 947 (2002) 59–68. 24

[14] A. Toumi, F. Hanisch, S. Engell, Optimal operation of continuous chromatographic processes: Mathematical optimization of the varicol process, Industrial and Engineering Chemistry Research 41 (2002) 4328–4337. 24

[15] Z. Zhang, H. Hidajat, A. Ray, M. Morbidelli, Multiobjective optimization of smb and varicol process for chiral separation, AIChE Journal 48 (2002) 2800–2816. 24

[16] L. Pais, A. Rodrigues, Design of simulated moving bed and varicol processes for preparative separations with a low number of columns, Journal of Chromatography A 1006 (2003) 33–44. 24

[17] M. Kearney, K. Hieb, Time variable simulated moving bed process, US Patent 5102553 (1992). 25

[18] Y. Zang, P. Wankat, Smb operation strategy-partial feed, Industrial and Engineering Chemistry Research 41 (2002) 2504–2511. 25

[19] Y. Zang, P. Wankat, Three-zone simulated moving bed with partial feed and selective withdrawal, Industrial and Engineering Chemistry Research 41 (2002) 5283–5289. 25, 28, 33

[20] E. Kloppenburg, E. Gilles, A new concept for operating simulated moving-bed processes, Chemical Engineering Technology 22 (1999) 813–817. 25

[21] Z. Zhang, M. Mazzotti, M. Morbidelli, Powerfeed operation of simulated moving bed units: changing flow-rates during the switching interval, Journal of Chromatography A 1006 (2003) 87–99. 25

[22] Z. Zhang, M. Mazzotti, M. Morbidelli, Continuous chromatographic processes with a small number of columns: Comparison of simulated moving bed with varicol, powerfeed, and modicon, Korean Journal of Chemical Engineering 21 (2004) 454–464. 25, 33

[23] Z. Zhang, M. Morbidelli, M. Mazzotti, Experimental assessment of powerfeed chromatography, AIChE Journal 50 (2004) 625–632. 25

[24] H. Schramm, M. Kaspereit, A. Kienle, A. Seidel-Morgenstern, Improving simulated moving bed processes by cyclic modulation of the feed concentration, Chemical Engineering Technology 25 (2002) 1151–1155. 26, 27

[25] H. Schramm, M. Kaspereit, A. Kienle, A. Seidel-Morgenstern, Improved operation of simulated moving bed processes through cyclic modulation of feed flow and feed concentration, Chemical Engineering Science 58 (2003) 5217–5227. 26, 27

[26] H. Schramm, A. Kienle, M. Kaspereit, A. Seidel-Morgenstern, Chromatographic separation of components of a multiple component fluid mixture using a simulated moving bed process comprises changing the concentration of the fluid mixture and/or composition of the solvent in a timing unit, DE Patent 10 235 385 (2004). 26

[27] D. Ruthven, C. Ching, Counter-current and simulated counter-current adsorption separation processes, Chemical Engineering Science 44 (1989) 1011–1038. 27

[28] C. Y. Chin, N.-H. L. Wang, Simulated moving bed equipment designs, Separation and Purification Reviews 33 (2004) 77–155. 28, 29, 33

[29] K. Lee, Continuous separation of glucose and fructose at high concentration using two-section simulated moving bed process, Korean Journal of Chemical Engineering 20 (2003) 532–537. 29

[30] W. Jin, P. Wankat, Two-zone smb process for binary separation, Industrial and Engineering Chemistry Research 44 (2005) 1565–1575. 29

[31] N. Abunasser, P. Wankat, One-column chromatograph with recycle analogous to simulated moving bed adsorbers: Analysis and applications, Industrial and Engineering Chemistry Research 43 (2004) 5291–5299. 29

[32] J. Mota, J. Araújo, Single-column simulated-moving-bed process with recycle lag, AIChE Journal 51 (2005) 1641–1653. 29

[33] K. Buhlert, M. Lehr, A. Jungbauer, Scale down of a single column smb unit for protein separation, in: 21st International Symposium, Exhibit & Workshops on Preparative / Process Chromatography, Ion Exchange, Adsorption/Desorption Processes & Related Separation Techniques, 2008. 29

[34] P. Wankat, Simulated moving bed cascades for ternary separations, Industrial and Engineering Chemistry Research 40 (2001) 6185–6193. 29

[35] J. Kim, Y. Zang, P. Wankat, Single-cascade simulated moving bed systems for the separation of ternary mixtures, Industrial and Engineering Chemistry Research 42 (2003) 4849–4860. 29

[36] J. Kim, P. Wankat, Designs of simulated-moving-bed cascades for quaternary separations, Industrial and Engineering Chemistry Research 43 (2004) 1071–1080. 29

[37] X. Wang, C. Ching, Chiral separation of β-blocker drug (nadolol) by five-zone simulated moving bed chromatography, Chemical Engineering Science 60 (2005) 1337–1347. 30

[38] R. Wooley, Z. Ma, N.-H. Wang, A nine-zone simulating moving bed for the recovery of glucose and xylose from biomass hydrolyzate, Industrial and Engineering Chemistry Research 37 (1998) 3699–3709. 30

[39] Y. Xie, C. Chin, D. Phelps, C.-H. Lee, K. Lee, S. Mun, N.-H. Wang, A five-zone simulated moving bed for the isolation of six sugars from biomass hydrolyzate, Industrial and Engineering Chemistry Research 44 (2005) 9904–9920. 30

[40] M. Ando, M. Tanimura, M. Tamura, Method of chromatographic separation, US Patent 4 970 002 (1990). 30

[41] T. Masuda, T. Sonobe, F. Matsuda, M. Horie, Process for fractional separation of multi-component fluid mixture, US Patent 5 198 120 (1993). 30

[42] V. Mata, A. Rodrigues, Separation of ternary mixtures by pseudo-simulated moving bed chromatography, Journal of Chromatography A 939 (2001) 2340. 30

[43] T. Jensen, T. Reijns, H. Billiet, L. van der Wielen, Novel simulated moving-bed method for reduced solvent consumption, Journal of Chromatography A 873 (2000) 149–162. 31

[44] D. Antos, A. Seidel-Morgenstern, Application of gradients in the simulated moving bed process, Chemical Engineering Science 56 (2001) 66676682. 31

[45] D. Antos, A. Seidel-Morgenstern, Two-step solvent gradients in simulated moving bed chromatography. numerical study for linear equilibria, Journal of Chromatography A 944 (2002) 77–91. 31

[46] S. Abel, M. Mazzotti, M. Morbidelli, Solvent gradient operation of simulated moving beds i. linear isotherms, Journal of Chromatography A 944 (2002) 23–39. 31

[47] C. Migliorini, M. Wendlinger, M. Mazzotti, Temperature gradient operation of a simulated moving bed unit, Industrial and Engineering Chemistry Research 40 (2001) 2606–2617. 31

[48] W. Jin, P. Wankat, Thermal operation of four-zone simulated moving beds, Industrial and Engineering Chemistry Research 46 (2007) 7208 – 7220. 31

[49] L. Aumann, M. Morbidelli, Method and device for chromatographic purification, EP patent 1 716 900 (2006). 32

[50] G. Ströhlein, L. Aumann, M. Mazzotti, M. Morbidelli, A continuous, counter-current multi-column chromatographic process incorporating modifier gradients for ternary separations, Journal of Chromatography A 1126 (2006) 338346. 32

[51] L. Aumann, M. Morbidelli, A continuous multicolumn countercurrent solvent gradient purification (mcsgp) process, Biotechnology and Bioengineering 98 (2007) 1043–1055. 32

[52] L. Aumann, M. Morbidelli, A semicontinuous 3-column countercurrent solvent gradient purification (mcsgp) process, Biotechnology and Bioengineering 99 (2008) 728–733. 32

[53] J. Mota, I. Esteves, M. Eusébio, Synchronous and asynchronous smb processes for gas separation, AIChE Journal 53 (2007) 1192–1203. 32

[54] K. Kostroski, P. Wankat, Separation of dilute binary gases by simulated-moving bed with pressure-swing assist: Smb/psa processes, Industrial and Engineering Chemistry Research 47 (2008) 3138–3149. 32

[55] F. Denet, W. Hauck, R. Nicoud, O. Giovanni, M. Mazzotti, J. Jaubert, M. Morbidelli, Enantioseparation through supercritical fluid simulated moving bed (sf-smb) chromatography, Industrial and Engineering Chemistry Research 40 (2001) 4603–4609. 32

[56] D. Azevedo, A. Rodrigues, Design methodology and operation of a simulated moving bed reactor for the inversion of sucrose and glucose-fructose separation, Chemical Engineering Journal 82 (2001) 95–107. 33

[57] M. Tanimura, M. Tamura, US Patent 5 556 546 (1996). 33

[58] J. Araújo, R. Rodrigues, J. Mota, Optimal design and operation of a certain class of asynchronous simulated moving bed processes, Journal of Chromatography A 1132 (2006) 76–89. 33

[59] G. Paredes, S. Abel, M. Mazzotti, M. Morbidelli, J. Stadler, Analysis of a simulated moving bed operation for three-fraction separations (3f-smb), Industrial and Engineering Chemistry Research 43 (2004) 6157–6167. 33

[60] H. Lorenz, P. Sheehan, A. Seidel-Morgenstern, Coupling of simulated moving bed chromatography and fractional crystallisation for efficient enantioseparation, Journal of Chromatography A 908 (2001) 201214. 33

[61] J. Kim, N. Abunasser, P. Wankat, Use of two feeds in simulated moving beds for binary separations, Korean Journal of Chemical Engineering 22 (2005) 619–627. 33

[62] Y. Kawajiri, L. Biegler, Optimization strategies for simulated moving bed and powerfeed processes, AIChE Journal 52 (2006) 1343–1350. 33

[63] A. Toumi, S. Engell, O. Ludemann-Hombourger, R. Nicoud, M. Bailly, Optimization of simulated moving bed and varicol processes, Journal of Chromatography A 1006 (2003) 15–31. 33

[64] K. Klatt, F. Hanisch, G. Dünnebier, S. Engell, Model-based optimization and control of chromatographic processes, Computers & Chemical Engineering 24 (2000) 1119–1126. 33

[65] E. Kloppenburg, E. Gilles, Automatic control of the simulated moving bed process for c8 aromatics separation using asymptotically exact input/output-linearization, Journal of Process Control 9 (1999) 41–50. 33

[66] H. Schramm, S. Grüner, A. Kienle, Optimal operation of simulated moving bed chromatographic processes by means of simple feedback control, Journal of Chromatography A 1006 (2003) 3–13. 33

[67] S. Abel, G. Erdem, M. Amanullah, M. Morari, M. Mazzotti, M. Morbidelli, Optimizing control of simulated moving bedsexperimental implementation, Journal of Chromatography A 1092 (2005) 2–16. 33

3

Simulated Moving Bed Modeling

Process modeling and simulation is an extremely important aspect in most chemical engineering processes and the SMB process is not an exception. An effective description of the SMB system is critical for the design of the process in order to find a suitable operating point among the infinite universe of possible choices.

Essentially an SMB model is constituted of the chromatographic column

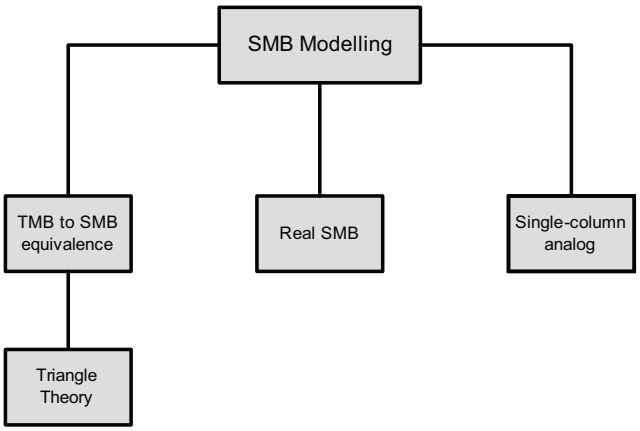

Figure 3.1: Schematic flowchart of the different approaches to model an SMB process.

model (described in Chapter 2) and the node equations. The column models describe the material balance for the single chromatographic columns and the node equations connect the various single column models to form the whole simulated moving bed system.

For process design, the initial transient SMB behavior is of little interest, except for unusually short campaigns, and only the CSS regime is relevant for process operation. The CSS is usually attained after a moderate number of cycles (each cycle is $N\tau$ long), and there is evidence that all memory of the initial condition is lost since multiple periodic states have never been reported for this process. Usually most modeling/optimization strategies directly compute the CSS behavior since its a faster and simpler approach.

Various models to predict and/or describe the performance of an SMB process with fair agreement with experimental results have been developed. In general, there are two main approaches for modeling an SMB process: simulate directly the real SMB, taking into account the τ-periodic behavior of the system, or assuming the equivalence of the SMB with the TMB process. More recently, efficient methods to directly calculate the cyclic steady state (CSS) of the SMB process based on single-column models were developed [1, 2].

3.1 Real SMB model

The real SMB approach analyzes each subsection individually. If one examine the SMB schematic diagram of Fig. 2.10, we can start by defining the simple overall balance:

$$Q_{\mathrm{E}} + Q_{\mathrm{F}} = Q_{\mathrm{X}} + Q_{\mathrm{R}} \tag{3.1}$$

Focusing the attention on the process node, Figure 3.2 shows the schematic representation of a generic node connecting two consecutive columns, say $j-1$ and j, of an SMB unit. As a reminder, the notation employed is as follows: Q is the liquid flow rate, $c^{\mathrm{out}}_{i,j-1}$ is the concentration of solute i at the outlet of column $j-1$ and c^{in}_{ij} is the corresponding solute concentration at the inlet of column

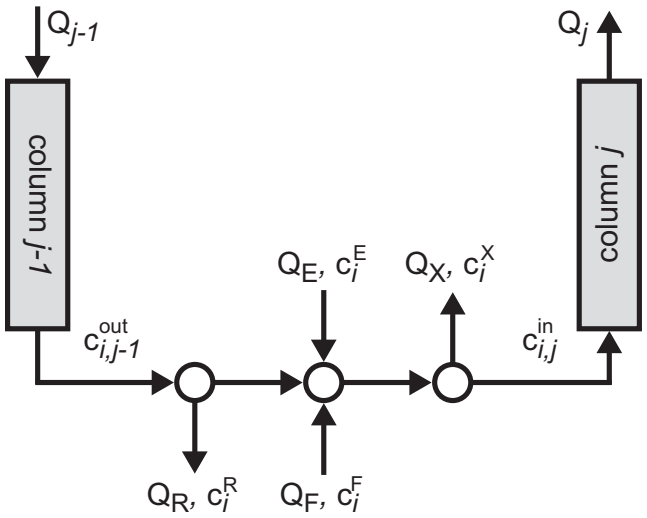

Figure 3.2: Schematic representation of the node connecting columns $j-1$ and j of an SMB unit. The concentration of solute i in liquid phase is c_i and Q is the volumetric flow rate. E, X, F, and R denote eluent, extract, feed and raffinate lines, respectively.

j. The solute concentration and flow rate of the external inlet/outlet lines are identified by scripts E (eluent), X (extract), F (feed), and R (raffinate).

Note that in the schematic diagram of Fig. 3.2 the sequence in which the inlet/outlet lines are connected to the node is such that it allows certain zones to cease to exist temporarily, while avoiding mixing issues and occurrence of short-cut streams. For example, an optimized asynchronous port switching typically suppresses zone I and zone IV over certain periods of the switching interval [3, 4, 2]. In the former case eluent is added and extract is withdrawn simultaneously on the same node, whereas in the latter case raffinate is withdrawn from the node into which eluent is being simultaneously introduced. The equations given below are of general applicability provided that lines do not cross each other and that adjacent zones do not cease to exist simultaneously.

Under these assumptions, the solute node balance can be written as:

$$\begin{cases} Q_{\mathrm{III}}\, c_{i,j}^{\mathrm{in}} = Q_{\mathrm{II}}\, c_{i,j-1}^{\mathrm{out}} + (Q_{\mathrm{III}} - Q_{\mathrm{II}})\, c_i^{\mathrm{F}} & \text{(feed node)} \\ Q_{\mathrm{I}}\, c_{i,j}^{\mathrm{in}} = Q_{\mathrm{IV}}\, c_{i,j-1}^{\mathrm{out}} + (Q_{\mathrm{I}} - Q_{\mathrm{IV}})\, c_i^{\mathrm{E}} & \text{(eluent node)}\ , \\ c_{i,j}^{\mathrm{in}} = c_{i,j-1}^{\mathrm{out}} & \text{(otherwise)} \end{cases} \tag{3.2}$$

where $Q_{\mathrm{I}}, \dots Q_{\mathrm{IV}}$ are the flow rates in the four sections of the SMB, and are determined by the global node balances:

$$Q_{\mathrm{I}} = Q_{\mathrm{IV}} + Q_{\mathrm{E}}, \tag{3.3}$$
$$Q_{\mathrm{II}} = Q_{\mathrm{I}} - Q_{\mathrm{X}}, \tag{3.4}$$
$$Q_{\mathrm{III}} = Q_{\mathrm{II}} + Q_{\mathrm{F}}, \tag{3.5}$$
$$Q_{\mathrm{IV}} = Q_{\mathrm{III}} - Q_{\mathrm{R}}. \tag{3.6}$$

Furthermore, the outlets are defined by:

$$\begin{cases} Q_{\mathrm{X}}\, c_i^X = Q_{\mathrm{I}}\, c_{i,j-1}^{\mathrm{out}} & \text{(extract node)} \\ Q_{\mathrm{R}}\, c_i^R = Q_{\mathrm{III}}\, c_{i,j-1}^{\mathrm{out}} & \text{(raffinate node)} \end{cases}, \tag{3.7}$$

The cyclic operation of the SMB process is achieved by moving the inlet and outlet ports one column downstream (i.e. in the direction of fluid flow) every τ time units, where τ is the switching interval. Mathematically, this can be expressed as

$$\Omega_j(t) = \Omega(t_j), \quad t_j = [t - (j-1)\tau] \bmod N\tau, \tag{3.8}$$

where Ω_j denotes the set of input variables for column j, which includes Q_j and the state (opened or closed) of the four inlet/outlet lines connected to its inlet node; "mod" defines the usual modulo operator: $a \bmod b \equiv a - b\,\mathrm{int}(a/b)$. Note that Eq. 3.8 imposes a $N\tau$ periodicity on $\Omega_j(t)$ and that:

$$\Omega_{j-1}(t) = \Omega_j(t + \tau). \tag{3.9}$$

3.2 TMB to SMB equivalence

Whereas the TMB, after the initial transient behavior, reaches a real steady state, the SMB on the other hand reaches a cyclic periodic state where the process exhibits the same dynamic behavior over each switching interval. However, despite this difference, the two units can be considered equivalent, with a degree of equality increasing with the number of columns of the discretized SMB unit. For instance, Pais et al. [5] showed that the TMB equivalence is a fair accurate approach for SMB processes with 2 or more columns per zone.

The analogy between the two units is made by keeping constant the fluid velocity relatively to the solid velocity:

$$\upsilon_j^{TMB} = \upsilon_j^{SMB} - \upsilon_s \tag{3.10}$$

where υ_j and υ_s are the fluid and solid phases velocities.

The solid velocity in the TMB model is also related to the switching interval τ of the SMB model:

$$\upsilon_s = \frac{L}{\tau} \tag{3.11}$$

where L is the length of one column in the SMB unit.

Because the volumetric flowrate can be described as:

$$Q_s = (1-\epsilon)\ A\ \upsilon_s \tag{3.12}$$

$$Q_j^{SMB} = \epsilon\ A\ \upsilon_j^{SMB} \tag{3.13}$$

Then, the solid and liquid velocities equivalence can be rewritten as:

$$\tau = \frac{(1-\epsilon)\ V}{Q_s} \tag{3.14}$$

$$Q_j^{SMB} = Q_j^{TMB} + \frac{\epsilon}{1-\epsilon}\ Q_s \tag{3.15}$$

With the logical equivalence to the zone lengths:

$$N_j\ V = V_j^{TMB} \tag{3.16}$$

where $V = AL$ is the SMB column volume, V_j^{TMB} is the volume for zone j in the TMB and N_j the number of columns in zone j in the SMB.

For visual clarity of the two setups equivalence, one can compare Figures 2.9 and 2.10 from chapter 2.

3.2.1 Triangle Theory

The most common analogy between the TMB and the SMB process is a method called "Triangle Theory". This method uses a simplified TMB model, based on the well known equilibrium theory, which ignores axial dispersion and resistance to mass-transfer effects, i.e. it assumes that the column has an infinite efficiency.

Under these assumptions (see chapter 2), if one consider a binary separation, the material balance equation for solute i in section j of the TMB unit is given by:

$$\epsilon \frac{\partial c_{ij}}{\partial t} + \beta \frac{\partial q_{ij}}{\partial t} + \frac{Q_j}{\epsilon A} \frac{\partial c_{ij}}{\partial z} = 0 \qquad (0 < z < L) \tag{3.17}$$

where A is the column cross-section area, L the length of the column and z the axial coordinate along the column. The symbol t represents the time coordinate, ϵ the column interparticle porosity, Q_j the volumetric flowrate of the fluid, c and q the concentrations in the liquid and solid phases.

With the help of additional parameters, m_j, so-called flowrate ratios, which define the ratio of the net fluid flowrate over the solid phase in each section, one can extend the analogy in terms of operating parameters of the equivalent SMB unit:

$$m_j = \frac{Q_j^{TMB}}{Q_s} = \frac{Q_j^{SMB} \tau}{(1-\epsilon)V} - \frac{\epsilon}{1-\epsilon} \tag{3.18}$$

To recover the most adsorbed species (B) in the extract stream and the less retained (A) in the raffinate stream, the operating parameters must be assigned appropriate values in order to ensure certain conditions:

- In zone I, the more retained species (B) must follow the movement of the fluid phase in order for the solid phase to be regenerated;

- In zones II and III the more retained compound (B) must migrate in the opposite direction of the fluid and A must go with the liquid phase;
- In zone IV, A must travel in the opposite direction of the fluid in order to effectively regenerate the eluent.

Mathematically, these three conditions can be expressed as:

$$\begin{gathered} m_1 > \overline{\left(\frac{\partial q_B^*}{\partial c_B}\right)}_{\mathrm{I}}, \\ \overline{\left(\frac{\partial q_A^*}{\partial c_A}\right)}_{\mathrm{II}} < m_2 < \overline{\left(\frac{\partial q_B^*}{\partial c_B}\right)}_{\mathrm{II}}, \overline{\left(\frac{\partial q_A^*}{\partial c_A}\right)}_{\mathrm{III}} < m_3 < \overline{\left(\frac{\partial q_B^*}{\partial c_B}\right)}_{\mathrm{III}}, \\ m_4 > \overline{\left(\frac{\partial q_A^*}{\partial c_A}\right)}_{\mathrm{IV}}, \end{gathered} \tag{3.19}$$

where $(\partial q_i^*/\partial c_i)_j$ is the average slope of the adsorption isotherm for species i in zone j.

Considering low feed concentrations, i.e. a linear adsorption isotherm ($q_i = K_i c_i$), the necessary and sufficient conditions for complete separation of two components A and B, with $K_B > K_A$, consist of the following inequalities [6]:

$$\begin{gathered} K_B < m_1 < \infty \\ K_A < m_2 < m_3 < K_B \\ \frac{-\epsilon_p}{1-\epsilon_p} < m_4 < K_A \end{gathered} \tag{3.20}$$

These conditions will define a region of complete separation of A and B in the operating parameter space through the frame of the ideal equilibrium model based on the equivalence between SMB and TMB. Normally only the triangular region of the (m_2, m_3) plane is used for graphical representation (see left graph of Fig. 3.3), but one has to keep in mind that this only applies provided that the constraints on the m_1 and m_4 plane are also fulfilled and the operating point in terms of m_1 and m_4 is chosen in the region of complete regeneration shown in the right graph of Fig. 3.3.

On the other hand, in the case of nonlinear adsorption isotherms the region of complete separation is dependent on the concentration of the components in the feed and the triangle shrinks with the increase of the feed concentration c_F as shown in Fig. 3.4. In a limiting case, the region can become so thin that one can only operate in the vertex of the pseudo-triangle, originating an extremely low robust operation very sensitive to process disturbances/fluctuations.

In practice, the SMB process performance is usually evaluated using productivity (maximized) and eluent consumption (minimized):

$$\text{Productivity} = \frac{Q_F\ c_F}{NV} = \frac{(m_3 - m_2)(1-\epsilon)c_F}{N\tau} \tag{3.21}$$

$$\text{Eluent consumption} = 1 + \frac{Q_E}{Q_F} = 1 + \frac{m_1 - m_4}{m_3 - m_2}. \tag{3.22}$$

Through equations 3.21 and 3.22 one can easily see that for constant switching interval τ, feed concentration c_F and $(m_1 - m_4)$ difference, the productivity

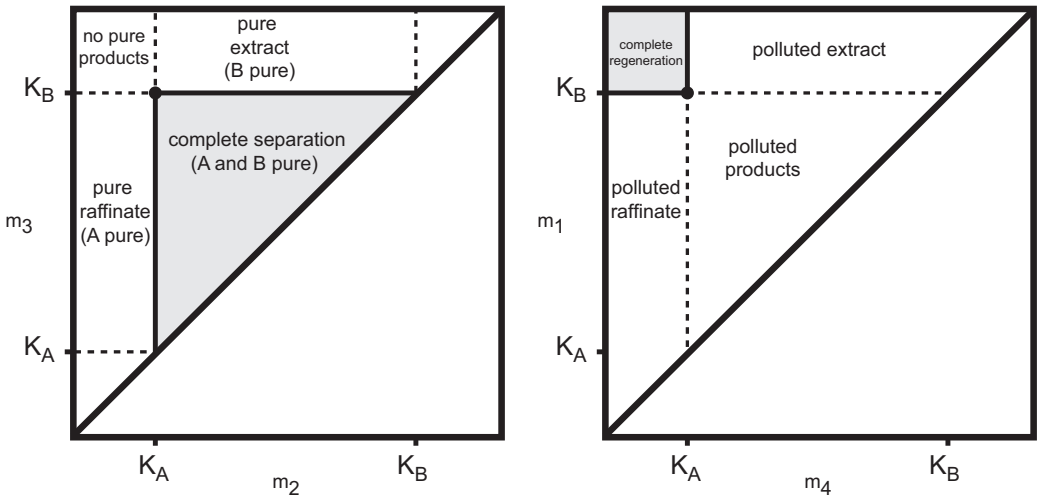

Figure 3.3: In the case of a linear adsorption isotherm, the left graph represents the region of complete separation in the m_2, m_3 operating parameter space; the right graph represents the complete regeneration region in the m_4, m_1 operating space. Note that A is the less and B the more retained component.

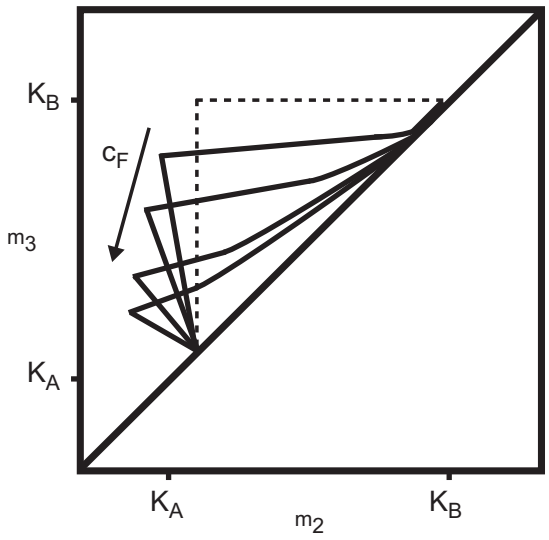

Figure 3.4: Behavior of the region of complete separation in the case of a nonlinear adsorption isotherm obtained from the triangle theory with increasing feed concentration c_F. Note that with the increase of the feed concentration the triangular separation region shifts and becomes more narrow.

increases and the eluent consumption decreases with the distance to the diagonal in the $m_2 - m_3$ plane. Consequently, the optimal operating point that maximizes productivity and minimizes the eluent consumption is the vertex of the triangular region of complete separation. In practice, the employed operating point is usually pushed inside the region of complete separation in order to create a safety margin and obtain a more robust operation.

Generally, the triangle theory is used in two different ways: to explain experimental results or to determine optimal operating conditions. The application of the triangle theory is well described elsewhere [6, 7, 8, 9].

Furthermore, the assumptions assumed in this theory, i.e. the infinite efficiency of the columns, can be surpassed with a more detailed modeling of the unit. Nevertheless, it is known that the area of the region of complete separation decreases with the reduction of the column efficiency [8, 10] due to axial dispersion and resistance to mass transfer.

3.3 Single-Column model

A detailed SMB process model is computationally expensive. While for exploratory or small parametric studies the computing time is not an issue, that may no longer be the case for rigorous model-based optimization, especially when the number of optimization variables is increased by the extra degrees of freedom in the operating conditions of nonstandard SMB processes. It is thus apparent that the increasing complexity of the optimization problems addressed in preparative chromatography calls for efficient methods to compute the periodic state. A general mathematical formulation based on a single-column chromatographic process that replicates the equivalent SMB operation can be used to efficiently calculate the periodic state of the SMB process. This approach is valid for classical or unconventional SMB modes of operation [1, 2] and has proved to efficiently reduce computational times in process simulation/optimization relatively to other modeling approaches [1].

As discussed before, for process design the initial transient SMB behavior is of little interest. By applying the CSS conditions, either backward or forward in time, to the solute node balance, the periodic state of the SMB process can be reproduced by two different single-column chromatographic models.

- A process model in which the part of its outlet stream that is not recovered

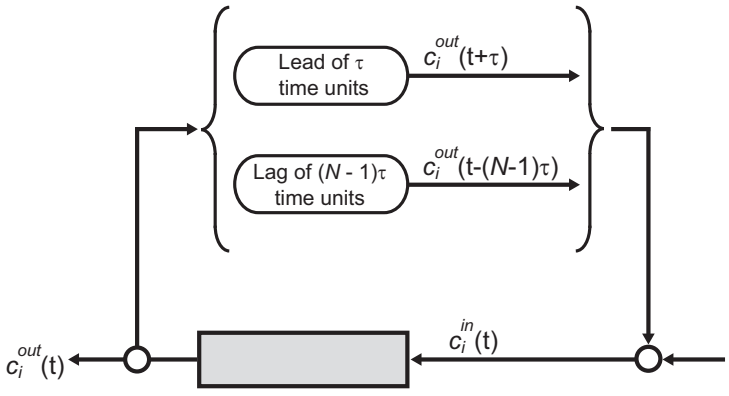

Figure 3.5: Block diagram of the node balance for the two ideal single-column chromatographic models analogous to an SMB process.

as product is recycled to the column with a time lag of $(N-1)\tau$ time units.

- Another process model in which the part of its outlet stream that is not recovered as product is recycled to the column with a time lead of τ time units.

Both single-column models are obtained by selecting an arbitrary column of the SMB unit and following its operation over a complete cycle. The recycle streams from the nonexisting columns are mimicked by recycling, with a time lag of $(N-1)\tau$ or a time lead of τ, the portion of the outlet stream of the column that is not withdrawn as product.

As described in the block diagram of Fig. 3.5, in a single-column model [1] one does not track the internal composition profile circulating around the multi-column loop, but instead follow its steady periodic behavior in one of the columns step by step over the cycle. To detach the selected column from the system, making it autonomous, while still maintaining the same CSS dynamics, its outlet stream is used as a replacement for that of the neighboring upstream column with a time lag of $(N-1)\tau$ [11] or a time lead of τ. This is equivalent to replacing Eq. 3.2 by

$$\begin{cases} Q_{\mathrm{III}}\, c_i^{\mathrm{in}}(t) = \; Q_{\mathrm{II}}\, c_i^{\mathrm{out}}(t') + (Q_{\mathrm{III}} - Q_{\mathrm{II}})\, c_i^{\mathrm{F}} & \text{(feed mode)} \\ Q_{\mathrm{I}}\, c_i^{\mathrm{in}}(t) = Q_{\mathrm{IV}}\, c_i^{\mathrm{out}}(t') + (Q_{\mathrm{I}} - Q_{\mathrm{IV}})\, c_i^{\mathrm{E}} & \text{(eluent mode)}\,, \\ c_i^{\mathrm{in}}(t) = \quad c_i^{\mathrm{out}}(t') & \text{(otherwise)} \end{cases} \tag{3.23}$$

where $t' = t-(N-1)\tau$ (lag) or $t' = t+\tau$ (lead) and, for simplicity, the j subscript is omitted because its value is fixed (we are tracking the dynamic behavior of a fixed column of the SMB unit). Clauses "feed mode" and "eluent mode" apply to the interval of the cycle during which the column is in the leftmost position of zone I and zone III, respectively. The choice of the value for j is arbitrary because all columns are assumed to be identical and undergo the same cycle.

These models establish a rigorous mathematical framework for all single-column chromatographic processes that replicate the equivalent SMB operation. Since the models employ a single chromatographic column, their numerical solution is easy to implement and is computationally cheap. Therefore, these models

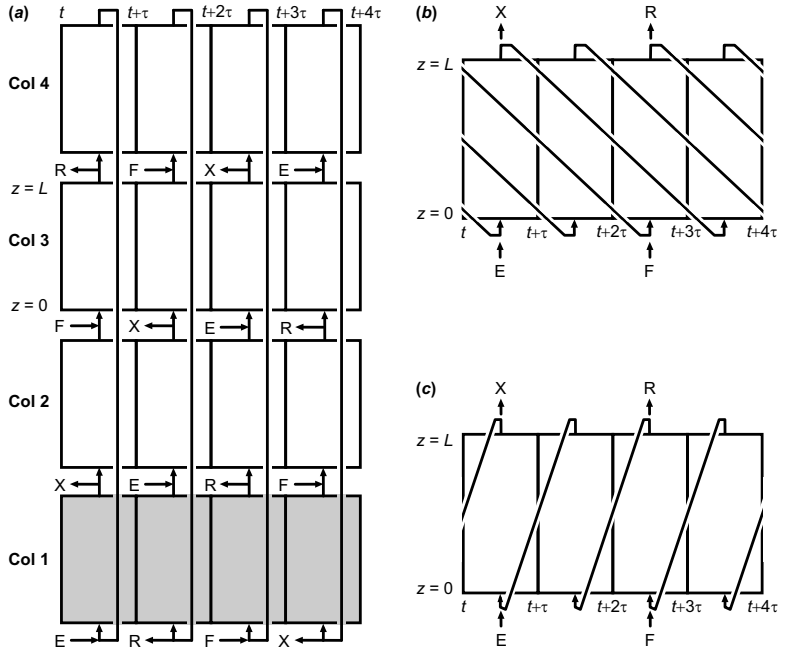

Figure 3.6: Schematic of an operating cycle for (a) a classical SMB with the port configuration 1/1/1/1, (b) its single-column analogue with recycle lag, and (c) its single-column analogue with recycle lead. Both single-column processes are obtained by selecting an arbitrary column of the SMB unit (i.e. column 1) and following its operation over a complete cycle. The recycle streams from the nonexisting columns are mimicked by recycling, with a time lag of $(N-1)\tau$ or time lead of τ, the portion of the outlet stream of the column that is not withdrawn as product.

are the basis for efficient methods to calculate the periodic state of the SMB process, which can be employed in process design and optimization [1].

References

[1] J. Araújo, R. Rodrigues, J. Mota, Use of single-column models for efficient computation of the periodic state of a simulated moving-bed process, Indus-

trial and Engineering Chemistry Research 45 (2006) 5314–5325. 42, 50, 51, 52

[2] J. Araújo, R. Rodrigues, J. Mota, Optimal design and operation of a certain class of asynchronous simulated moving bed processes, Journal of Chromatography A 1132 (2006) 76–89. 42, 43, 50

[3] A. Toumi, F. Hanisch, S. Engell, Optimal operation of continuous chromatographic processes: Mathematical optimization of the varicol process, Industrial and Engineering Chemistry Research 41 (2002) 4328–4337. 43

[4] A. Toumi, S. Engell, O. Ludemann-Hombourger, R. Nicoud, M. Bailly, Optimization of simulated moving bed and varicol processes, Journal of Chromatography A 1006 (2003) 15–31. 43

[5] L. S. Pais, J. M. Loureiro, A. E. Rodrigues, Modeling strategies for enantiomers separation by smb chromatography, AIChE Journal 44 (1998) 561–569. 45

[6] M. Mazzotti, G. Storti, M. Morbidelli, Optimal operation of simulated moving bed units for nonlinear chromatographic separations, Journal of Chromatography A 769 (1997) 3–24. 47, 49

[7] C. Migliorini, A. Gentilini, M. Mazzotti, M. Morbidelli, Design of simulated moving bed units under non-ideal conditions, Industrial and Engineering Chemistry Research 38 (1999) 2400–2410. 49

[8] C. Migliorini, M. Mazzotti, M. Morbidelli, Design of simulated moving bed multicomponent separations: Langmuir systems, Separation and Purification Technology 20 (2000) 79–96. 49

[9] P. S. Gomes, M. Minceva, A. Rodrigues, Simulated moving bed technology: old and new, Adsorption 12 (2006) 375–392. 49

[10] G. Biressi, O. Ludemann-Hombourger, M. Mazzotti, R. Nicoud, M. Morbidelli, Design and optimization of a smb unit: role of deviations from equilibrium theory, Journal of Chromatography A 876 (2000) 3. 49

[11] J. Mota, J. Araújo, Single-column simulated-moving-bed process with recycle lag, AIChE Journal 51 (2005) 1641–1653. 51

4

Single-column analog to SMB

4.1 Brief introduction

Simulated moving-bed (SMB) is a continuous chromatographic separation process with numerous applications, many of which are difficult to handle using other modes of production chromatography.

The scale-down of the original SMB process [1] into smaller SMB units has been gaining an increasing interest over the last decade for the separation of pure substances in the pharmaceutical, fine chemistry and biotechnology industries [2]. The recent rapid growth of newly emerging SMB applications has been accompanied by the development of novel SMB schemes that are substantially different from the conventional process. These include new concepts such as the Varicol [3, 4, 5], the ModiCon [6, 7] and PowerFeed [8, 9, 10, 11, 12] processes. These advances are pushing the trend for units with a small number of columns, since the inventory of stationary phase is reduced, the setup is more economical, and the overall pressure drop can be lowered. In this chapter, we are particularly interested in two classes of nonstandard cyclic operating schemes: zone length manipulation and flowrate modulation.

The Varicol scheme [3, 4] typically consists of performing a predetermined sequence of asynchronous port switchings over every switching interval, resulting in

a time-periodic modulation of the zone lengths. The possibilities for asynchronous port switching are endless. In the more general case, the optimization of a Varicol process requires solving a mixed integer nonlinear programming problem [13]. A few authors, however, have proposed different approaches to substantially reduce the dimension of the searchable Varicol space and eliminate the integer nature of the optimization problem [5, 14].

The use of time-variable flowrates as a way to improve process performance creates also additional time-variable degrees of freedom. All of the aforementioned studies on flowrate modulation are theoretical or numerical. One exception is a recent study where a simplified PowerFeed scheme was implemented experimentally [12]. The possibility of combining Varicol and PowerFeed operating modes into a single hybrid scheme has also been considered [14, 15] and shown to provide further enhancements to process performance.

When these schemes are applied in practice the process becomes more complex, because of the increased degrees of freedom that must be optimized. It is also less robust and more difficult to operate because it is more demanding on hardware, particularly in regard to the flowrate profiles imposed on the pumps. This additional complexity requires highly versatile SMB equipment [16], advanced optimization tools [5, 14, 17, 18, 19, 20], and robust control procedures [21, 22, 23, 24, 25].

In the present chapter we analyze the performance of Varicol and PowerFeed processes, as well as their combination into a single hybrid scheme, both experimentally and by numerical simulation. The experimental feasibility and effectiveness of each scheme are assessed by running and comparing optimized configurations for the linear separation of two nucleosides on a high-performance reversed-phase stationary phase. The experimental setup employed in this work is based on a single-column apparatus for reproducing the steady periodic behavior of multi-column countercurrent chromatography.

4.2 Single-column Setup

As described in chapter 3, equation 3.23 defines, by means of a time lead or lag, a single-column batch chromatographic system that has the same CSS dynamics

Table 4.1: Outline of the nonlinear optimization problem.

Degrees of freedom:

$\tau > 0, \quad Q_{\mathrm{I}} \geq 0, \ldots, Q_{\mathrm{IV}} \geq 0, \quad N_{\mathrm{I}} \geq 0, \ldots, N_{\mathrm{IV}} \geq 0$

Objective function:

f_{obj} =max$\{Q_{\mathrm{F}}\}$

Basic constraints:

$Q_{\mathrm{I}} \leq Q_{\max}, \quad \sum N_j = N$

Feasibility constraints on internal flowrates:

$Q_{\mathrm{II}} < Q_{\mathrm{I}}\,(Q_{\mathrm{X}} > 0), \quad Q_{\mathrm{III}} > Q_{\mathrm{II}}\,(Q_{\mathrm{F}} > 0), \quad Q_{\mathrm{IV}} < Q_{\mathrm{III}}\,(Q_{\mathrm{R}} > 0), \quad Q_{\mathrm{I}} > Q_{\mathrm{IV}}\,(Q_{\mathrm{E}} > 0)$

Feasibility constraints on section length:

$N_{\mathrm{I}} + N_{\mathrm{II}} \geq 1, \quad N_{\mathrm{II}} + N_{\mathrm{III}} \geq 1, \quad N_{\mathrm{III}} + N_{\mathrm{IV}} \geq 1, \quad N_{\mathrm{IV}} + N_{\mathrm{I}} \geq 1$

Purity requirements:

$$P_{\mathrm{R}} = \frac{\int_t^{t+N\tau} Q_{\mathrm{R}} c_1^R dt}{\int_t^{t+N\tau} Q_{\mathrm{R}}(c_1^R + c_2^R)dt} \geq P_{\mathrm{R}}^{\min}, \quad P_{\mathrm{X}} = \frac{\int_t^{t+N\tau} Q_{\mathrm{X}} c_2^X dt}{\int_t^{t+N\tau} Q_{\mathrm{X}}(c_1^X + c_2^X)dt} \geq P_{\mathrm{X}}^{\min}$$

as a fixed column of the equivalent multi-column chromatographic process (see Fig. 4.1). In this chapter we will focus the attention on the model with a time lag of $(N-1)\tau$, which is a consequence of the circular column arrangement and of the periodic nature of the SMB [26]. With this model in mind, the resulting outline of the nonlinear programming (NLP) problem is described in Table 4.1. The NLP problem is formulated in AMPL [27] and solved using a efficient interior-point solver [28] as recently advocated by Kawajiri and Biegler [17].

In recent work [29, 30] we proposed a single-column model as the basis for two efficient methods to calculate the periodic state of the analogous multi-column process. In one of the methods, the governing equations are integrated over a sufficiently large number of cycles until CSS is attained. However, instead of the traditional approach of integrating the multi-column equations, the method employs the reduced set of equations for a single column. To numerically implement the recycle lag, a record is kept of the simulated outlet composition profile sampled at discrete points in time over the past $(N-1)\tau$ time units. The lagged

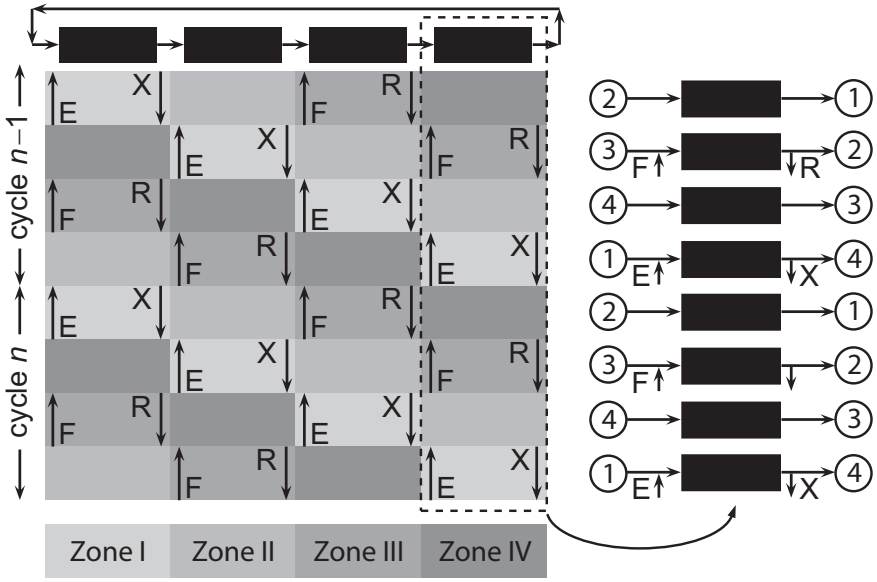

Figure 4.1: Schematic diagram showing the sequence of port switching for two cycles of a four-column SMB and the analogous single-column process.

composition profile, $c_i^{\mathrm{out}}(t-(N-1)\tau)$, which is required to determine the inlet composition at each simulated point in time, is reconstructed by a suitable polynomial interpolation of the previously stored discrete values of c_i^{out}.

The idea behind the experimental single-column apparatus presented in this chapter is to replace numerical integration by the real dynamics of the chromatographic column. Basically, the time-periodic composition profile of the inlet effluent, $c_i^{\mathrm{in}}(t)$, is experimentally reproduced from the online measured outlet composition profile, $\{c_i^{\mathrm{out}}(t)\}^{\mathrm{exp}}$, while simultaneously satisfying the flow-rate profile imposed on the column, $Q(t)$. The instantaneous value of $c_i^{\mathrm{in}}(t)$ is determined from Eq. 3.23:

$$c_i^{\mathrm{in}}(t) = \begin{cases} \dfrac{Q_{\mathrm{II}}\left\{c_i^{\mathrm{out}}(t')\right\}^{\mathrm{exp}} + (Q_{\mathrm{III}} - Q_{\mathrm{II}})\, c_i^{\mathrm{F}}}{Q_{\mathrm{III}}} & \text{(feed mode)} \\ \dfrac{Q_{\mathrm{IV}}\left\{c_i^{\mathrm{out}}(t')\right\}^{\mathrm{exp}} + (Q_{\mathrm{I}} - Q_{\mathrm{IV}})\, c_i^{\mathrm{E}}}{Q_{\mathrm{I}}} & \text{(eluent mode)} \\ \left\{c_i^{\mathrm{out}}(t')\right\}^{\mathrm{exp}} & \text{(otherwise)} \end{cases}, \tag{4.1}$$

The setup employs standard chromatographic equipment, comprising a column, a suitable detection system for online monitoring of the outlet effluent composition, and three variable speed HPLC pumps with computer-controlled flow rate.

The whole system must be fully automated with an integrated computer capable of handling the control procedures of recording, conditioning and processing the signal from the detector and feeding back the processed information into the HPLC pumps.

By combining the three pump flows it is possible to manipulate the composition and flow rate of the effluent fed into the column as desired. Each pump delivers part of the inlet flow to the column at a controlled flow-rate by pumping liquid from a different source solution. One pump delivers pure mobile phase

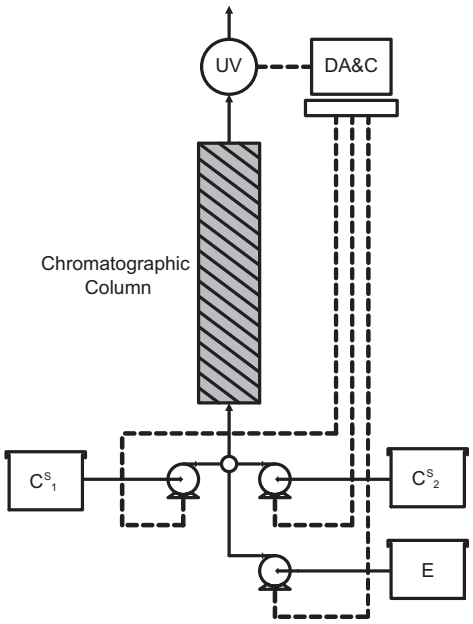

Figure 4.2: Schematic diagram of experimental setup. The main equipment comprises a chromatographic column, three HPLC pumps and an UV detector. Pumps and detector are connected to an automated data acquisition and control unit.

(Q_0), whereas the other two pumps (Q_1 and Q_2) deliver a different solute dissolved in the mobile phase at a prescribed concentration c_i^{S}. The three pump outlets are connected to a common low-volume mixing junction to provide a well-mixed stream that is fed directly into the chromatographic column.

To get the desired flow rate and composition when the three streams are combined, i.e.

$$Q_0 + Q_1 + Q_2 = Q \quad \text{and} \quad \frac{Q_i c_i^{\mathrm{S}}}{Q} = c_i^{\mathrm{in}}, \tag{4.2}$$

the instantaneous values of the three pump flow-rates are determined as follows:

$$Q_1 = \frac{Q\, c_1^{\mathrm{in}}}{c_1^{\mathrm{S}}}, \tag{4.3}$$

$$Q_2 = \frac{Q\, c_2^{\mathrm{in}}}{c_2^{\mathrm{S}}}, \tag{4.4}$$

$$Q_0 = Q - Q_1 - Q_2. \tag{4.5}$$

The flow rate of mobile phase is obtained from the global material balance, Eq. 4.5, and since $Q_0(t) \geq 0$, the condition

$$\frac{c_1^{\mathrm{in}}}{c_1^{\mathrm{S}}} + \frac{c_2^{\mathrm{in}}}{c_2^{\mathrm{S}}} \leq 1 \tag{4.6}$$

must always be verified. This imposes lower limits $(c_i^{\mathrm{S}})^{\mathrm{min}}$ on the minimum values of c_1^{S} and c_2^{S} for the system to be physically realizable. The values of $(c_i^{\mathrm{S}})^{\mathrm{min}}$ are best determined from the simulated composition profile $\{c_i^{\mathrm{in}}(t)\}^{\mathrm{sim}}$ obtained from a suitable chromatographic model of the column. However, provided that the outlet solute concentration never exceeds the corresponding feed value, i.e. $\{c_i^{\mathrm{out}}(t)\}^{\mathrm{exp}} \leq c_i^{\mathrm{F}}$ (absence of roll-up), which is generally the case, one can safely set $c_i^{\mathrm{S}} = 2c_i^{\mathrm{F}}$. This choice is always feasible for a racemic mixture, because the solubilities of the two enantiomers are mutually exclusive, i.e. the solubility of one enantiomer increases by as much as the concentration of the other in the same solution is decreased. Although one should expect the solubility of a given solute to be larger when it is not competing with other solutes in the same solution, it is not guaranteed that $c_i^{\mathrm{S}} = 2c_i^{\mathrm{F}}$ can always be set for mixtures involving solutes with

different chemical structure when the feed concentration is close to the solubility limit.

An alternative solution to overcome the solubility problem, which is also advantageous when it is difficult or expensive to obtain the two solutes separately, is to install an extra pump (Q_{12}) delivering regular feed solution with composition c_i^{F}. In this case, the instantaneous values of the four flow rates are determined as:

$$Q_{12} = Q \min\left\{\frac{c_1^{\mathrm{in}}}{c_1^{\mathrm{F}}}, \frac{c_1^{\mathrm{in}}}{c_2^{\mathrm{F}}}\right\} \tag{4.7}$$

$$Q_1 = Q\,\frac{c_1^{\mathrm{in}}}{c_1^{\mathrm{S}}} - Q_{12} \tag{4.8}$$

$$Q_2 = Q\,\frac{c_2^{\mathrm{in}}}{c_2^{\mathrm{S}}} - Q_{12} \tag{4.9}$$

$$Q_0 = Q - Q_{12} - Q_1 - Q_2. \tag{4.10}$$

To summarize, Eq. 4.1, together with Eqs. 4.3–4.5 or Eqs. 4.7–4.10, and the imposed flow-rate profile, $Q(t)$, determine the instantaneous flow rate of each HPLC pump. The compositions of the two product streams are determined from the measured values of c_i^{out} as follows:

$$c_i^{\mathrm{X}} = \frac{Q\,\{c_i^{\mathrm{out}}\}^{\mathrm{exp}} + \,(Q_{\mathrm{I}} - Q)\,c_i^{\mathrm{E}}}{Q_{\mathrm{I}}} \quad \text{(extract withdrawal)}, \tag{4.11}$$

$$c_i^{\mathrm{R}} = \frac{Q\,\{c_i^{\mathrm{out}}\}^{\mathrm{exp}} + (Q_{\mathrm{III}} - Q)\,c_i^{\mathrm{F}}}{Q_{\mathrm{III}}} \quad \text{(raffinate withdrawal)}. \tag{4.12}$$

These expressions take into account the possibility of temporary or full suppression of zone I or zone III. In the former case eluent is added and extract is withdrawn simultaneously at the same node, whereas in the latter case feed is added and raffinate is collected at the same node (this situation is unlikely to occur in practice).

4.2.1 Model-based Startup Procedure

The simplest way to carry out an experimental run is to start with a clean column and assume that for $t < 0$ it had been fed with eluent, i.e. $\{c_i^{\mathrm{out}}(t < 0)\}^{\mathrm{exp}} = 0$.

This closely mimics the transient startup behavior of an SMB, though not exactly. In most cases, however, the initial transient is of no interest, but only the fully established periodic state. For those cases, the duration of the experiment can be significantly reduced by applying a fast model-based startup procedure. It should be pointed out that this scheme cannot be directly applied to a real SMB process because the multicolumn unit lacks the capability of artificially generating a prescribed inlet concentration profile. Other authors [31], however, have satisfactorily solved the problems of shortening the transient period and recovering the remaining products in a real SMB shutdown process. This is especially important when processing short batches where the transient operational time is comparable to the steady-state operational time. The proposed fast startup scheme is described next.

It is assumed that a more or less detailed dynamic model of the chromatographic process is available. This is practically a must in SMB chromatography for determining suitable operating conditions and for advanced process optimization. Let $\{c_i^{\text{out}}(t)\}^{\text{sim}}$ $(i = 1, 2)$ be the simulated outlet composition profile at cyclic steady state for the fixed column of the multi-column process that is being experimentally reproduced. By definition $\{c_i^{\text{out}}(t)\}^{\text{sim}}$ is $N\tau$-periodic:

$$\{c_i^{\text{out}}(t)\}^{\text{sim}} = \{c_i^{\text{out}}(t \bmod N\tau)\}^{\text{sim}}. \tag{4.13}$$

Hopefully, one expects $\{c_i^{\text{out}}(t)\}^{\text{sim}}$ to be as close as possible to $\{c_i^{\text{out}}(t)\}^{\text{exp}}$, but there will always be some mismatch due to model uncertainty and experimental variability.

Figure 4.3 shows typical axial composition profiles in the liquid phase at the beginning of each switching interval of the cycle under CSS conditions for the rightmost column of Figure. 4.1 The mimicked SMB unit has a 1-1-1-1 configuration and the selected operating parameters provide high product purity and yield. At the start of the cycle the column has just been regenerated and during the first switching interval it is operated in pure recycle mode. During the second switching interval the column is charged with an effluent enriched with feed while at the same time the outlet flow is partially diverted for raffinate collection. Over the third switching interval the column reverts to pure recycle operation.

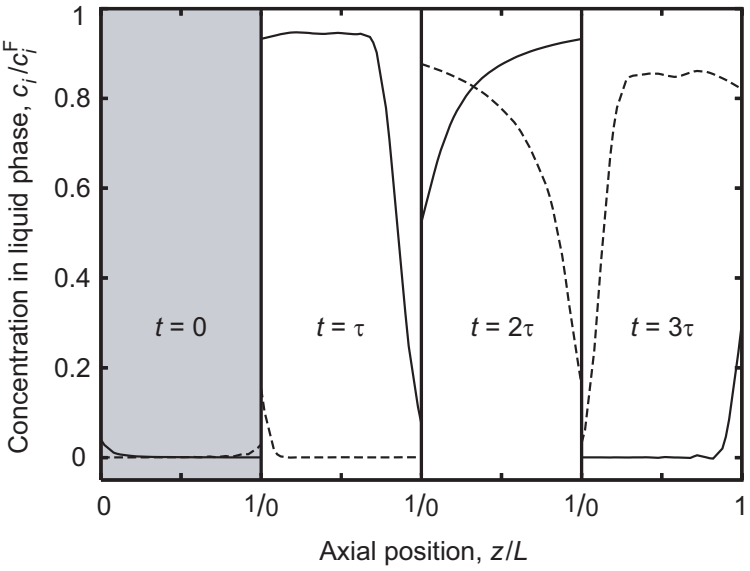

Figure 4.3: CSS axial concentration profiles in liquid phase at the beginning of each switching interval of the cycle for the rightmost column of Figure 4.1. (__) Fast migrating solute; (- - -), slow migrating solute. The cycle starts after eluent addition, during the second switching interval fresh feed is added and raffinate is collected, during the fourth switching interval the column is regenerated while extract is obtained. If the regeneration step is effective, at the start of the cycle the column is nearly solute free (shaded area) and its status is well approximated by that of a clean column.

Finally, during the fourth switching interval the column is regenerated by diluting the inlet flow with fresh eluent while simultaneously withdrawing extract.

The point to note is that if the regeneration step is effective, at the start of the cycle the column is nearly solute free (shaded area) and its status is well approximated by that of a clean column. Thus, if the startup condition $\{c_i^{\text{out}}(t < 0)\}^{\text{exp}} = 0$ is replaced by $\{c_i^{\text{out}}(t < 0)\}^{\text{exp}} = \{c_i^{\text{out}}(t)\}^{\text{sim}}$, i.e. the inlet composition profile over the first $(N-1)\tau$ time units of operation is taken from the simulated column behavior at CSS, then the system should approach the cyclic steady state very fast. In fact, as demonstrated in the next section the CSS is experimentally attained in just one or two cycles of operation.

Let τ_{sim} be the initial period during which the inlet composition profile for the single-column setup is determined by the chromatographic model. Since the single-column process delays its recycle by $(N-1)\tau$ time units, τ_{sim} is constrained by this lower bound:

$$\tau_{\text{sim}} \geq (N-1)\tau. \tag{4.14}$$

Given $\{c_i^{\text{out}}(t)\}^{\text{sim}}$, $\{c_i^{\text{out}}(t)\}^{\text{exp}}$ and τ_{sim}, one define

$$c_i^{\text{out}}(t) = \begin{cases} \{c_i^{\text{out}}(t)\}^{\text{sim}}, & t \leq \tau_{\text{sim}} - (N-1)\tau \\ \{c_i^{\text{out}}(t)\}^{\text{exp}}, & t > \tau_{\text{sim}} - (N-1)\tau \end{cases} \tag{4.15}$$

as holding all the information about the outlet composition profile required to experimentally reproduce the composition profile of the inlet effluent. In practice, the above definition for c_i^{out} replaces $\{c_i^{\text{out}}\}^{\text{exp}}$ in Eq. 4.1.

Note that if τ_{sim} is set equal to the duration of the experiment then the inlet composition profile is obtained solely from the output of the chromatographic model and the experimental outlet composition profile is never fed back into the system. This situation might be helpful to identify model mismatches.

4.2.2 Data Sampling and Filtering

The continuous signal from the concentration detector, $\{c_i^{\text{out}}(t)\}^{\text{exp}}$, is sampled at discrete points in time, t_0, t_1, ..., to obtain the sampled data, $\{c_i^{\text{out}}(t_k)\}^{\text{exp}}$, $k = 0, 1, 2, \ldots$, which are then stored for future feedback into the system. In this case, the sampling rate of the detector and the sampling rate at which the pump flow rates are updated are not necessarily identical. Therefore, there must be means to update the actuating signal on the pumps at instants which are not in phase with the discrete measurements of the detector. Furthermore, the detector must provide an accurate and noise-free signal for the system to work properly. An excessive noise level in the detector signal would have a detrimental impact on the HPLC pumps. This means that in many cases the signal must be conditioned.

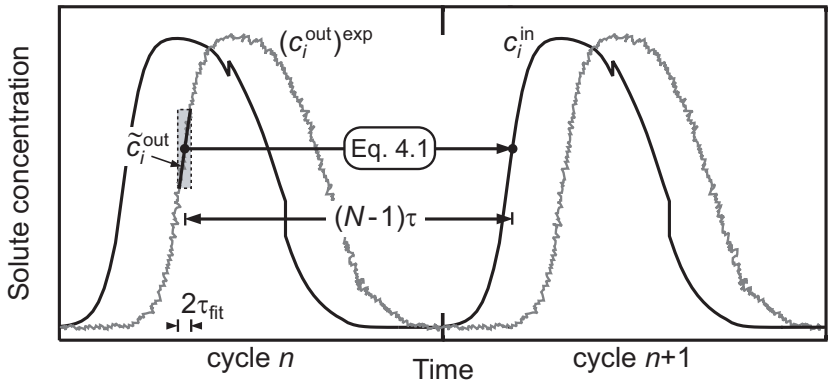

Figure 4.4: Schematic diagram of moving-polynomial fit to generate a continuous noise-free signal from the sampled data of the online composition detector.

In this implementation, these problems are solved by resorting to a moving-polynomial-fit filter, $\tilde{c}_i^{out}(t)$, which is applied to $c_i^{out}(t)$ defined in Eq. 4.15 and replaces it in Eq. 4.1. The procedure is shown schematically in Fig. 4.4.

The filtered signal $\tilde{c}_i^{out}(t)$ is the second-order polynomial that provides the best fit to the sampled data $c_i^{out}(t_k)$ over the range $t - \tau_{fit} \leq t_k \leq t + \tau_{fit}$. This moving polynomial is an effective method of generating a continuous signal from the sampled data of the detector, thus providing the value of $c_i^{out}(t)$ for any required value of t, and simultaneously reducing the noise level by locally fitting the data with a small number of degrees of freedom. The value of τ_{fit} must be smaller than the switching interval, typically $\tau_{fit} \approx 0.05\tau$, yet large enough to accommodate more sampled data than the three polynomial coefficients.

4.3 Experimental

To experimentally evaluate and demonstrate the feasibility of the proposed setup, the separation of nucleosides uridine and guanosine on reversed-phase Source^{TM} 30RPC (GE Healthcare , Uppsala, Sweden) was considered [25].

This stationary phase has a matrix based on rigid polystyrene/divinyl benzene 30 μm monosized beads, and is designed for high-performance preparative separations of bio-molecules, such as proteins, peptides and oligonucleotides. A

Table 4.2: Characteristics of the stationary phase Source^{TM} 30RPC.

Matrix	Polystyrene/divinyl benzene
Bead Form	Rigid, spherical, porous, monosized
Particle size	30 μm
Chemical stability	Stable in all aqueous buffers
pH stability	1-12 (working), 1-14 (cleaning)
Typical flow velocity range	100-1000 cm/h
Operating temperature	4-40°C

description of the main characteristics of the stationary phase can be viewed in Table 4.2. The composition of the mobile phase was fixed at 5% (v/v) ethanol (HPLC grade,Panreac, Spain) in distilled water, which has previously been found to be suitable for the separation under study [25]. The system was operated isothermally at 25°C.

The chemical structure of the two nucleosides is presented in Figure 4.5. Nucleosides are glycosylamines consisting of a nucleobase (often referred to simply as base) bound to a ribose or deoxyribose sugar. In medicine several nucleoside analogues are used as antiviral or anticancer agents.

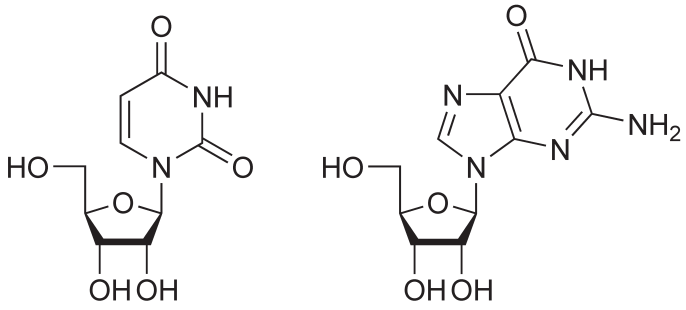

Figure 4.5: Chemical structure of the nucleosides uridine and guanosine.

4.3.1 Online Monitoring

A multi-wavelength UV detector (USB2000, Ocean Optics, USA) equipped with a DH-2000-S-DUV light source (Micropack, Ostfildern, Germany) and a variable attenuator (FVA-UV, Ocean Optics, USA), was employed to continuously monitor the composition of the outlet effluent. Since the concentrations of the two components cannot be discriminated from the UV measurement at a single wavelength because they contribute additively to the total absorbance, at least two UV absorbances measured simultaneously at two different wavelengths are required to calculate the concentration of each component. For better measurement accuracy the UV absorbance was simultaneously measured at 6 suitably chosen wavelengths to provide a well-conditioned estimation procedure.

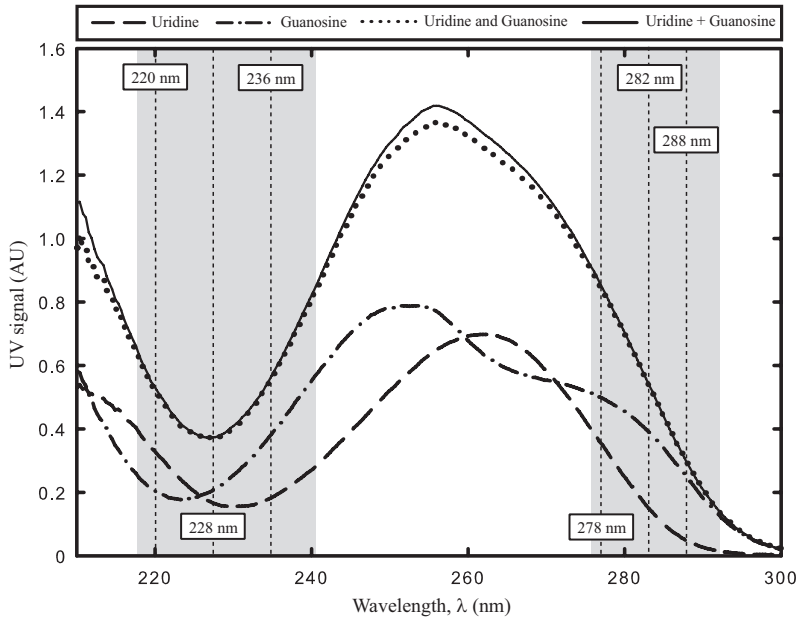

Figure 4.6: UV spectra of uridine (- - -), $A_U(\lambda, c_U)$, and guanosine (- -), $A_G(\lambda, cG)$, measured with a multi-wavelength detector, and their additive range (shaded areas), for $cU = cG = 0.05$ g/l. The dotted line represents the experimental spectrum $A(\lambda, cU + cG)$, whereas the solid line corresponds to the sum of the two individual spectra, $AU(\lambda, cU) + A_G(\lambda, cG)$. The six wavelengths selected for online monitoring are identified in the graph.

In practice, prior to the experiments was determined the UV spectrum of each separate nucleoside at feed concentration, $A_i(\lambda; c_i^{\mathrm{F}})$, and the wavelength region $[\lambda_{\min}, \lambda_{\max}]$ over which the two spectra are additive (Fig. 4.6):

$$A(\lambda; c_1^{\mathrm{F}} + c_2^{\mathrm{F}}) = A_1(\lambda; c_1^{\mathrm{F}}) + A_2(\lambda; c_2^{\mathrm{F}}), \quad \lambda_{\min} \leq \lambda \leq \lambda_{\max}. \tag{4.16}$$

The MatLab (MathWorks, USA) software was then employed to select from a large number (1000 in the case of the experiments reported here) of randomly generated sets of 6 wavelengths in the additive spectrum region, the one, say $\{\lambda_{j(j=1,\ldots,6)} : \lambda_{\min} \leq \lambda_1 < \ldots < \lambda_6 \leq \lambda_{\max}\}$, whose 6×2 absorbance matrix

$$[S_\lambda] = \begin{bmatrix} \dfrac{A_1(\lambda_1; c_1^{\mathrm{F}})}{c_1^{\mathrm{F}}} & \dfrac{A_2(\lambda_1; c_2^{\mathrm{F}})}{c_2^{\mathrm{F}}} \\ \ldots & \ldots \\ \dfrac{A_1(\lambda_6; c_1^{\mathrm{F}})}{c_1^{\mathrm{F}}} & \dfrac{A_2(\lambda_6; c_2^{\mathrm{F}})}{c_2^{\mathrm{F}}} \end{bmatrix} \tag{4.17}$$

had the smallest condition number with respect to inversion. The condition number of a matrix measures the sensitivity of the solution of a system of linear equations to errors in the data. It gives an indication of the accuracy of the results from matrix inversion and the linear equation solution. Condition numbers near 1 indicate a well-conditioned matrix, whereas large condition numbers indicate a nearly singular matrix. The selected wavelengths are shown in Fig. 4.6.

At each sampling instant, the solute concentrations c_i were calculated by computing the L_1 solution to the over-determined linear algebraic system

$$\begin{bmatrix} A(\lambda_1; c_1 + c_2) \\ \ldots \\ A(\lambda_6; c_1 + c_2) \end{bmatrix} = [S_\lambda] \begin{bmatrix} c_1 \\ c_2 \end{bmatrix}, \tag{4.18}$$

where the left-hand vector is the vector of experimental absorbances measured simultaneously at the 6 selected wavelengths. This is done by employing the ma20 fortran package of the Harwell software library archive. If the vector of experimental measurements contains some "wild" points (i.e. measurements that are wildly inaccurate to the overall accuracy of the data) it is advisable to calculate an L_1 approximation rather than an L_2 (least-squares) approximation. The sampling rate of the UV was fixed at 0.25 s^{-1}.

The system was operated with feed concentrations low enough to allow the use of the UV detector in the linear range of the calibration curve. The concentration limit imposed by the UV detector restricted the separation to the linear range of the adsorption equilibrium. Since the system was operated far from the solubility limit of the two nucleosides, the adopted setup configuration is the one with three HPLC pumps [Eq. 4.3–4.5] and $c_i^{\mathrm{S}} = 2c_i^{\mathrm{F}}$.

4.3.2 Chromatographic Model

As discussed in detail in chapter 2, the dispersed plug-flow model with linear driving-force approximation for mass transfer is a sufficiently general model to provide a realistic representation of most chromatographic columns [32]. Under linear conditions, as in the case considered here, the model can be simplified to an equilibrium dispersed plug flow model [32, 33, 34]. For a linear adsorption isotherm, i.e. $q_i^* = K_i c_i$:

$$(1+\beta K_i)\frac{\partial c_i}{\partial \theta} = \frac{\tau \upsilon}{L}\left(\frac{h_i}{2}\frac{\partial^2 c_i}{\partial x^2} - \frac{\partial c_i}{\partial x}\right) \quad (0 < x < 1), \tag{4.19}$$

and

$$h_i = \frac{H_i}{L} = \frac{2}{\mathrm{Pe}_i'} = \frac{2}{\mathrm{Pe}_i} + \frac{\beta K_i}{(1+\beta K_i)^2}\frac{2\upsilon}{k_i L} \tag{4.20}$$

is the dimensionless plate height. The usual boundary conditions are

$$c_i - \frac{1}{\mathrm{Pe}_i'}\frac{\partial c_i}{\partial x} = c_i^{\mathrm{in}} \quad \text{for} \quad x = 0, \tag{4.21}$$

$$\frac{\partial c_i}{\partial x} = 0 \quad \text{for} \quad x = 1. \tag{4.22}$$

In this working range of fluid velocity, the contribution of axial molecular diffusion is negligible [35], then the influence of υ on column efficiency can be simplified into a linear relationship:

$$\frac{h_i}{2} = \frac{1}{\mathrm{Pe}_i} + \alpha_i \upsilon, \quad \alpha_i = \frac{\beta K_i}{k_i L (1+\beta K_i)^2}. \tag{4.23}$$

4.3.3 Materials and System Characterization

The stationary phase was slurry packed into one jacketed Superformance 10 mm I.D. glass column (Götec Labortechnik, Germany) to a bed height of $L = 60$ mm. The nucleosides were purchased from SigmaAldrich (Schnelldorf, Germany) with a purity of 99% for uridine and 98% in the case of guanosine. Extra-column dead volumes in our setup were estimated from Blue Dextran (MW 2.10^6 from SigmaAldrich) pulse experiments with and without the chromatographic column. The packing porosity was obtained by measuring the retention times of several dilute pulses of Blue Dextran (interparticle void fraction, ϵ) and sodium nitrate (overall porosity, ϵ^*). For reference, the obtained value was $\epsilon_p = (\epsilon^* - \epsilon)/(1-\epsilon) = 0.546$, though the used chromatographic model is based on ϵ only.

The Henry constants, K_i, and coefficients, Pe_i and α_i, of the simplified Van Deemter plot (Fig. 4.7), were determined by fitting Eq. 4.19 to a series of experimental chromatograms obtained from the injection of several diluted pulses (500 μl at 0.2 g/l) of uridine and guanosine at different liquid flowrates. The time lag, due to the dead volume in the system, was subtracted from the sampling instants before fitting Eq. 4.19 to each experimental chromatogram. A representative set of the fitted chromatograms is shown in Fig. 4.8. All parameter fitting was made by means of a developed chromatographic column model in

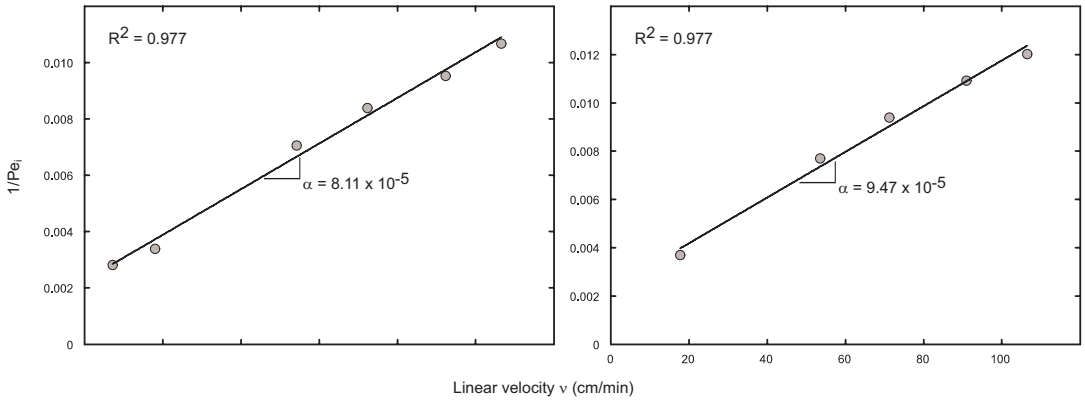

Figure 4.7: Measured values of apparent Péclet number, Pe_i, for uridine (left) and guanosine (right), as a function of linear fluid velocity, and corresponding fits to a linear van Deemter plot.

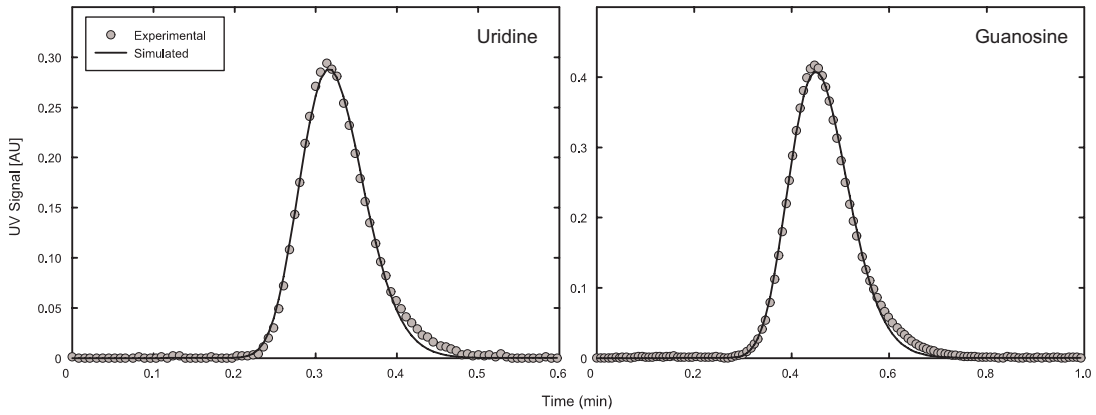

Figure 4.8: Experimental (symbols) and fitted lines (lines) chromatograms for at a interstitial flow velocity of $\upsilon = 90$ cm/min for a injection loop of 500μl and a concentration of 0.1 g/l each.

gProms (Process Systems Enterprise, London, United Kingdom) software. The obtained parameters are listed in Table 4.3.

The HPLC pumps employed in the experiments are model K-501 from Knauer (Berlin, Germany) with 10 and 50 ml pump heads, controlled by the RS232 communication protocol. The whole setup is fully automated and driven in-house developed Labview (National Instruments, USA) based software system (BioCTR) for monitoring and control of chromatographic processes [36].

Figure 4.9 shows a snapshot of the monitoring window of the process automation system software. The top-left graph monitors the actuating signal (flowrate)

Table 4.3: Column characterization and adsorption parameters.

L (cm)	d (cm)	$V_{ex}(cm^3)^a$	ϵ	ϵ^*
6.0	1.0	0.143	0.265	0.667
	K	Pe	αL (s)	$k(s^{-1})$
Uridine	1.197	441.8	0.029	6.10
Guanosine	1.907	436.8	0.034	3.93

$\epsilon^* = \epsilon + (1-\epsilon)\epsilon_p$, where ϵ_p is the intraparticle porosity.

[a] Extra column dead volume

on each HPLC pump, whereas the top-right graph displays the recorded cumulative weight of the outlet effluent measured on a Sartorius TE3102S balance (Göttingen, Germany) via the RS232 interface. This information is used to check the overall accuracy and reproducibility of the pumps, since the weight change is directly related to the flowrate:

$$\frac{dW}{dt} = \rho Q(t) \tag{4.24}$$

where W is the recorded weight and ρ is the density of the mobile phase. The bottom graph monitors the two solute concentrations resulting of the deconvolution of the absorbances measured at the six different flowrates.

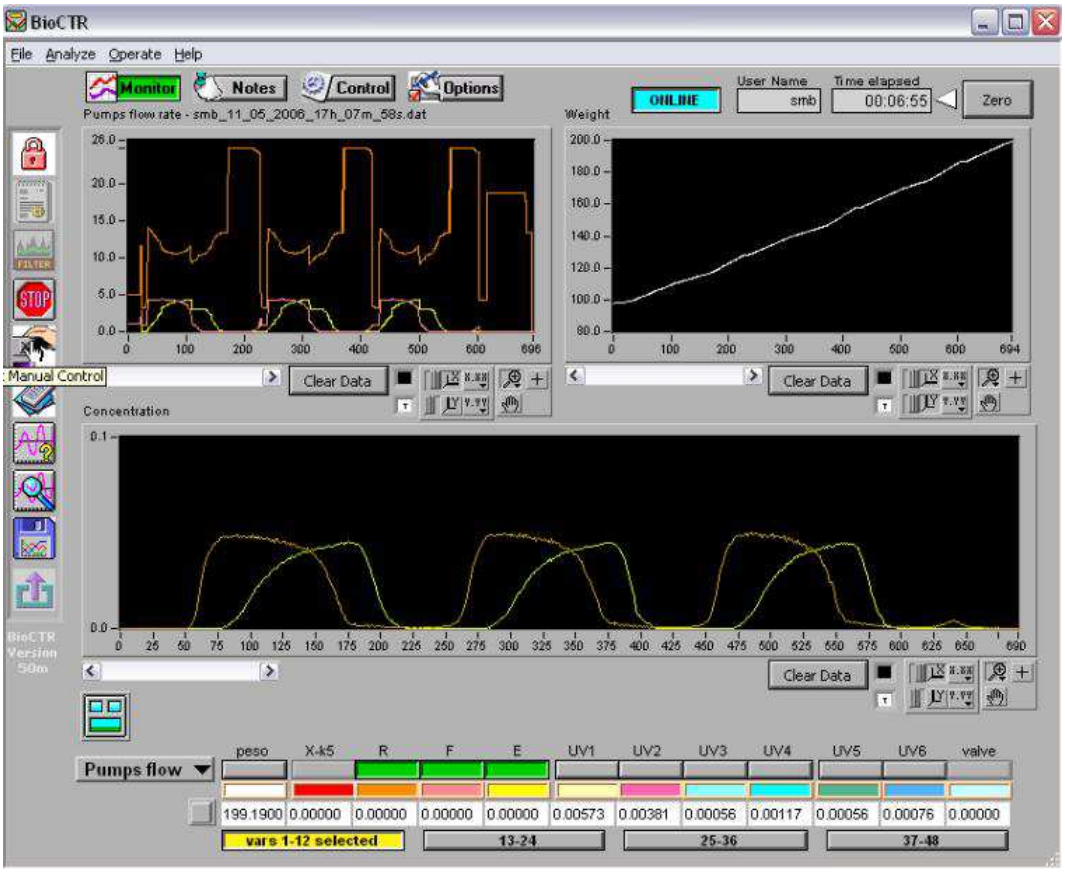

Figure 4.9: Snapshot of the monitoring window of the process automation system.

4.4 Results and Discussion

Recently [14], we have derived a compact representation for a broad class of physically realizable asynchronous SMB processes, which are univocally defined by four real parameters $N_{\mathrm{I}}, \ldots, N_{\mathrm{IV}}$ (provided that $N = \sum N_j$ is an integer), defining the average number of columns in each zone. If the N_j values are all integers, a classical SMB process is obtained.

To define a particulary cycle, one has to specify the intervals during which the clauses of Eq. 4.1 apply, the temporal profile of liquid flowrate in the column and the intervals for product withdrawal. To achieve that, it is convenient to define the following auxiliary parameters:

$$\begin{cases} \theta_4 = N_{\mathrm{IV}} \\ \theta_3 = N_{\mathrm{III}} + \theta_4 = N_{\mathrm{IV}} + N_{\mathrm{III}} \\ \theta_2 = N_{\mathrm{II}} + \theta_3 = N_{\mathrm{IV}} + N_{\mathrm{III}} + N_{\mathrm{II}} \\ \theta_1 = N_{\mathrm{I}} + \theta_2 = N_{\mathrm{IV}} + N_{\mathrm{III}} + N_{\mathrm{II}} + N_{\mathrm{I}} = N \end{cases} . \tag{4.25}$$

The temporal profile of liquid flow-rate in the column is then given by the following $N\tau$-periodic piecewise-constant function:

$$Q(\theta) = \begin{cases} Q_{\mathrm{IV}}, & 0 < \theta' < \theta_4 \\ Q_{\mathrm{III}}, & \theta_4 < \theta' < \theta_3 \\ Q_{\mathrm{II}}, & \theta_3 < \theta' < \theta_2 \\ Q_{\mathrm{I}}, & \theta_2 < \theta' < \theta_1 \end{cases} , \tag{4.26}$$

where $\theta' = \theta \bmod N$ (the process is $N\tau$-periodic). The intervals during which the clauses in Eq. 4.1–4.12 apply are listed in Table 4.4.

Six different optimized processes were experimentally reproduced; the corresponding port configurations and operating parameters are listed in Table 4.5. The parameter values for the NLP constraints are $Q_{\max} = 25$ ml/min and $P_{\mathrm{R}}^{\min} = P_{\mathrm{X}}^{\min} = 0.98$. The feed concentration was fixed at 0.05 g/l of each

Table 4.4: Intervals during which the clauses in Eq. 4.1–4.12 are valid.

Equation	Clause	Valid range	
4.1	Feed mode	$\theta_3 - 1 < \theta' < \theta_3$	
4.1	Eluent mode	$\theta_1 - 1 < \theta' < \theta_1$	
4.11	Extract withdrawal	$\theta_4 < \theta' < \theta_4 + 1$	
4.12	Raffinate withdrawal	$\theta_2 < \theta' < \theta_2 + 1$	$(N_\mathrm{I} \geq 1)$
		$0 < \theta' < \theta_2 + 1 - \theta_1$ and $\theta_2 < \theta' < \theta_1$	$(N_\mathrm{I} < 1)$

θ_j is defined in Eq. 4.25, $\theta' = (t/\tau) \bmod N$.

nucleoside. Run 1 is an experimental replica of the classical 1/1/1/1 SMB process. For the aforementioned constraints, the maximum specific productivity achieved by the process is $Q_\mathrm{F}/N = 0.96$ ml/min with a specific eluent consumption $Q_\mathrm{E}/Q_\mathrm{F} = 2.98$. For this solution all constraints are active, i.e. $Q_\mathrm{I} = Q_\mathrm{max}$, $P_\mathrm{R} = P_\mathrm{R}^\mathrm{min}$ and $P_\mathrm{X} = P_\mathrm{X}^\mathrm{min}$.

To get optimized parameters for run 2, the zone lengths were unfixed and added to the set of optimization variables, more precisely, only N_I, N_II and N_III are considered as degrees of freedom (N_IV is obtained from the relation $\sum N_j = N$). The optimized scheme is a Varicol process with average column configuration 1.2/1.2/1.6/0; the chronogram of its port switching is displayed in the top-left schematic of Fig. 4.10. The desynchronization of port switching increases the specific productivity by 64% to $Q_\mathrm{F}/N = 1.57$ ml/min, but at the cost of a 34% increase on specific eluent consumption ($Q_\mathrm{E}/Q_\mathrm{F} = 3.98$). Note that the optimized solution turns out to be a three-zone open-loop Varicol process. Zone IV has been eliminated, i.e. fresh mobile phase is admixed with the remaining portion of the outlet stream from zone III that is not withdrawn as raffinate. Moreover, $Q_\mathrm{IV} = 0$ which means that the effluent leaving zone III is fully recovered as raffinate and none is recycled back to zone I. Thus, the system effectively operates in an open-loop configuration. This is consistent with the optimization study of Kawajiri and Biegler [37], who obtained a similar optimized configuration for a linear problem

Table 4.5: Optimized operating parameters for the six processes which have been reproduced experimentally. The first four runs simulate four-column processes, whereas the other two simulate three-column configurations. In runs 3, 4 and 6 the flowrates are modulated using piecewise-constant profiles with five steps per switching interval (PowerFeed operation); the reported values of $Q_{\mathrm{E}}/Q_{\mathrm{F}}$ and Q_{F}/N for these cases are the averages over a switching interval. Runs 4 and 6 combine Varicol and PowerFeed operating modes into a single hybrid scheme. The parameter values for the NLP constraints are $Q_{\max} = 25$ ml/min, $P_{\mathrm{R}}^{\min} = P_{\mathrm{X}}^{\min} = 0.98$. Flowrates are expressed in ml/min and τ in min.

Run	$N_{\mathrm{I}}/\ldots/N_{\mathrm{IV}}$	τ	Q_{IV}	Q_E	Q_F	Q_X	Q_R	Q_E/Q_F	Q_F/N
1	1.0/1.0/1.0/1.0	0.36	13.49	11.51	3.86	9.10	6.26	2.98	0.96
2	1.2/1.2/1.6/0	0.35	0.0	25.00	6.29	9.15	22.13	3.98	1.57
3	1.0/1.0/1.0/1.0	0.34	25.00	0	0	0	0	1.51	1.65
			4.84	20.16	0	0	20.16		
			0	25.00	17.79	25.00	17.79		
			20.27	4.73	15.30	20.03	0		
			25	0	0	0	0		
4	1.0/1.2/1.4/0.4	0.33	25.00	0	0	0	0	2.11	1.78
			25.00	0	21.16	21.16	0		
			0	25.00	14.46	19.54	19.92		
			0	25.00	0	1.96	23.04		
			0	25.00	0	0	25.00		
5	1.0/0.9/1.1/0	0.38	0.0	25.00	3.01	9.15	18.86	8.30	1.00
6	1.0/0.8/0.8/0.4	0.35	25.00	0	0	0	0	2.35	2.13
			25.00	0	0	0	0		
			0	25.00	0	0	25.00		
			0	25.00	16.46	23.79	17.67		
			0	25.00	15.47	22.36	18.11		

of sugar separation. Notice also that all constraints are again active, but this time $Q_{\mathrm{E}} = Q_{\mathrm{I}} = Q_{\max}$, i.e. fresh mobile phase is added to the system at the maximum allowable flowrate.

It is reported in the literature [16] that the open-loop system has better pump stability than the closed-loop configuration. However, the synchronous three-zone

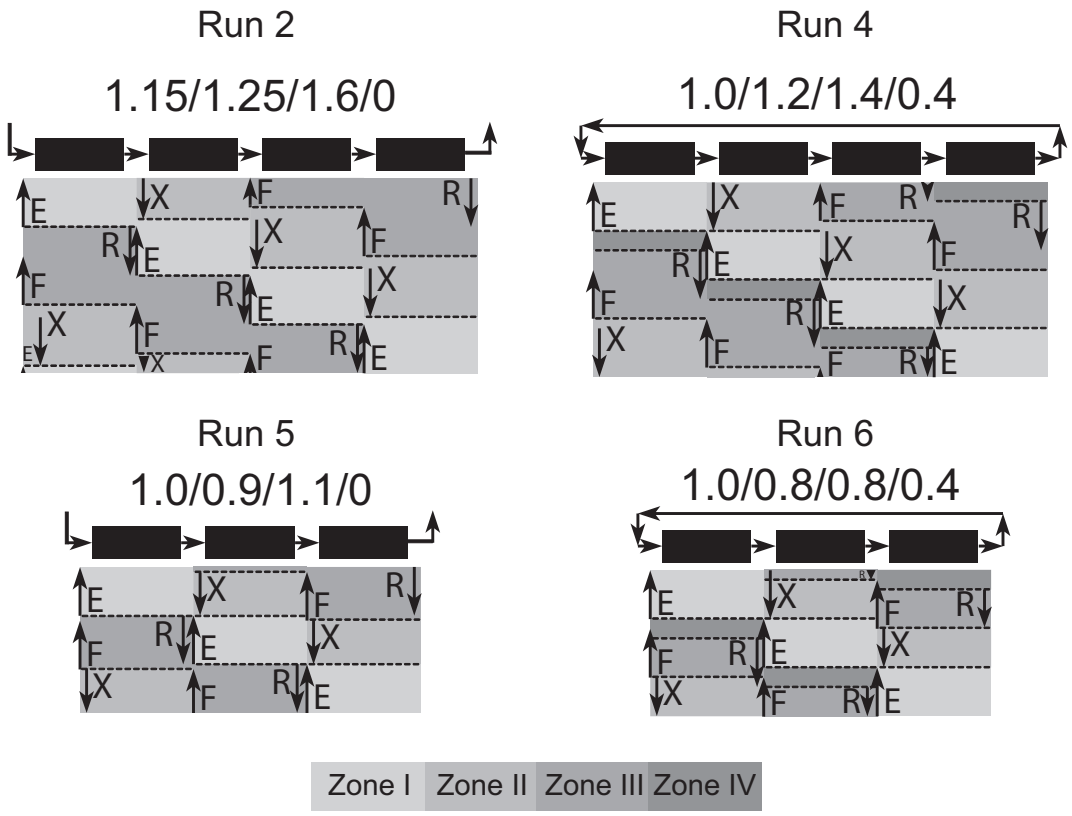

Figure 4.10: Chronograms of port switching for the four asynchronous configurations listed in Table 4.5. Note that the two leftmost schemes are open-loop configurations.

SMB is also known to increase eluent usage and dilution of the raffinate. To a certain extent both remarks hold true for the present scheme, since the raffinate flowrate is increased from $Q_R^{(1)} = 6.26$ ml/min to $Q_R^{(2)} = 21.83$ ml/min, whereas the extract stream is withdrawn at about the same flowrate as for the classical closed-loop SMB scheme.

Run 3 is an optimized PowerFeed process for which the four internal flowrates are allowed to be piecewise-constant τ-periodic functions with five subdivisions per switching interval. Note that the column configuration is fixed at 1/1/1/1. Because of the increased degrees of freedom available with PowerFeed, when compared to the standard SMB process, the specific productivity is increased by

72% to $Q_F/N = 1.65$ ml/min and the specific eluent consumption is reduced by 51% to $Q_E/Q_F = 1.51$. This scheme performs better than the optimized Varicol scheme, not only in productivity but especially in eluent consumption. Notice that $Q_I = Q_{max}$ for all steps of the flowrate modulation.

Run 4 shows that by combining Varicol and PowerFeed schemes into a single hybrid process, the productivity can be increased further with respect to those of the second and third runs. The increase, however, is only marginal. For this solution all constraints are again active and $Q_I = Q_{max}$ for all steps of the flowrate modulation. The optimized port configuration for this run is no longer a three-zone, open-loop configuration, as for the pure Varicol scheme; instead it is the usual four-zone, closed-loop configuration. The corresponding chronogram of port switching is depicted in the top-right schematic of Fig. 4.10.

In agreement with other authors [5, 20], the optimized asynchronous port switching increases the lengths of zones II and III and reduces those of zone IV and/or zone I. By increasing the lengths of zones II and III, the system can withstand more heavily loaded columns which allows for an increase in productivity. However, since zone IV was reduced in length, the eluent is less efficiently regenerated. Therefore, more fresh mobile phase is required to properly regenerate the adsorbent in zone I.

The desynchronization of port switching allows for the operation of certain low-column processes which both the classical SMB and PowerFeed schemes cannot handle. A typical example is a four-zone SMB process operated with only three columns. Run 5 was meant to illustrate this, but the optimized Varicol scheme turned out to be a three-zone, open-loop configuration, in accordance with the optimized solution obtained for run 2. The chronogram of port switching is depicted in the bottom-left schematic of Fig. 4.10. Note that the amount of stationary phase for this run was reduced by 25% with respect to the amount employed in the previous runs, because of the removal of one column. This configuration requires significantly more mobile phase than the classical four-column SMB process and only gives a marginal increase in specific productivity.

On the other hand, very good results are obtained when the three-column process is operated with the hybrid combination of Varicol and PowerFeed schemes.

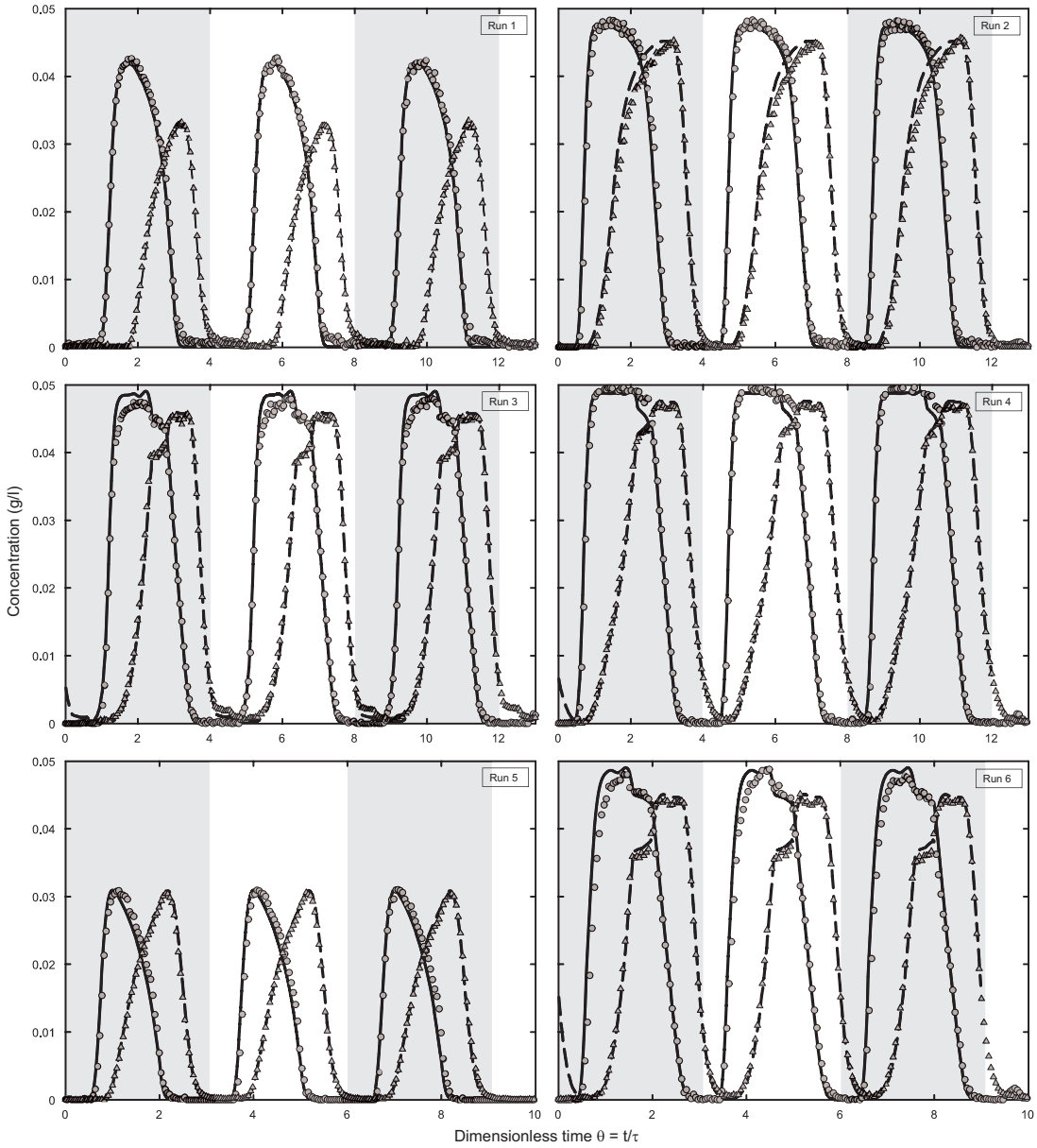

Figure 4.11: Experimental (symbols) temporal profiles of outlet effluent composition measured over three cycles of operation for the six optimized schemes listed in Table 4.5, and their comparison with the steady periodic solutions (lines) of the process model.

The results for this scheme are reported as run 6 in Table 4.5 and the corresponding chronogram of port switching is given in the bottom-right schematic of Fig. 4.10. This process has the highest specific productivity of all six runs, $Q_F/N = 2.13$ ml/min, which corresponds to a 121% increase with respect to the classical four-column SMB, and a low solvent consumption ($Q_E/Q_F = 2.35$). These results suggest that the combined use of Varicol and PowerFeed with a low number of columns may be a very promising process.

Figure 4.11 shows that all six configurations were successfully reproduced experimentally by our single-column setup. Each plot of Fig. 4.11 compares the experimental outlet effluent composition $\{c^i_{out}\}^{exp}$ with the steady periodic solution $\{c^i_{out}\}^{sim}$, obtained from the process model, for the duration of the experiment which spanned three cycles of operation. The agreement between experimental and simulated data is excellent for all cases. Note that each plot provides the steady periodic dynamics for a single column. The other columns would have similar dynamics, but shifted in time according to Eq. 3.8.

Note that the column whose behavior is reproduced experimentally, is the one whose upstream effluent has just been admixed with fresh mobile phase during the last switching interval of the cycle (for example, it is the right-most column in the chronograms of Fig. 4.10). Hence, it is the column whose steady periodic state at the start of every cycle is closer to that of a clean column. But this is precisely the state of the column at the startup of the experiment. Fig. 4.11 clearly shows that in the second cycle of each plot one have already attained the cyclic steady state.

Fig. 4.11 also provides evidence that the simulation model captures all essential features of the chromatographic process and that it can be confidently applied to explore other regions of the operational space. This is done in Fig. 4.12, where the Pareto optimal solutions for the six SMB schemes are compared. Each Pareto curve corresponds to the set of optimal solutions for a two objective optimization problem in which Q_F is to be maximized and Q_E has to be minimized, subject to a number of constraints. They were generated by carrying out a series of single-objective optimizations in which Q_F was maximized for progressively larger values of Q_E. They could also have been generated by minimizing Q_E for progressively larger values of Q_F. The symbols in Fig. 4.12 identify the six experimental runs

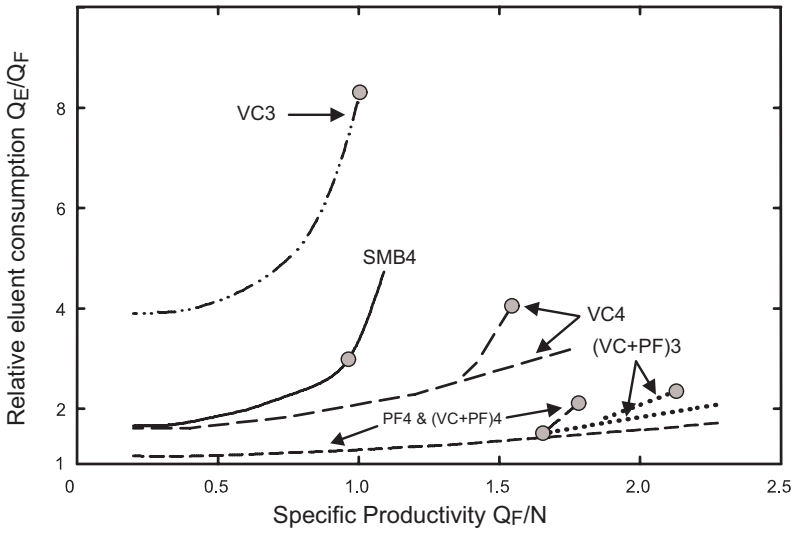

Figure 4.12: Pareto optimal solutions for the various SMB schemes analyzed in this chapter. The labeling is as follows: SMB, classical SMB process; VC, Varicol process; PF, PowerFeed scheme; VC+ PF, combination of VC and PF into a single hybrid scheme. The number attached to each label indicates the number of columns. The circles locate the experimental runs listed in Table 4.5. Two Pareto curves are drawn for each scheme: one for $Q_{\max} = 25$ ml/min, which ends on a circle, and the other for $Q_{\max} = \infty$, which extends to higher productivity values.

reported in Table 4.5; at those points the constraint on the maximum allowable flowrate is active.

Each Pareto curve represents the opposing objectives of maximizing productivity and minimizing solvent consumption for a given number of columns and operating scheme. Any point above the Pareto curve has worse performance than the points constituting the Pareto curve, because there is always one element of the Pareto set which has a lower solvent consumption for the same productivity. The points located below the Pareto curve are not feasible because the purity requirements are not fulfilled. When moving along the Pareto curve, each point is nondominant with respect to the others. The choice of a particular point in the Pareto curve over all other points requires additional considerations about

the problem, such as the overall separation cost and profit functions.

Fig. 4.12 also shows the extended Pareto curves for $Q_{\max} = \infty$ (unconstrained maximum flowrate), which for lower values of Q_F/N are superposable onto the previously discussed Pareto curves. This may be misleading for some of the SMB schemes, because it appears that there is a single Pareto curve, which bifurcates in the higher feed throughput region, when in fact there are two distinct curves. The reason for the apparent bifurcation is that there is a small region around the experimental point where the process can operate at lower Q_E/Q_F values if the constraint on $Q_{\max}$ is relaxed. For both the four-column SMB and three-column Varicol processes the superposition of the Pareto curves for $Q_{\max} = 25$ ml/min and $Q_{\max} = \infty$ gives rise to a single smooth curve. Note that the Pareto curves exist only in finite domains of the (Q_F/N, Q_E/Q_F) plane; for convenience their extents are not completely covered by the x- and y-scale of Fig. 4.12. Only the Pareto curve for SMB4 is displayed in its entirety. The extent of the domain enclosing a given Pareto curve is a measure of versatility of the corresponding operating scheme [38].

Overall, the results show that the best schemes are those whose flowrates are modulated. The hybrid combination of Varicol and PowerFeed applied to the four-column configuration gives little improvement over the flowrate modulation with synchronous port switching. It is possible that a more complex Varicol scheme than those considered here would perform better and bring the corresponding Pareto curve closer to the one for PowerFeed operation. On the other hand, the use of Varicol is a prerequisite to obtain a workable three-column scheme, which can be turned into a high-performance process by simultaneously modulating the flowrates. Furthermore, Varicol is a scheme which is easier and more robust to operate than flowrate modulation.

For a linear separation, the thermodynamic limit for the specific eluent consumption without adding energy to the system is $Q_E/Q_F = 1.0$ [39]. Fig. 4.12 shows that this limit is approached by the Pareto curves for the flowrate modulated schemes as Q_F/N approaches zero, despite the thermodynamic limit been obtained from an equilibrium analysis of the TMB model, which neglects finite mass-transfer resistances and assumes an infinite number of column partitions.

4.5 Summary

In this chapter, we have presented an experimental setup and procedure to experimentally reproduce the periodic state of multicolumn countercurrent chromatography with just one column. The feasibility of the proposed system has been demonstrated on the separation of two nucleosides using six different process configurations. Furthermore, we have investigated the performance of Varicol and PowerFeed processes, as well as their combination into a single hybrid scheme, both experimentally and by numerical simulation. The experimental feasibility and effectiveness of the various schemes were assessed by running and comparing optimized configurations in the proposed single-column setup.

A single-column experimental setup was employed to demonstrate the feasibility of the various schemes, explore the effect of their operating parameters, and illustrate the performance enhancements that are obtained by modulating the zone lengths or flowrates, or even the combination of both schemes. The simulated outlet effluent composition was in excellent agreement with the measured one for the six experimental runs reported here.

For the separation under study, the PowerFeed scheme always outperformed the classical SMB process and Varicol operating mode, both in productivity and eluent consumption. For very low feed throughputs the SMB and Varicol processes are coincident. At higher feed flowrates, the asynchronous scheme quickly diverges from a four-zone, closed-loop configuration toward a three-zone, open-loop process. Finally, it was shown that the Varicol scheme allows for the operation of three-column processes, which both the classical SMB and PowerFeed schemes cannot handle, and that its combination with PowerFeed in a single hybrid scheme can turn a three-column unit into a very competitive alternative.

Through the described single-column procedure, the process periodic state can be attained in a minimum number of cycles. Therefore, mobile phase and solute consumptions required to experimentally reproduce the periodic state of the equivalent multi-column process can be substantially reduced. The proposed system may be an economic, optimal manner of experimentally testing a set of operating conditions, or cycle policy, to achieve a given separation performance for a new multi-column chromatographic separation.

References

[1] D. Broughton, C. Gerhold, Continuous sorpion process employing fixed bed of sorbent and moving inlets and outlets, US Patent 2985589 (1961). 55

[2] M. Juza, M. Mazzotti, M. Morbidelli, Simulated moving-bed chromatography and its application to chiroyechnology, Trends in Biotechnology 18 (2000) 108–118. 55

[3] P. Adam, R. Nicoud, M. Bailly, O. Ludemann-Hombourger, Process and device for separation with variable-length, US Patent 6 136 198 (2000). 55

[4] O. Ludemann-Hombourger, R. Nicoud, M. Bailly, The varicol process - a new multicolumn continuous chromatographic process, Separation Science and Technology 35 (2000) 1829–1862. 55

[5] A. Toumi, F. Hanisch, S. Engell, Optimal operation of continuous chromatographic processes: Mathematical optimization of the varicol process, Industrial and Engineering Chemistry Research 41 (2002) 4328–4337. 55, 56, 77

[6] H. Schramm, M. Kaspereit, A. Kienle, A. Seidel-Morgenstern, Improving simulated moving bed processes by cyclic modulation of the feed concentration, Chemical Engineering Technology 25 (2002) 1151–1155. 55

[7] H. Schramm, M. Kaspereit, A. Kienle, A. Seidel-Morgenstern, Improved operation of simulated moving bed processes through cyclic modulation of feed flow and feed concentration, Chemical Engineering Science 58 (2003) 5217–5227. 55

[8] M. Kearney, K. Hieb, Time variable simulated moving bed process, US Patent 5102553 (1992). 55

[9] E. Kloppenburg, E. Gilles, A new concept for operating simulated moving-bed processes, Chemical Engineering Technology 22 (1999) 813–817. 55

[10] Y. Zang, P. Wankat, Smb operation strategy-partial feed, Industrial and Engineering Chemistry Research 41 (2002) 2504–2511. 55

[11] Z. Zhang, M. Mazzotti, M. Morbidelli, Powerfeed operation of simulated moving bed units: changing flow-rates during the switching interval, Journal of Chromatography A 1006 (2003) 87–99. 55

[12] Z. Zhang, M. Morbidelli, M. Mazzotti, Experimental assessment of powerfeed chromatography, AIChE Journal 50 (2004) 625–632. 55, 56

[13] Z. Zhang, H. Hidajat, A. Ray, M. Morbidelli, Multiobjective optimization of smb and varicol process for chiral separation, AIChE Journal 48 (2002) 2800–2816. 56

[14] J. Araújo, R. Rodrigues, J. Mota, Optimal design and operation of a certain class of asynchronous simulated moving bed processes, Journal of Chromatography A 1132 (2006) 76–89. 56, 73

[15] Z. Zhang, M. Mazzotti, M. Morbidelli, Continuous chromatographic processes with a small number of columns: Comparison of simulated moving bed with varicol, powerfeed, and modicon, Korean Journal of Chemical Engineering 21 (2004) 454–464. 56

[16] C. Y. Chin, N.-H. L. Wang, Simulated moving bed equipment designs, Separation and Purification Reviews 33 (2004) 77–155. 56, 75

[17] Y. Kawajiri, L. Biegler, Optimization strategies for simulated moving bed and powerfeed processes, AIChE Journal 52 (2006) 1343–1350. 56, 57

[18] G. Dünnebier, J. Fricke, K. Klatt, Optimal design and operation of simulated moving bed chromatographic reactors, Industrial and Engineering Chemistry Research 39 (2000) 2290–2304. 56

[19] A. Jupke, A. Epping, H. Schmidt-Traub, Optimal design of batch and simulated moving bed chromatographic separation processes, Journal of Chromatography A 944 (2002) 93–117. 56

[20] A. Toumi, S. Engell, O. Ludemann-Hombourger, R. Nicoud, M. Bailly, Optimization of simulated moving bed and varicol processes, Journal of Chromatography A 1006 (2003) 15–31. 56, 77

[21] K. Klatt, F. Hanisch, G. Dünnebier, S. Engell, Model-based optimization and control of chromatographic processes, Computers & Chemical Engineering 24 (2000) 1119–1126. 56

[22] E. Kloppenburg, E. Gilles, Automatic control of the simulated moving bed process for c8 aromatics separation using asymptotically exact input/output-linearization, Journal of Process Control 9 (1999) 41–50. 56

[23] K. Klatt, F. Hanisch, G. Dünnebier, Model-based control of a simulated moving bed chromatographic process for the separation of fructose and glucose, Journal of Process Control 12 (2002) 203–219. 56

[24] H. Schramm, S. Grüner, A. Kienle, Optimal operation of simulated moving bed chromatographic processes by means of simple feedback control, Journal of Chromatography A 1006 (2003) 3–13. 56

[25] S. Abel, G. Erdem, M. Amanullah, M. Morari, M. Mazzotti, M. Morbidelli, Optimizing control of simulated moving bedsexperimental implementation, Journal of Chromatography A 1092 (2005) 2–16. 56, 65, 66

[26] J. Mota, J. Araújo, Single-column simulated-moving-bed process with recycle lag, AIChE Journal 51 (2005) 1641–1653. 57

[27] R. Fourer, D. Gay, B. Kernighan, AMPL - a Modeling Language for Mathematical Programming, 2nd Edition, Brooks/Cole Thomson Learning, 2003. 57

[28] A. Wächter, L. Biegler, On the implementation of an interior-point filter line-search algorithm for large-scale nonlinear programming, Mathematical Programming 106 (2005) 25–57. 57

[29] R. Rodrigues, J. Araújo, M. Eusébio, J. Mota, Experimental assessment of simulated moving bed and varicol processes using a single-column setup, Journal of Chromatography A 1142 (2007) 69–80. 57

[30] R. Rodrigues, J. Araújo, J. Mota, Optimal design and experimental validation of synchronous, asynchronous and flow-modulated, simulated moving-bed processes using a single-column setup, Journal of Chromatography A 1162 (2007) 14–23. 57

[31] Y. Xie, S.-Y. Mun, N.-H. Wang, Startup and shutdown strategies of simulated moving bed for insulin purification, Industrial and Engineering Chemistry Research 42 (2003) 1414–1425. 62

[32] D. Ruthven, Principles of Adsorption and Adsorption Processes, Wiley, 1984. 69

[33] H. Haynes, P. Sarma, A model for the application of gas chromatography to measurements of diffusion in bidisperse structured catalysts, AIChE Journal 19 (1973) 1043–1046. 69

[34] G. Guiochon, S. Golshan-Shirazi, A. Katti, Fundamentals of Preparative and Nonlinear Chromatography, Academic Press, 1994. 69

[35] O. Ludemann-Hombourger, M. Bailly, R. Nicoud, Design of a simulated moving bed: Optimal particle size of the stationary phase, Separation Science and Technology 35 (2000) 1285–1305. 69

[36] M. Eusébio, Development of an universal interface for monitoring and control of chemical and biochemical processes, Ph.D. thesis, Universidade Nova de Lisboa (2006). 71

[37] Y. Kawajiri, L. Biegler, Nonlinear programming superstructure for optimal dynamic operations of simulated moving bed processes, Industrial and Engineering Chemistry Research 45 (2006) 8503–8513. 74

[38] G. Paredes, M. Mazzotti, Optimization of simulated moving bed and column chromatography for a plasmid dna purification step and for a chiral separation, Journal of Chromatography A 1142 (2007) 56–68. 81

[39] P. Wankat, Large-scale Adsorption and Chromatography, CRC Press, 1986. 81

5

Experimental Setup of a Compact and Flexible SMB Unit

In practical and simple terms, an SMB unit consists of input and output streams and a number of columns filled with a stationary phase. From the equipment design point of view, the valving system is the nucleus of the SMB operation because it determines the operational flexibility of a separation and its ability to apply various SMB schemes.

In chapter 2 many different schemes of SMB processes are illustrated. Each different scheme dictates different equipment requirement and posology. The major challenge in designing an SMB system is to maximize the flexibility and versatility in order to be able to accommodate the different modes of operation of classical and unconventional SMB processes. Besides being able to reproduce a whole class of operating schemes, such as changes in zone configuration or open-loop operations, an SMB unit must allow an easy adding/removal of the chromatographic columns or any additional modification of the unit. Another extremely important issues in all SMB units are contamination and dead volume problems; contamination may occur due to equipment leakage or by a simple bad design and dead volume plays a crucial role, specially in small-scale units, and may lead to poor productivity or even non-separation problems [1].

5.1 Compact SMB unit design

The main objective of this chapter is to describe the design and implementation of a compact SMB unit with only two columns; however, for further development we have decided that a three column setup is more suitable. Starting with the column distribution, the main goal is to minimize the tubing volumes between columns and at the same time maintain the system as symmetrical as possible; to achieve that all columns must split from each other the same distance and this distance must be small enough to minimize the volumes of the intercolumn connection but sufficiently large to allow an easy column replace operation. Because we are employing 3 columns, the most suitable column distribution, as shown in Figure 5.1, is to place them in the vertices of an equilateral triangle, this way all the columns span the same distance. Additionally, as seen in Figure 5.1, the columns were placed one column diameter in distance from each other which was found the suitable space for easy column exchange.

Because the system must be able to operate without some of the standard

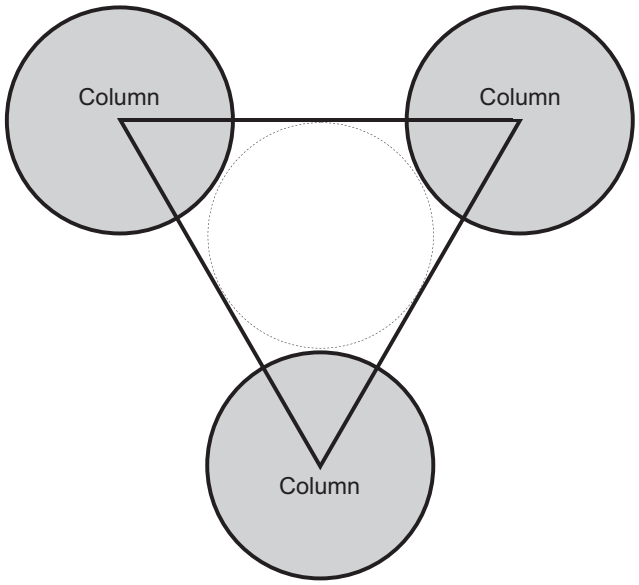

Figure 5.1: Column setup disposition - In order to achieve a symmetrical system, the disposition of the three columns is in a way to form an equilateral triangle.

zones of an SMB, particularly zone IV, the line between two adjacent columns, the so called node, has to be able to accommodate this feature. Figure 5.2(a) shows the position of the inlet/outlet lines when all four zones are brought together between two adjacent columns. The inlet line for the eluent stream is repeated twice, because it precedes the extract outlet port when zone I is suppressed, but follows the raffinate withdrawal port when zone IV is temporarily or permanently removed. However, in fact not all port configurations have to be realized in practice, for instance adding before collecting is not a logical happening since we are polluting or diluting the outlet line. Consequently, the node design can be simplified to the setup shown in Figure 5.2(b), where the outlet lines are placed before the inlet streams and between them an extra valve ensures for cases of total column output withdrawal (open-loop configurations). As seen in Figure 5.2(c), for the possibility of schemes with recycling streams or partial withdrawal an extra pump can be added to the node.

As said before, the valve design is an essential part of an SMB unit [1]. Different designs have been described in literature, but usually two major options are available: single rotary and on-off distributed valves. The single rotary valves, like the UOPs or ISEP valves (see Figure 5.3), consists of a unique central valve for the whole system. It is a more expensive and specialized design but has the big advantage of extreme minimization of the dead volume and contamination issues, however its only suitable for certain and predetermined SMB schemes and do not allow for asynchronous switching and scheme manipulation.

Since the developed system is far from being a standard SMB, one need a valve design that allows total and independent manipulation of the inlet/outlet lines to easily perform synchronous, asynchronous, open- or closed-loop schemes. In order to achieve that, the best solution is to place a two-way valve on each of the streams to independently control all process lines. This design have been used in several commercial SMB systems, like the NOVASEP varicol units or the JO process setups, it is the more versatile one and it presents the extra advantage of not having contamination problems since all lines are individually separated. However, it could lead to high dead volume problems since a high number of valves (at least four per column) and consequent tubing and connectors is needed,

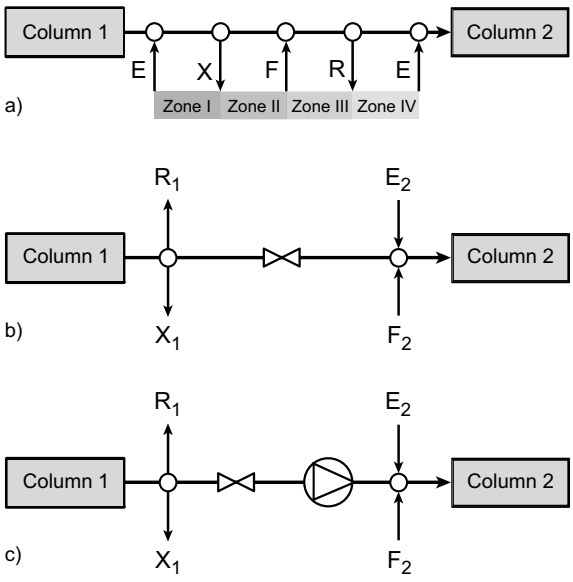

Figure 5.2: Schematic of (a) inlet/outlet lines when all four zones are brought together onto the junction between two adjacent columns, (b) node design for a simple two-column open-loop process, and (c) node design for a process with recycle and/or partial withdrawal. Notation is as follows: E, eluent inlet; X, extract outlet; F, feed inlet; R, raffinate outlet.

therefore minimization of the volume of connecting lines is essential, specially in this case of a small-scale unit.

The two-way valve design has been used for many application, such as sugar [2] and enantiomer [3] separations. Figure 5.4 shows the proposed piping and instrumentation diagram of the unit. As previously discussed it consists of three chromatographic columns interconnected in a way to form a closed loop, between each is placed the node with the connection of the inlet and outlet streams. Each node consists of two cross connections and one on-off valve placed between the outlet and the inlet junction and the UV cell is located on the outlet stream of column 1. Additionally, and not represented in Figure 5.4, there are two pumps that provide the eluent and feed streams. Furthermore, to allow closed loop operations one can easily place one or more extra pumps between the node valve and the inlet junction (actually it substitutes the node check valve).

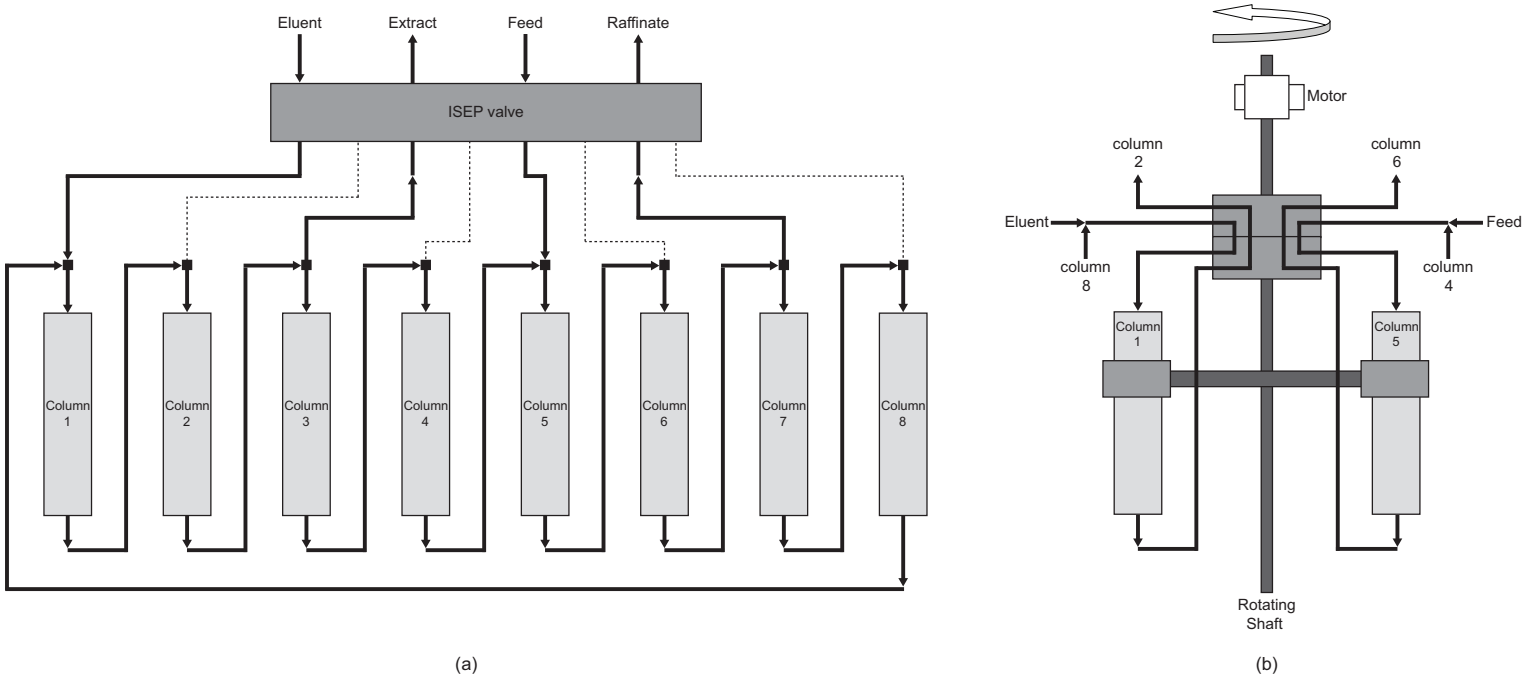

Figure 5.3: ISEP valve example [1]. In (a) a example of a setup comprising 8 columns with a central single rotary valve, these valve is very efficient however not very versatile since only allows a predetermined port scheme. In (b) a cutaway of the valve is presented.

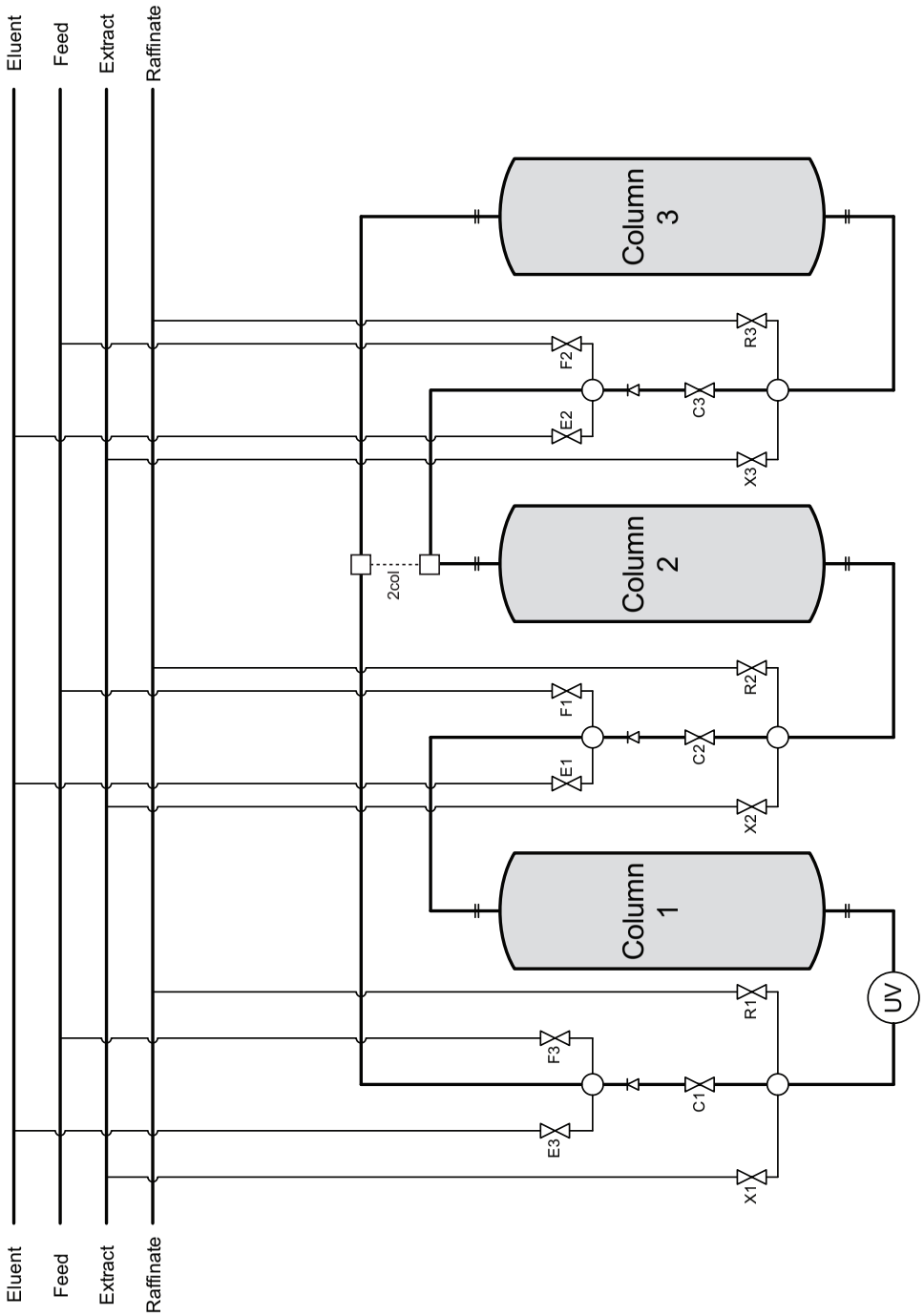

Figure 5.4: Diagram of process piping and instrumentation.

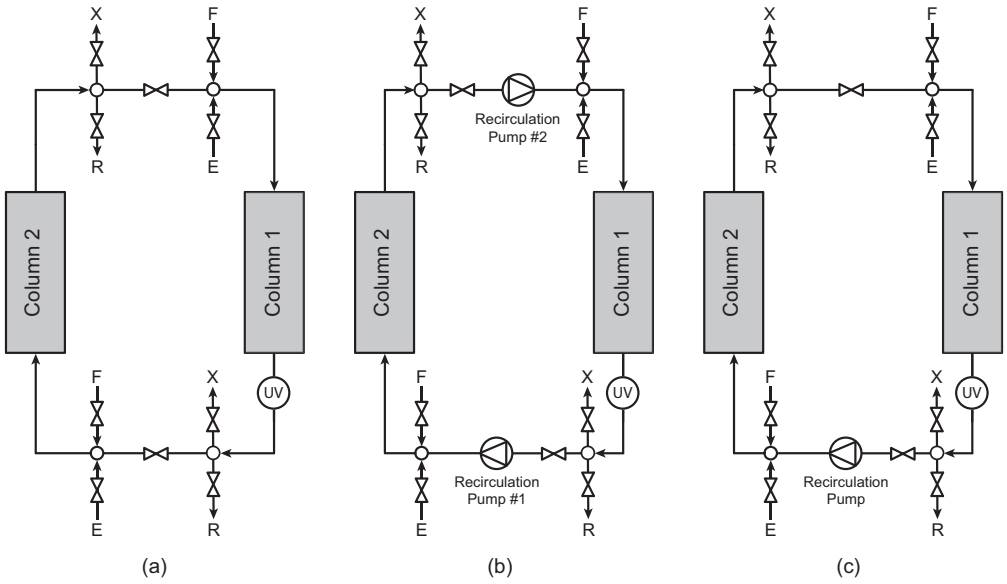

Figure 5.5: Various schematic diagrams of the two-column SMB unit. In (a) one has the design for open-loop configurations, for a process with partial withdrawal one apply the (b) design and for an open-loop scheme with a simple recycle step the (c) design is employed. These various potential designs show the versatility of the experimental setup.

As said before, easily the system can operate with only two columns by simply activating the "2col" line in Figure 5.4 and consequently eliminate column 3, resulting in the scheme shown in Figure 5.5(a). With the addition of an extra pump in order to allow recirculation steps one obtains the scheme represented in Figure 5.5(c) or with two spare pumps we can perform partial stream recycling from one column to the other (Figure 5.5(b)).

In summary, we obtained a flexible and simple practical setup which is capable of reproducing all known SMB schemes (of course limited to 3 columns); a photo of the experimental unit can be viewed in Figure 5.6.

However, in order to implement in practise the aimed setup, an accurate choose of all required equipment is essential. This problematic is discussed in the next section of this chapter.

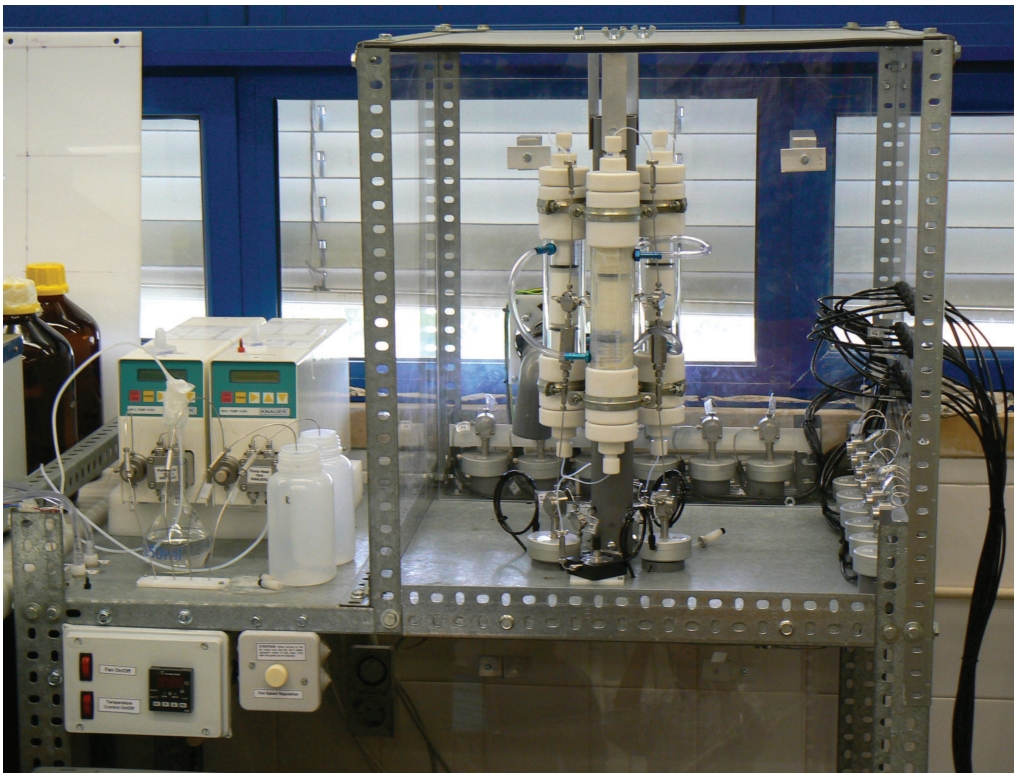

Figure 5.6: Picture of the built-up experimental unit.

5.2 Instrumentation

5.2.1 Pumps

If we consider the method that pumps use to move a fluid from a lower to a higher pressure, they can be classified into two major groups: rotodynamic centrifugal and positive displacement pumps (see flowchart of Fig. 5.7).

A centrifugal pump is a pump that uses a rotating impeller to increase the velocity of a fluid. The fluid enters the pump impeller along the rotating axis and is accelerated by the impeller, flowing radially outward into a diffuser or volute chamber, from where it exits into the downstream. Centrifugal pumps are used for large discharge and are commonly used in industrial piping systems.

Positive displacement pumps are one in which a finite volume of fluid is delivered for each cycle of pump operation. This volume is constant regardless of

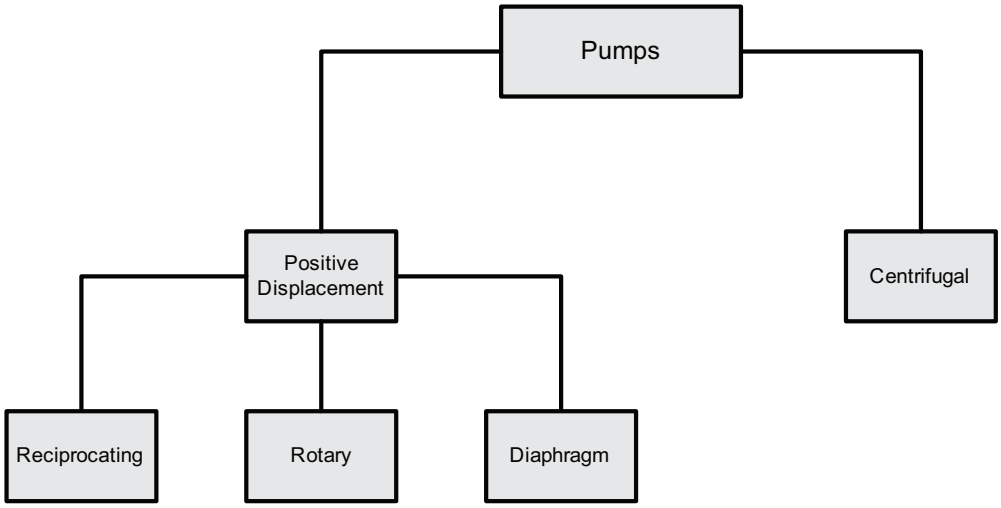

Figure 5.7: Flowchart representing the different types of pumps.

the resistance to flow offered by the system the pump is in (neglecting slippage effects), provided the capacity of the power unit driving the pump or pump component strength limits are not exceeded. The positive displacement pump delivers liquid in separate volumes with no delivery in between, although a pump having several chambers may have an overlapping delivery among individual chambers, which minimizes this effect. The positive displacement pump differs from centrifugal pumps, which deliver a continuous flow for any giving pump speed and discharge resistance.

All positive displacement pumps operate on the same basic principle: it consists of a single piston in a cylinder with a suction and a discharge port as shown in Figure 5.8; during the suction stroke, the piston moves to the left and liquid is admitted to the chamber; during the discharge stroke, the piston moves to the right and the volume of admitted liquid is pushed through the discharge port. The volume of liquid moved by the pump in one cycle (one suction and one discharge stroke) is equal to the change in the liquid volume of the cylinder. Regarding to how the displacement is obtained, a positive displacement pump can be further classified as: diaphragm, rotary or reciprocating pumps.

Diaphragm pumps are positive displacement pumps that use a combination of the reciprocating action of a thermoplastic or teflon diaphragm and suitable

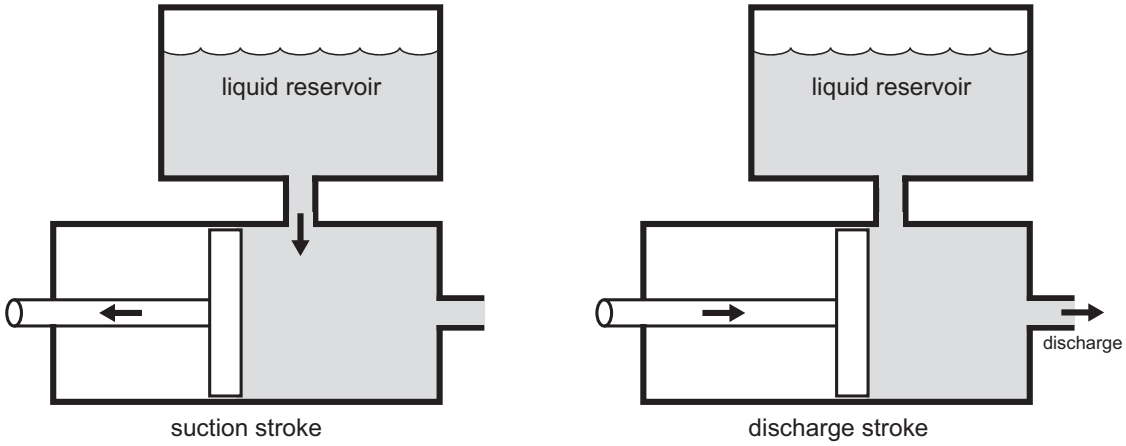

Figure 5.8: Positive displacement pump operation principle.

non-return check valves to pump a fluid. Sometimes this type of pump is also called a membrane pump. Mainly they are applied for pumping slurries with a moderate amount of solid content.

A rotary pump is a positive displacement pump that consists of vanes mounted to a rotor that rotates inside of a cavity to create the displacement. They are

Table 5.1: Technical data of the Knauer pump K-501.

Delivery system	Double-piston pump with main and auxiliary piston
Flow rate range	10 ml pump head: 0.001 − 9.999 ml/min (external control) 50 ml pump head: 0.01 − 49.99 ml/min
Flow accuracy	$< 1\%$ at 1 ml/min and 12 MPa
Residual pulsation	$< 1.5\%$ at 1 ml/min methanol:water (8:2) and 12 MPa
System protection	P_{min} and P_{max} adjustable
Maximum operating pressure	40 MPa (10 ml pump head) 15 MPa (50 ml pump head)
Control	RS232 interface
Power supply	90-260 V, 47-63 Hz, 100 W
Dimensions	105 x 185 x 345 mm (W x H x D)
Weight	3.9 kg

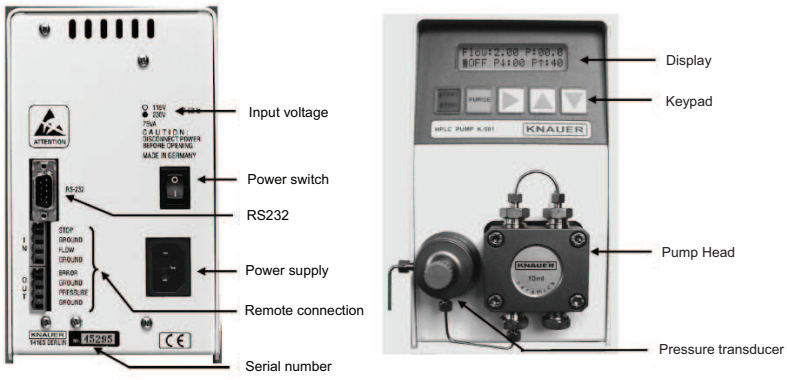

Figure 5.9: Picture of the used HPLC pump. All the pumps used in the system are Knauer K-501 pumps (Berlin, Germany) with 10 ml/min pump heads.

generally used in mid-range pressure applications or as vacuum pumps.

A reciprocating pump is a positive displacement plunger pump. It is often used where relatively small quantity of fluid is to be handled and delivery pressure is quite large. This type of pump was found to be the most suitable for our system since it handles small amounts of liquid but can be subject to high pressure (typical of preparative chromatography processes).

All the pumps used in the system are HPLC pumps K-501 from Knauer (Berlin, Germany) equipped with 10 (A4033) and 50 (A4034) ml/min capacity pump heads. A detailed description of the pumps technical data can be viewed in table 5.1. This type of pumps were chosen mainly for the simple reason that they largely eliminate the characteristic pulsing flow behavior present in many other reciprocating pump models due to a positive displacement head with a double-piston that works in a alternating way. They also have the advantage of having stainless steel pump heads which allows a broad variety solvents and a high operating pressure. Furthermore, it can be controlled in external mode through the RS232 protocol which is very handy for applying flow modulated processes.

5.2.2 Columns

The chromatographic column plays a central role in all chromatographic processes. In order to obtain an effective system, mainly the columns must ensure:

- Easy and flexible packing and repacking procedure.
- Efficient temperature control of the bed.
- Effective liquid injection and distribution through the chromatographic bed.
- Resistance to a broad class of liquid solvents and liquid flowrates.

All the columns chosen for this unit are Superformance hight performance glass columns from Götec Labortechnik (Merck company, Germany). A summary

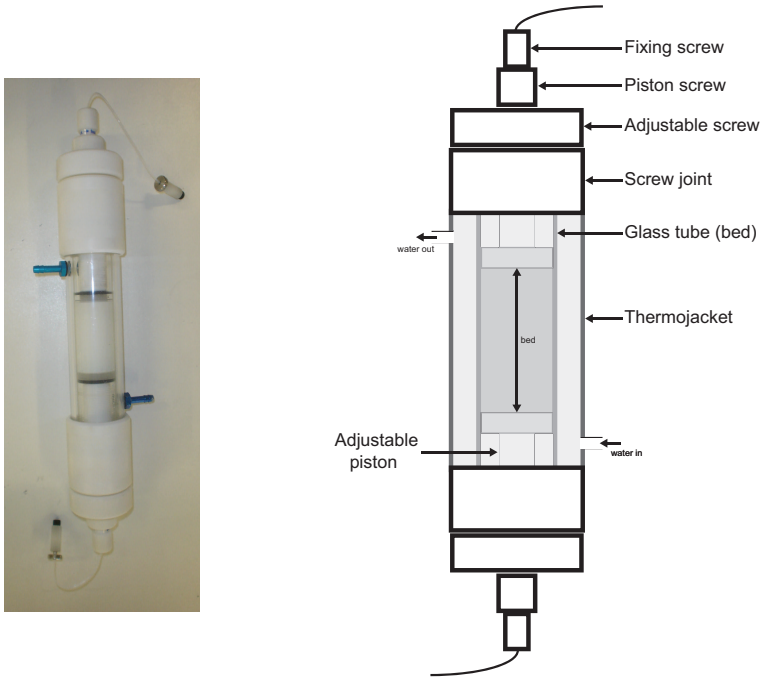

Figure 5.10: Picture and schematic diagram of a chromatography columns. The figure in the right presents a schematic representation of the column; i the left a real picture of the chromatographic column is showed.

Table 5.2: Chromatographic columns technical data sheet.

Model	Superformance glass-columns
Supplier	Götec Labortechnik
Supplier reference	G.20211 and G.20251
ID (mm)	10 and 26
Length (mm)	from 60 to 150
Maximum operating pressure	100 and 60 bar
Chemical resistance	resistence to aqueous and most organic liquids
Capillaries connections	1/16”

of the columns technical data can be viewed in Table 5.2. These are high performance glass columns that offer an effective system for chromatography analysis and method development. They are easy to handle, present an high flexibility and because it comprises an inert glass interior column it is chemical resistant to a large family of liquid solvents. Additionally, the use of glass aids in the control of the column bed height during packing by means of a piston design with a sealing lip and it guarantees good sample placement after injection with no dead volume problems directly above the bed. It presents also the flexility of being able to chose a bed height from 6 to 15 cm and a high pressure drop tolerance. Furthermore, the column incorporate a thermojacket which allows a efficient temperature control and stability by means of an external water bath system.

As described in Table 5.2, two different column models were used which are identical to each other and only differ in their internal diameter: ID of 1 and 2.6 cm.

5.2.3 Two-way valves and UV Detector

For the complete system a total of 15 individual two-way valves were used. The chosen equipment are air-actuated Valco high pressure on/off valves (ASFVO model from VICI Valco Instruments, USA) mainly because of its extremely low internal volume ($< 2\mu$l) and leak-tight operation up to 690 bar and 100°C. In

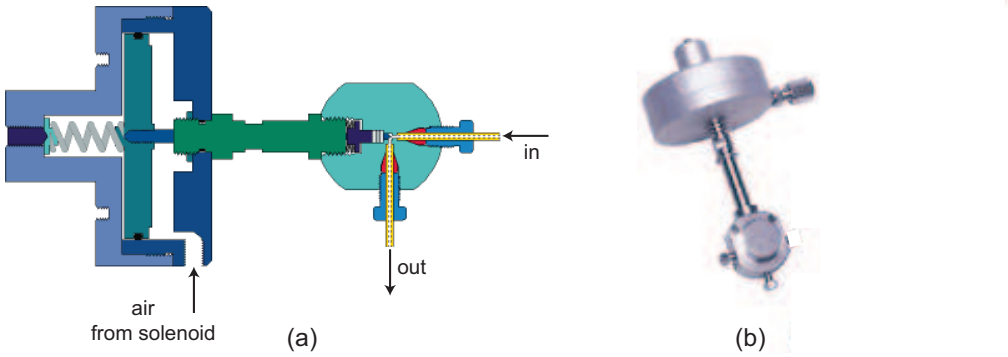

Figure 5.11: The two-way valves used in the setup are VALCO VICI air-actuated valves. In (a) one can see a cutaway of the valve; notice the solenoid connection system which opens the valve when is subjected to a 3.5 bar air pressure and is normally closed in the absence of pressure. In (b) one can see a real picture of the apparatus of the valve.

figure 5.11 (a) a cutaway of the valve is presented, it comprises of a special high strength alloy which is resistant even to buffer salts which might accidentally precipitate inside the valve, the seals are fluorocarbon with valve bodies machined from HPLC grade stainless steel that insures long lifetime in even the most demanding situations. The automated system uses a single three-way solenoid: application of around 3.5 bar opens the valve and a consequent venting of the air allows the spring to return the valve to the closed position. A real picture of one valve is showed in figure 5.11 (b).

For monitoring the outlet effluent composition from column 1 a multi-wavelength USB2000/4000 UV detector from Ocean Optics (Dunedin, FL, USA) equipped with a DH-2000-S-DUV light source (Micropack, Ostfildern, Germany) and variable light attenuator (FVA-UV, Ocean Optics, USA) was employed (same as used for the detection in chapter 4).

In Figure 5.12 (a) a schematic diagram of how light moves through the optical bench of the spectrometer is shown. Basically, the light which comes from the detection cell enters through the spectrometer by means of an optical fiber path in

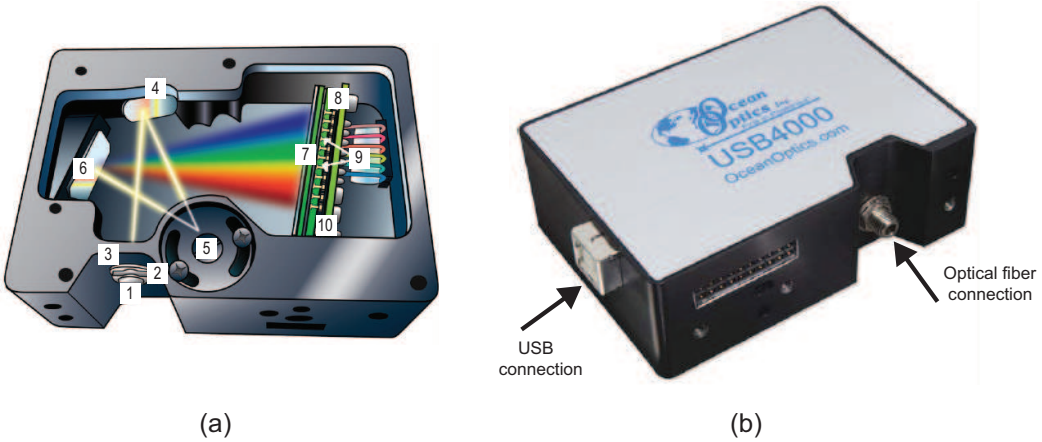

Figure 5.12: The used spectrometer is an USB4000 from Ocean Optics. In (a) is represented a schematic of the inside of the device and how light travels inside of it; in (b) a picture of the spectrometer is presented.

what is called the SMA connector (1), next passes in the slit (2) which regulates the size of the aperture (from 5 μm to 200 μm) to control the amount of light that enters the optical bench and then go through a filter (3) to restrict the light radiation to certain wavelength regions, after the light reflects off in the collimating mirror (4) onto the grating (5) in where is diffracted onto the focusing

Table 5.3: UV detector USB4000/2000 specifications

Detector	Toshiba TCD1304AP Linear CCD array
Sensitivity	130 photons/count at 400 nm
Data transfer	Full spectrum every 4 ms via USB 2.0 port
Wavelength range	200-1100 nm
Possible simultaneous wavelengths acquisition	3648 (USB4000), 2048 (USB2000)
Signal-to-noise ratio	300:1 (at full signal)
Integration time	3.8 ms - 10 seconds
Power consumption	250 mA @ 5 VDC
Dimensions	89 x 63 x 34 mm (W x H x D)
Weight	190 g

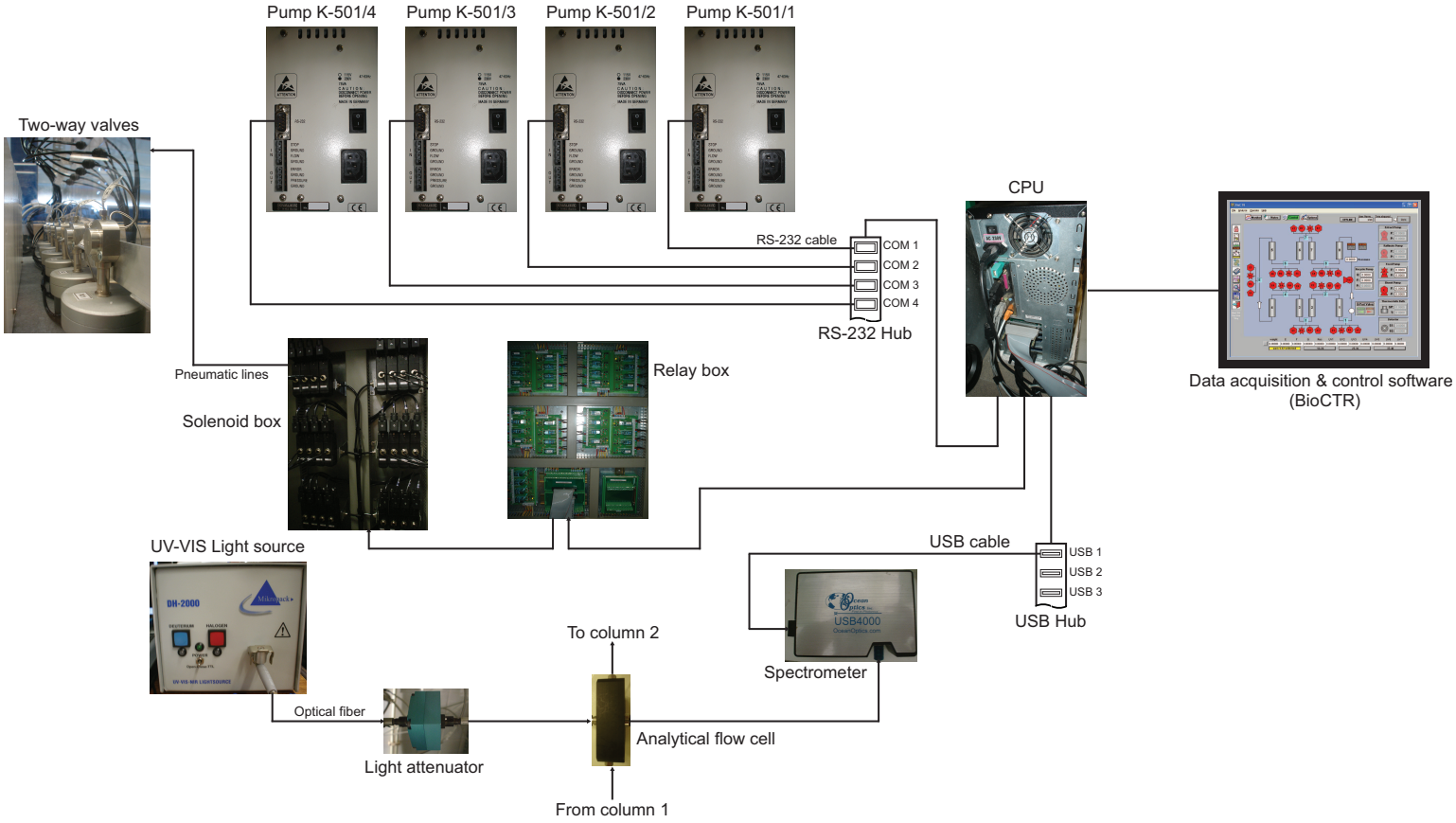

Figure 5.13: Wiring of the spectrometer, valve and pump system.

mirror (6) and next to the detector plane (7). In the detector (8) the the optical signal is converted to a digital signal that is transmitted to the software application via the USB connection protocol. Additionally, the spectrometer can have an extra filter called the OFLV (9) and an enhanced quartz window (10) to raise its performance.

On figure 5.12 (b) a simple picture of the aspect of an USB4000 UV detector is illustrated (the USB2000 model is similar).

As an example of how the valve and detection system functions a schematic diagram of the wiring is presented in figure 5.13.

5.2.4 Temperature Control

An efficient temperature control system is essential in order to reduce uncertainty on the adsorption parameters. The main objective is to maintain the operating zone with the most uniform and constant temperature as possible, to achieve that first one begin by limiting the unit area (column and main operating line) into a closed box since its more easy to temperature control the atmosphere temperature of a small area than of a large room.

The temperature of the system is controlled at two different points: in the columns and in the surrounding environment. In the columns the temperature

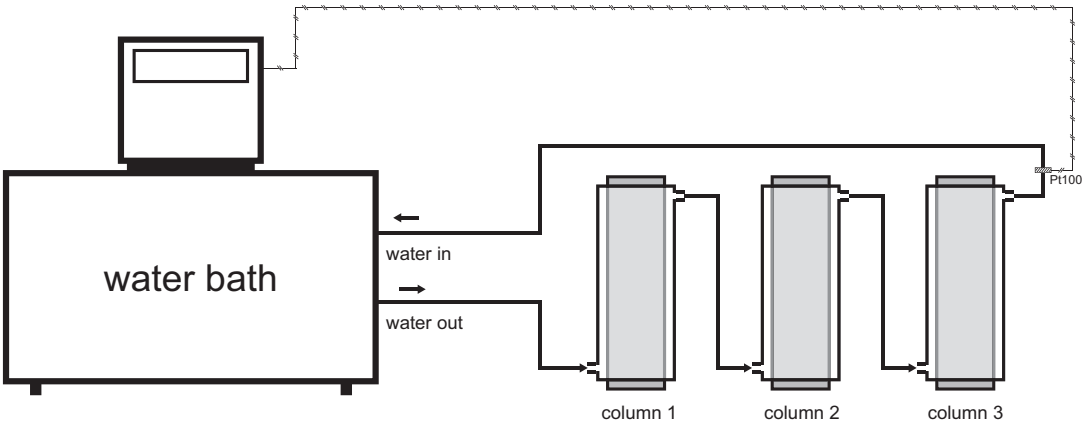

Figure 5.14: Temperature control scheme for the columns. It comprises of a standard water bath with an external Pt100 thermocouple measurement.

Table 5.4: Specifications of the equipment for the columns bed temperature control.

Water Bath	
Supplier	SELECTA Ultratherm PT (Spain)
Model	6000383
Temperature range	-20°C to 200°C
Accuracy	0.1% full scale
Temperature Probes (thermocouple)	
Supplier	RS Amidata (Spain)
Model	Pt100
Temperature range	0°C to 850°C
Accuracy	Class B: ± 0.12 Ω at 0.3°C

is ensured by means of a thermal controlled bath that pumps distilled water through the thermojackets of the columns. It consists of a standard thermal bath (model 6000383 from SELECTA Ultratherm PT, Spain) pumping water through the three columns in a series mode, the control is made by measuring the temperature of the water at the output of the third column by means of a Pt100 thermocouple. A simplified scheme of the water temperature control can be viewed in Figure 5.14.

A Pt100 temperature probe is a 4-wire temperature sensor with platinum resistance that exhibit a typical resistance of 100 Ω at 0°C; it consists of a thin film of platinum on a plastic film inside a stainless steel involucrum, and the relationship between resistance and temperature presents a relatively linear behavior. A description of the characteristics of the bath and the Pt100 probe is reported in Table 5.4.

Additionally, the air temperature inside the unit is also object of control. The simplified electric scheme of the air temperature control system is shown in Figure 5.16. One begin by placing another Pt100 thermocouple right in the middle of the three columns (see Figure 5.1) because there is where one want to more accurately control the temperature of the air; the temperature is registered in a PID digital control unit (model LDS491030000 from ERO ELECTRONIC)

which will trigger on a relay (the relay is placed for protection of the controller relative to electric spikes) accordingly to the decision flowchart of Figure 5.15, the relay will directly actuate on a standard resistance heater (100 W) that is connected in series with a permanently working constant speed fan (160 m^3/h) placed in a cross-section of the back panel of the unit box in a way that the fan will blow air to the inside. The basic idea is when the air temperature inside the unit is lower the our set-point temperature (Tsp) the system will turn on the heater which is being crossed by air coming from the fan, therefore the air will heat up and consequently raise the temperature inside the operating box, on the other case if the temperature is higher than our set-point the heater will remain off and the fan will blow room temperature air inside the unit hence decreasing the temperature inside. Additionally, as seen in Figure 5.16, a rheostat was placed in the fan line so that the rotating speed of it could be adjusted and two switches were added to be able to manually turn on and off both the heater (switch 2) and the fan (switch 1).

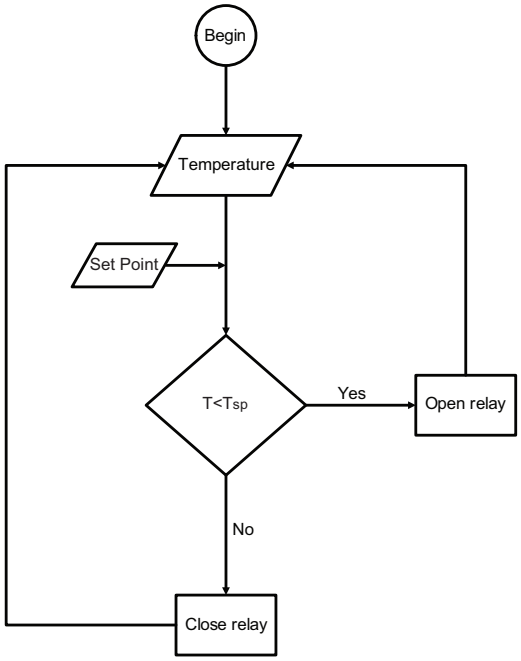

Figure 5.15: Air temperature control decision flowchart.

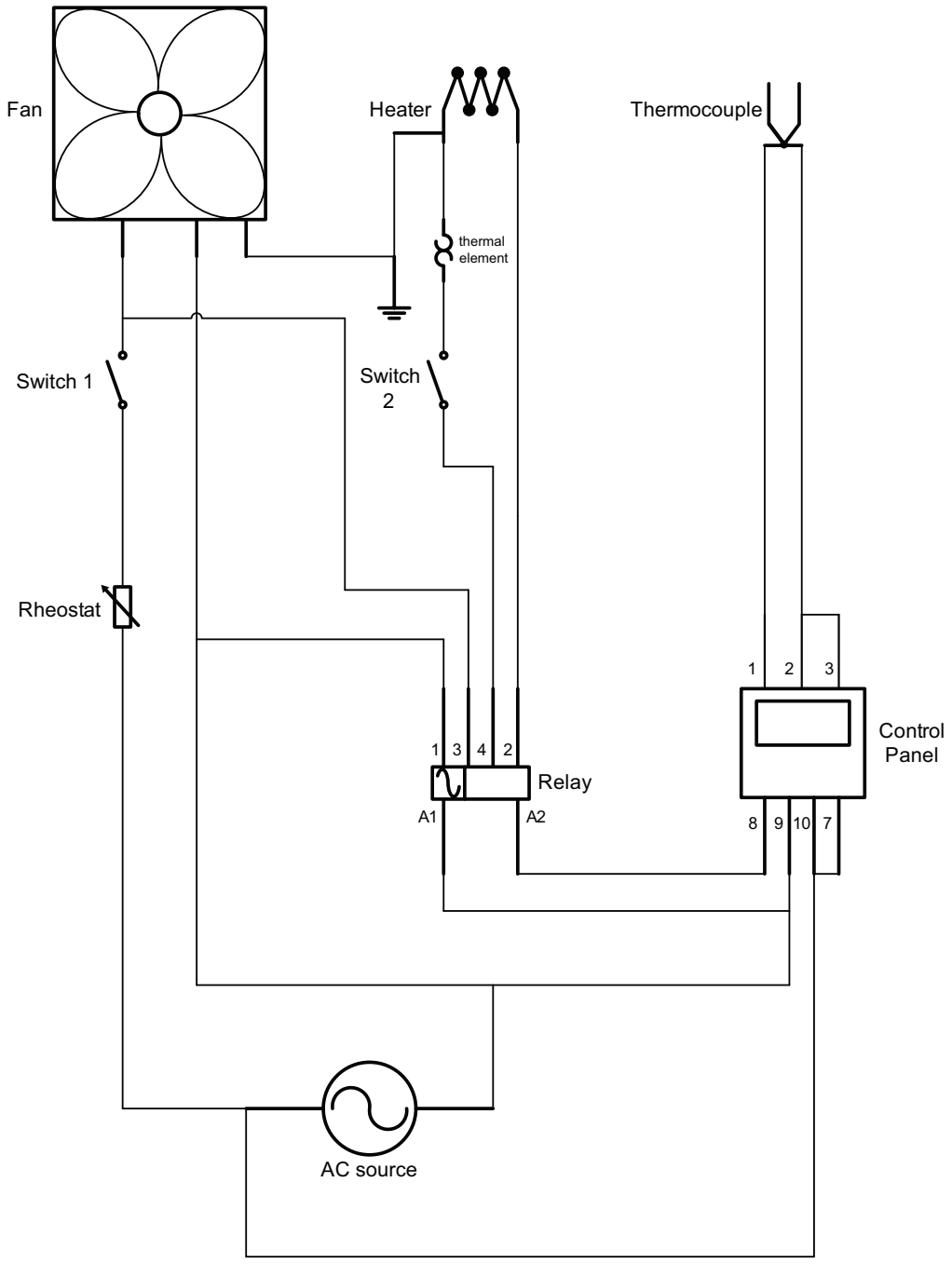

Figure 5.16: Electrical scheme of the air temperature control.

Table 5.5: Air temperature control equipment specifications.

Heater	
Supplier	RS Amidata (Spain)
Model	282-1045
Power	100 W
Air Fan	
Supplier	RS Amidata (Spain)
Model	211-9314
Air Flowrate	160 m^3/h
Speed	2650 rpm
Power	19 W
Digital Controller	
Supplier	ERO Electronic
Model	LDS 491030000
Sampling time	500 ms
Accuracy	$\pm$0.3 fsv $\pm$1 digit @ 25C
Temperature drift	$<$ 200 ppm/°C of fsv selected
Algorithm	PID

5.2.5 Other equipment

All capillaries, t- and cross-connectors and various fittings are from Knauer (Berlin, Germany). The pneumatic connecting system was supplied from Legris (France) and the electronic relay control board was provided by Paralab SA (Portugal).

The CPU employed for the automation of the unit is a typical Intel Pentium IV processor with 1 Gb of RAM and the connection to the relay system is made via a PCI board (model PCI-6509 from National Instruments). A resume of the characteristics of these equipments can be found in Tables 5.6 and 5.7.

Table 5.6: Capillaries and fittings specifications.

Capillaries and fittings	
Dimensions	1/16" OD and 0.7 mm ID
Supplier	Knauer (Berlin, Germany)
Supplier references	A0133, A0121, A0120 and A0117

Table 5.7: Hardware Equipment specifications.

CPU unit	
Processor	Intel Pentium IV 3.2 GHz)
RAM	1 Gb DDR2
Hard-drive	160 Gb
Operating system	Windows XP SP2
Acquisition Board	
Model	PCI-6509
Supplier	National Instruments (USA)
Number of Digital Channels	96 8-bit I/O
I/O connector	100-pin female 0.050 series SCSI

5.3 Data control and acquisition software

In order to fully control and manipulate the experimental setup, a process automation system was developed in-house using LabView software (National Instruments, USA). The system is designed for real-time control and monitoring of chromatography systems and is discussed elsewhere [4].

Generally its a very versatile software that allows fully independent control and manipulation of all valves and pumps and it has integrated up to two spectrometer windows. A schematic flowchart of the of how the software operates is presented in Figure 5.18. Basically the software core is constituted by the bioCTR module which represents the user interface and is where one define our equipment drivers and impose the user preferences; externally, by means of a foreign library file, one can easily impose a process setup i.e. the valves scheme, flowrates profile and monitoring parameters. In the BioCTR unit, we can acquire and watch

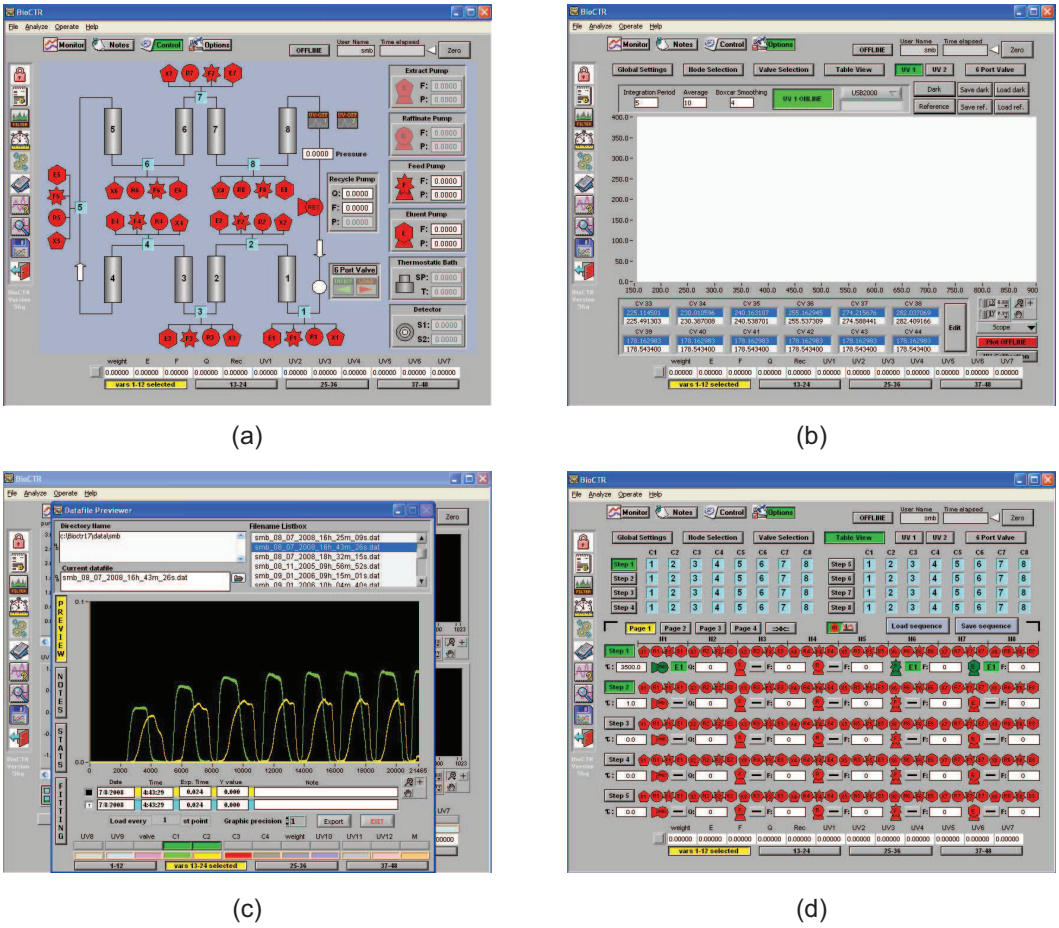

Figure 5.17: Snapshots of the monitoring window of the process automation system. In (a) is presented the main window of the software where one have represented the process scheme, pumps and valves with simultaneous actualization of the state (on/off and value); (b) is the UV spectrum window; (c) represents an example of the preview and exportation of the output Excel file; (d) is an extra process table where one can define a pre-determined scheme instead of using the external library file.

online (in the monitoring window) the evolution of the concentration profiles for the imposed SMB scheme. Furthermore, both the imposed parameters and the monitoring variables can be saved into a external Excel file.

Different snapshots of the BioCTR system are introduced in Figure 5.17.

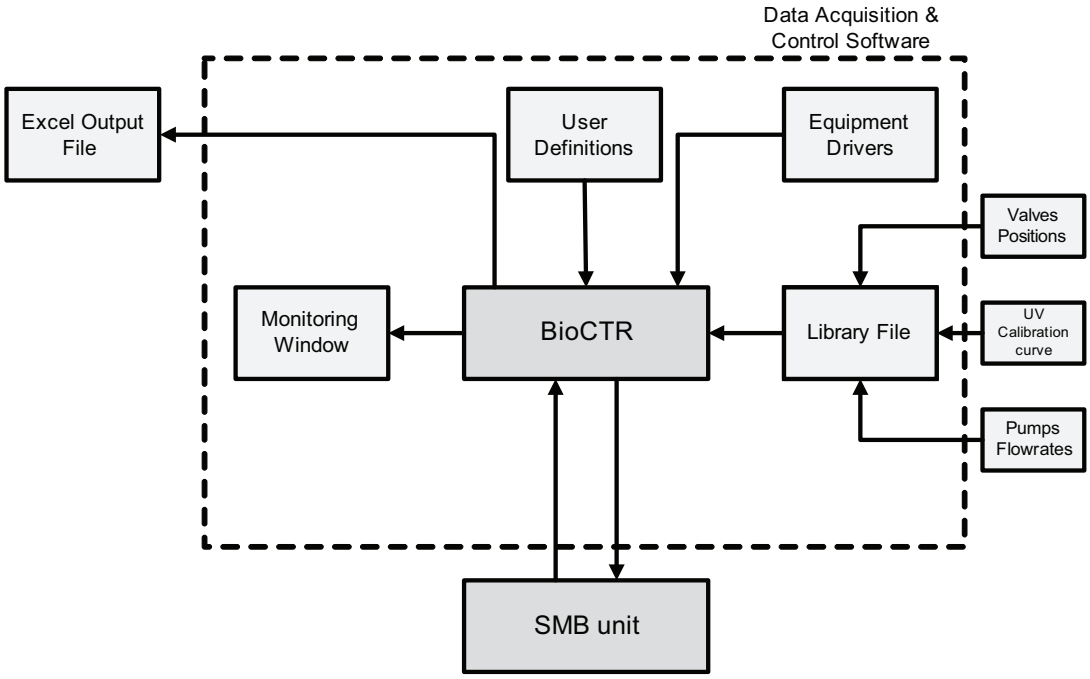

Figure 5.18: Data control & acquisition software flowchart.

References

[1] C. Y. Chin, N.-H. L. Wang, Simulated moving bed equipment designs, Separation and Purification Reviews 33 (2004) 77–155. xxvi, 87, 89, 91

[2] Y. Beste, M. Lisso, G. Waozny, W. Arlt, Optimization of simulated moving bed plants with low efficient stationary phases: separation of fructose and glucose, Journal of Chromatography A 868 (2000) 169–188. 90

[3] E. Cavoy, M.-F. Deltent, S. Lehoucq, D. Miggiano, Laboratory-developed simulated moving bed for chiral drug separations: design of the system and separation of tramadol enantiomers, Journal of Chromatography A 769 (1997) 49–57. 90

[4] M. Eusébio, Development of an universal interface for monitoring and control of chemical and biochemical processes, Ph.D. thesis, Universidade Nova de Lisboa (2006). 108

6

Two-Column Simulated Moving-Bed Processes for Binary Separation

6.1 Brief introduction

The increasing use of the SMB as a multipurpose unit in the pharmaceutical and fine chemistry industries has led to the development of novel cyclic operating schemes, some of which are substantially different from the conventional process. Broadly speaking, the new operating schemes introduce periodic modulations of selected control parameters into the operating cycle. Concepts such as asynchronous port switching [1, 2, 3], cyclic modulation of feed concentration [4, 5], time-variable manipulation of the flow rates [6, 7, 8, 9, 10], and solvent-gradient operation [11, 12, 13], have been thoroughly analyzed. The extra degrees of freedom available with these schemes improve the separation efficiency, thus allowing for the use of units with smaller number of columns. The advantages are apparent: less stationary phase is used, the set-up is more economic, and the overall pressure drop can be reduced. Furthermore, switching from one mixture to another is easier and takes less time than with more columns.

In the present chapter, the design of a two-column SMB system for binary separation is presented. Emphases is given to the use of two columns rather

than two zones, because with three or more columns it is always possible to implement a better SMB scheme which uses more zones with roughly the same ancillary equipment. In fact, running a two-zone configuration with three columns can be detrimental to the separation because the zone lengths become highly asymmetrical [14].

In this two-column process, both the port switching and the flow rates are modulated over the cycle. The feasibility and effectiveness of the proposed two-column processes are demonstrated experimentally on the linear separation of two nucleosides by reversed phase.

6.2 Two-column SMB process

The developed experimental unit to reproduce the two-column SMB scheme is described in detail in chapter 5. Generally speaking, if we consider the node scheme represented in Figure 5.2(c), one can reproduce several different node port configurations. Fig. 6.1 shows all the different port configurations that can

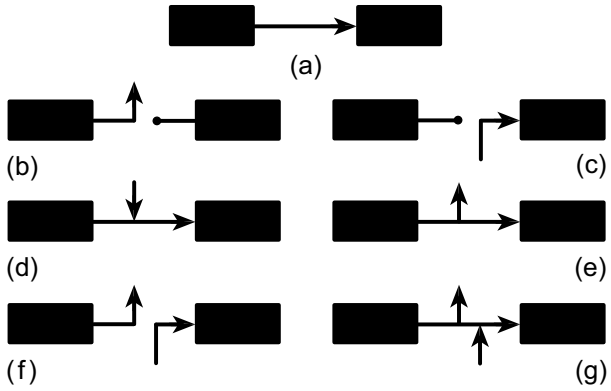

Figure 6.1: Flow diagram for the different types of port configuration that can be implemented with the proposed node design: (a) complete direction of flow to the next column, (b) downstream frozen bed, (c) upstream frozen bed, (d) flow addition to circulating stream, (e) partial withdrawal, (f) complete withdrawal and flow injection on the same node, and (g) partial withdrawal and flow addition at the same node. Steps b, c, and f, allow for open-loop operation.

be achieved with this node design. Streams can be partially or totally added or removed, or flown to the next column; an inlet port and an outlet port can be simultaneously open at the same node, and the flow through a column can be temporarily frozen. These port configurations can be thought of as the building blocks for establishing the cyclic operating scheme for the proposed two-column process.

A schematic diagram of the proposed setup is shown in Fig. 5.5(b). Overall, our base system employs two inlet pumps for supplying feed and eluent to the system, two internal recirculation pumps to manipulate the flow rate of stream that is directed from one column to the next, and 10 two-way valves to control the port switching. The used pumps have 10 ml pump heads, and are controlled via RS232 communication protocol. The experimental setup is fully automated and driven by an in-house developed automation system [15].

6.3 Procedure for optimal cycle design

Because the two columns are assumed to be identical, the cycle can be divided into two steps of equal length, τ, where τ is equivalent to the switching interval of a standard SMB. At the end of each step, i.e. every τ time units, the inlet/outlet ports are switched, and the columns, as well as the two internal pumps, reverse roles.

To achieve maximum process performance, the flow rates (feed, eluent, and two internal pumps) are fully modulated in time. This will usually give rise to better productivity and less eluent consumption than a simpler partial-feed strategy. For simplicity, the τ-periodic modulations implemented in the present work are piecewise constant. In practice, each step of the cycle is divided into a given number n_{Q} of subintervals of equal length, and the flow rates are kept constant over each subinterval before jumping discretely to different values over the next subinterval. The same assumption applies to the port configuration.

A rigorous model-based optimization approach [16] is employed to determine the optimal operating scheme. The purpose of the optimization procedure is to guarantee the fulfillment of product and process specifications, such as minimum

purities and maximum operating flow rates, while optimizing process performance in terms of productivity and eluent consumption.

The adopted formulation does not explicitly track the port switching over the cycle; instead, the status of the two-way valves is inferred from the piecewise-constant flow-rate profiles. For example, if in Fig. 5.2(c) $F_j = 0$ over a subinterval of the step then the two-way valve that connects the feed pump to the inlet of column j is closed, otherwise it is opened. Similarly, if $Q_j = 0$ or $X_j + R_j = Q_j$ then the two-way valve near the inlet of the internal recirculation pump located downstream of column j is closed, otherwise it is opened. This formulation is highly flexible and has the advantage of eliminating the integer nature of the design problem, since the only remaining degrees of freedom are the switching interval and time-variable flow rates.

At each step of the flow-rate modulation, the following basic conditions must be fulfilled:

$$0 \leq E_j \leq Q_{\max}, \quad X_j \geq 0, \quad 0 \leq F_j \leq Q_{\max}, \quad R_j \geq 0, \tag{6.1}$$

$$0 \leq Q_j - X_j - R_j \leq Q_{\max}, \tag{6.2}$$

where $Q_{\max}$ is the capacity of the installed pumps. These constraints guarantee that the solution is physically realizable. Eq. 6.2 prevents product from being withdrawn at a higher flow rate than that provided by the column and sets the maximum flow rate for the two internal recirculation pumps.

Product quality is enforced through the following constraints:

$$P_{\mathrm{R}} \geq P_{\mathrm{R}}^{\min}, \quad P_{\mathrm{X}} \geq P_{\mathrm{X}}^{\min}, \tag{6.3}$$

$$R_{\mathrm{R}} \geq R_{\mathrm{R}}^{\min}, \quad R_{\mathrm{X}} \geq R_{\mathrm{X}}^{\min}, \tag{6.4}$$

where P and R denote product purity and recovery, respectively, and the 'min' script their minimal admissible values; these performance variables are defined

in Figure 6.2. In a first instance the objective function, f_{obj}, is chosen to be the maximization of productivity, or feed throughput:

$$f_{\text{obj}} = \max \overline{F}, \quad \overline{F} = \int_0^1 (F_1 + F_2)\, d\theta = \int_0^2 F_j\, d\theta, \tag{6.5}$$

where $\theta = t/\tau$ is a dimensionless time coordinate and $\overline{F}$ is the average feed

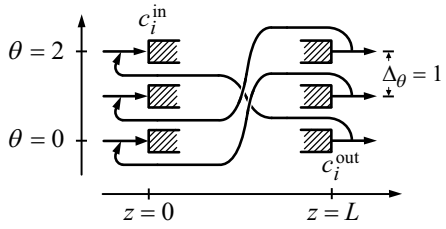

Dimensionless time coordinate:

$$\theta = t/\tau, \quad \theta' = \theta \bmod 1, \quad \overline{\theta} = \theta \bmod 2$$

Computational domain:

$$\Omega = \Omega_z \times \Omega_\theta, \quad \Omega_\theta = [0, 2], \ \Omega_z = [0, L]$$

Formulate column model with cyclic condition:

$$c_i(z, 2) = c_i(z, 0), \ q_i(z, 2) = q_i(z, 0), \ \forall z \in \Omega_z$$

Condition for simulated countercurrent (SCC) flow:

$$c_i(z, \overline{\theta+1}) = c_i(z, \theta), \ q_i(z, \overline{\theta+1}) = q_i(z, \theta), \ \forall z \times \theta \in \Omega$$

Overall node balance with embedded SCC condition:

$$(Q_E)_\theta = (Q - Q_F)_\theta + (Q_X + Q_R - Q)_{\overline{\theta+1}}, \ \forall \theta \in \Omega_\theta$$

Solute node balance with embedded SCC condition:

$$\left(Q c_i^{\text{in}} - Q_F c_i^F\right)_\theta = \left[(Q - Q_X - Q_R) c_i^{\text{out}}\right]_{\overline{\theta+1}}, \ \forall \theta \in \Omega_\theta$$

Physical realizability of the flow rates ($\forall \theta \in \Omega_\theta$):

$$Q_E \geq 0, \ Q_X \geq 0, \ Q_F \geq 0, \ Q_R \geq 0, \ Q_X + Q_R \leq Q$$

Extract (P_X) and raffinate (P_R) purities:

$$P_X = \frac{\int_{\Omega_\theta} Q_X\, c_2^{\text{out}}\, \mathrm{d}\theta}{\int_{\Omega_\theta} Q_X\, (c_1^{\text{out}} + c_2^{\text{out}})\, \mathrm{d}\theta}, \quad P_R = \frac{\int_{\Omega_\theta} Q_R\, c_1^{\text{out}}\, \mathrm{d}\theta}{\int_{\Omega_\theta} Q_R\, (c_1^{\text{out}} + c_2^{\text{out}})\, \mathrm{d}\theta}$$

Figure 6.2: Schematic diagram and main governing equations of single-column model that replicates the cyclic steady state of the two-column SMB process.

flow rate per cycle. However, we shall also address the more general case of multi-objective optimization in which productivity is to be maximized and eluent consumption is to be minimized.

To enforce the use of a single feed pump and a single eluent pump, the flow rates are also subjected to the following additional constraints:

$$F_1(\theta)F_2(\theta) = 0, \quad E_1(\theta)E_2(\theta) = 0. \tag{6.6}$$

The optimization problem is formulated with a single-column analog model that replicates the cyclic steady state of the two-column unit [17, 18], together with a full-discretization approach for steady period dynamics. For this purpose, a full-discretization (in both time and space) method is applied to the single-column model in which the time coordinate is discretized over a full cycle (2τ time units) and the CSS conditions are directly imposed [19]. The computational domain and governing equations are given in Fig. 6.2, together with a schematic diagram of the single-column model (see Figure 3.6).

Discretization is handled via collocation, using 15 cubic Hermite elements [20] for the spatial domain and $10N = 20$ Radau elements (with two interior points) for the time domain. The latter type of collocation elements is especially suitable for handling process dynamics with frequent discontinuities in time [21]. The flow rates remain constant over each Radau element, but are allowed to change discretely to different values across elements. This means that the largest number of subintervals that can be allocated per step for the piecewise-constant flow-rate modulation is $n_{\mathrm{Q}} = 10$. This is perfectly adequate for virtually every practical application, since higher resolutions have little impact on process performance.

As proposed by Kawajiri and Biegler [16, 21], the nonlinear programming problem obtained after discretization is formulated in AMPL [22] and solved using IPOPT 3.2.3 [23]. This solution strategy has been previously employed with success on a broad class of SMB problems [24]. IPOPT implements a primal-dual interior-point method, and uses line searches based on filter methods. It directly exploits first and second derivative (Hessians) information provided by AMPL via automatic differentiation.

In order to obtain the initial dynamic behavior of the process, after obtaining the optimal solution parameters, it is simulated in gProms (Process Systems

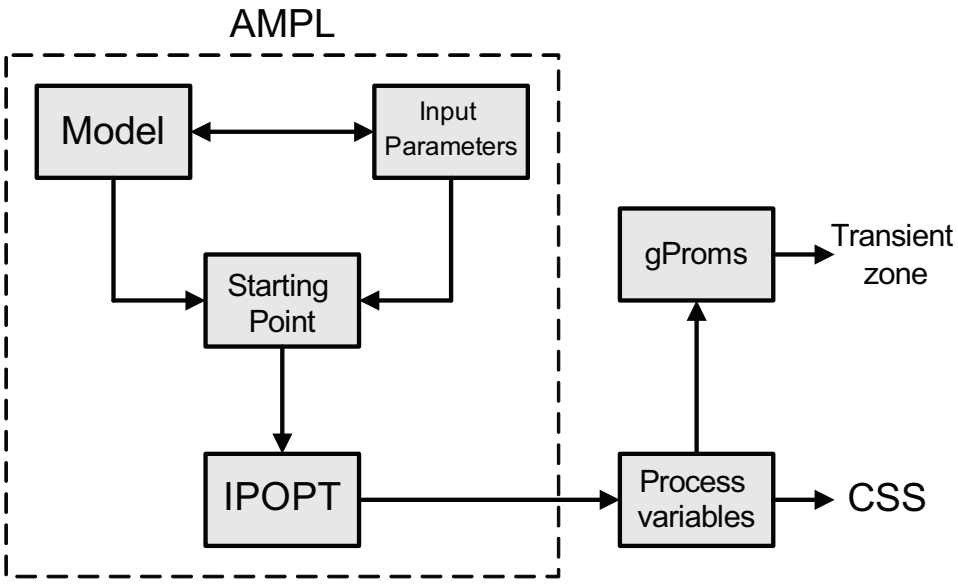

Figure 6.3: Optimization procedure flowchart. The optimal parameters are obtained for CSS conditions via a formulated AMPL [22] program and solved using the IPOPT [23] solver; after, for the initial transient zone of the process, the obtained optimal parameters are computed in a developed gProms code.

Enterprise Limited, London, United Kingdom) and the whole process data is obtained. A flowchart of the optimization procedure is shown in Fig. 6.3.

6.4 Materials and methods

To experimentally evaluate and demonstrate the feasibility of the proposed two-column process, the separation of two nucleosides uridine and guanosine on reversed-phase stationary phase was considered (for further details see chapter 4). The mobile phase was fixed at 5% (v/v) ethanol in water [25] and the system was operated isothermally at 25°C.

Uridine (99%) and guanosine (98%) were purchased from SigmaAldrich (Steinheim, Germany), and HPLC-grade ethanol (99.9%) from Panreac Quimica (Spain). The chromatographic columns are Superformance 26 mm I.D. thermojacketed glass columns. The stationary phase was slurry packed into each column to a bed

height $L = 6$ cm, with a flow rate of mobile phase of 25 ml/min, back-pressure of 30 bar, and 30 min packing time.

A multi-wavelength USB2000 UV detector (Ocean Optics, USA), equipped with a DH-2000-S-DUV light source (Micropack, Ostfildern, Germany) and attenuator, was employed for monitoring the outlet effluent composition from one of the columns. The individual nucleoside concentrations were obtained by deconvoluting the UV measurements taken at several suitably chosen wavelengths to provide a well-conditioned estimation procedure (as described in chapter 4). The sampling rate of the UV was fixed at 0.25 s^{-1}. An identical monitoring scheme was employed in the experiments for column characterization and estimation of adsorption parameters. In the preparative experiments the feed concentration was fixed at 0.05 g/l of each nucleoside to allow the use of the UV detector in the linear range of the calibration curve. The concentration limit imposed by the UV detector restricted the separation to the linear range of the adsorption equilibrium.

6.5 Characterization of adsorption equilibrium and band broadening

The chromatography column model employed is the equilibrium dispersed plug-flow model [26] previously described in chapters 2 and 4.

Prior to performing the preparative experiments, the porosity (interparticle void fraction, ϵ) of each column was estimated by measuring the retention time of

Table 6.1: Column dimensions and packing characterization based on the analysis of blue-dextran chromatograms.

Column	L (cm)	d (cm)	ϵ	Pe
# 1	6.0	2.6	0.320	738
# 2	6.0	2.6	0.317	742

diluted pulses of blue dextran (SigmaAldrich, Germany). Packing reproducibility was assessed by comparing the peak shapes and retention times of the chromatograms. The results, listed in Table 6.1, suggest that both columns were identically, and reasonably well, packed. It should be pointed out that the reported values of ϵ do not account for the contribution from extra-column volumes, since these were removed from the calculations by performing a blank experiment with an empty column.

The two columns were then connected in series by means of a very short junction and subjected to further pulse experiments for determining the Henry's constants, K_i, and coefficients, Pe_i and α_i, of the simplified van Deemter plot (Equation 2.12). The procedure consisted of fitting the column model (Equations 2.8, 2.10 and 2.11), with $L = 2 \times 6$ cm, to a series of experimental chromatograms obtained by injecting several diluted pulses (500 μl at 0.2 g/l) of each nucleoside at different liquid flow rates. The results are listed in the top rows of Table 6.2, and correspond to average values for the two columns. The interparticle porosity, $\epsilon = 0.349$, estimated from the blue-dextran chromatograms, is slightly larger than the one listed in Table 6.1, since it now includes the contribution from extra-column volumes. These parameters were then used in the design and optimization of the cycle for the two-column process.

6.6 Two-column SMB experiments

The optimal cycle for the two-column process was determined by solving the design problem with the chromatographic parameters listed in Table 6.2, subject to minimal extract and raffinate purity requirements, $P_{\mathrm{X}}^{\mathrm{min}} = P_{\mathrm{R}}^{\mathrm{min}} = 98\%$. Five subdivisions per step were allocated for the piecewise-constant modulation of the flow rates ($n_{\mathrm{Q}} = 5$), and Q_{max} was fixed at 9.5 ml/min, which is only 5% lower than the maximum capacity of the installed pumps. The optimized operating parameters are listed in the bottom rows of Table 6.2. Broadly speaking, the cycle can be classified as an open-loop 1/0/1/0 column configuration with partial feed and selective withdrawal. For this reason, the flow rates in Table 6.2 are reported in terms of the standard four zones of an SMB. The cycle is discussed in detail below, but before doing so we focus on its experimental validation.

Table 6.2: Adsorption parameters for the serial arrangement of the two columns, and corresponding optimal operating cycle for the two-column process. The parameter values for the NLP problem ($f_{\text{obj}} = \max \overline{F}$) are: $n_{\text{Q}} = 5$, $Q_{\max} = 9.5$ ml/min, $P_{\text{R}}^{\min} = P_{\text{X}}^{\min} = 0.98$.

$\epsilon = 0.349^a$		K	Pe	αL (s)	k (s^{-1})
Uridine (U)		1.397	744	0.108	1.85
Guanosine (G)		2.353	640	0.163	0.93
$N_{\text{I}}/\ldots/N_{\text{IV}}$	τ (min)	P_{X}		P_{R}	
1/0/1/0	2.70	0.98		0.98	
Step	Q_{I}	Q_{II}	Q_{III}	Q_{IV}	F	E
1	7.623	7.623	7.623	0.0	0.000	7.623
2	9.500	0.000	6.699	0.0	6.699	9.500
3	9.500	0.000	6.643	0.0	6.643	9.500
4	9.500	0.000	6.726	0.0	6.726	9.500
5	9.500	1.907	1.907	0.0	0.000	9.500
Average					4.014	9.125

Flow rates are expressed in ml/min. The Péclet numbers are reported for an individual column. [a]Determined from blue-dextran pulses.

The optimized two-column SMB scheme was reproduced experimentally over 10 operating cycles. Actually, the run could have been shorter since the cyclic steady state was attained in only 5 to 6 cycles. Figure 6.4 compares the experimental concentration profiles at the outlet of column 1, measured during the 10th cycle, with those predicted by process simulation. The symbols are the deconvoluted values of the multi-wavelength UV data, and are plotted at 1/15th of the experimental sampling rate for visual clarity. There is a clear mismatch between experimental and simulated profiles, but the shapes are qualitatively similar. This is not surprising, given that the porosity value listed in Table 6.2 does not account for the volumes introduced by the extra tubing, connecting tees, UV detector, and additional pumps present in the two-column setup. Extra-column volumes increase the residence time of solutes in the system, and their impact is

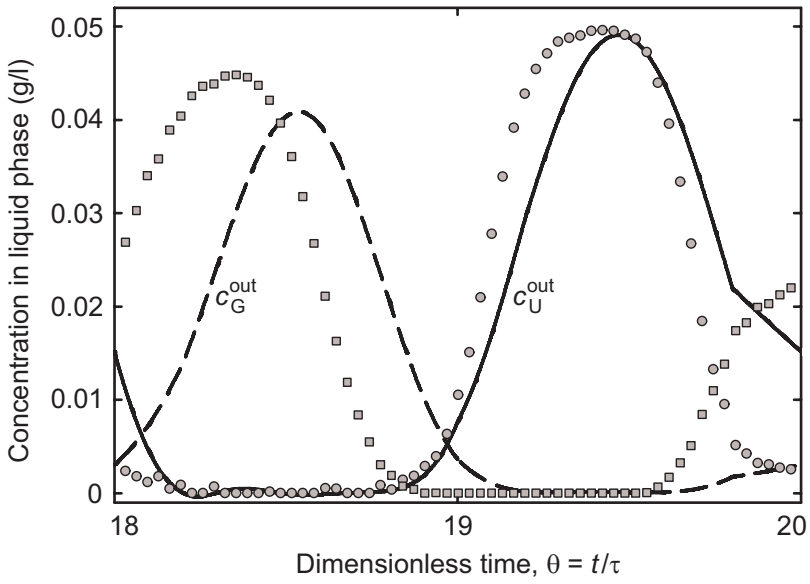

Figure 6.4: Solute concentration profiles at the outlet of column 1, measured over the 10th cycle of operation, for the optimized scheme listed in Table 6.2. Symbols denote experimental measurements (□, guanosine; ○, uridine), whereas lines represent the steady periodic solution of the process model. For visual clarity, only 1/15th of the UV measurements are plotted.

larger with decreasing solute retentivity. The product purity values, determined by post-processing the experimental data, are $P_X = 0.963$ and $P_R = 0.885$, which clearly do not meet the intended process specification.

To incorporate the effect of the extra-column volumes, the steady periodic solution of the two-column process was fitted to the experimental composition profile shown in Fig. 6.4, with the interparticle porosity, ϵ, as an adjustable parameter. The Henry constant for the less-retained nucleoside (uridine) was also slightly altered to provide a better fit of the experimental profile. The adjusted values of the column parameters are listed in Table 6.3. The value of ϵ was increased from 0.349 to 0.445, and K_U was reduced by only 3.4%. Figure 6.5 demonstrates that the agreement between the experimental concentration profiles and those predicted by the simulation model improved considerably for the newly estimated values of the chromatographic parameters.

Table 6.3: Readjusted values of chromatographic parameters and corresponding optimal operating cycle for the two-column process. The parameters were estimated by fitting the steady periodic solution of the two-column model to the composition profile plotted in Fig. 6.4 for the cycle defined in Table 6.2. The NLP problem is the same as in Table 6.2.

$\epsilon = 0.445$		K	Pe	αL (s)	$k(s^{-1})$
Uridine (U)		1.350	744	0.108	1.87
Guanosine (G)		2.353	640	0.163	0.93
$N_{\mathrm{I}}/\ldots/N_{\mathrm{IV}}$	τ (min)	P_{X}		P_{R}	
1/0/1/0	2.70	0.98		0.98	
Step	Q_{I}	Q_{II}	Q_{III}	Q_{IV}	F	E
1	7.395	7.395	7.395	0.0	0.000	7.395
2	9.500	0.000	6.723	0.0	6.723	9.500
3	9.500	0.000	6.666	0.0	6.666	9.500
4	9.500	0.000	6.739	0.0	6.739	9.500
5	9.500	1.878	1.878	0.0	0.000	9.500
Average					4.026	9.079

It is worth mentioning that this fitting procedure is one of several possibilities within a more general approach for isotherm estimation by the inverse method based on experimental SMB data. For the process under analysis, this approach is particularly appealing because the cyclic steady state is attained in a small number cycles, thus leading to an inexpensive and quick estimation procedure.

The operating cycle for the two-column process was optimized for the newly adjusted values of the chromatographic parameters. The values of the switching interval and piecewise-constant flow rates are listed in the bottom rows of Table 6.3. Notice that their values were only slightly changed with respect to those listed in Table 6.2. The newly optimized scheme was experimentally reproduced in another 10-cycle run, and the measured composition profile at the outlet of column 1 was compared with the one predicted by process simulation. The

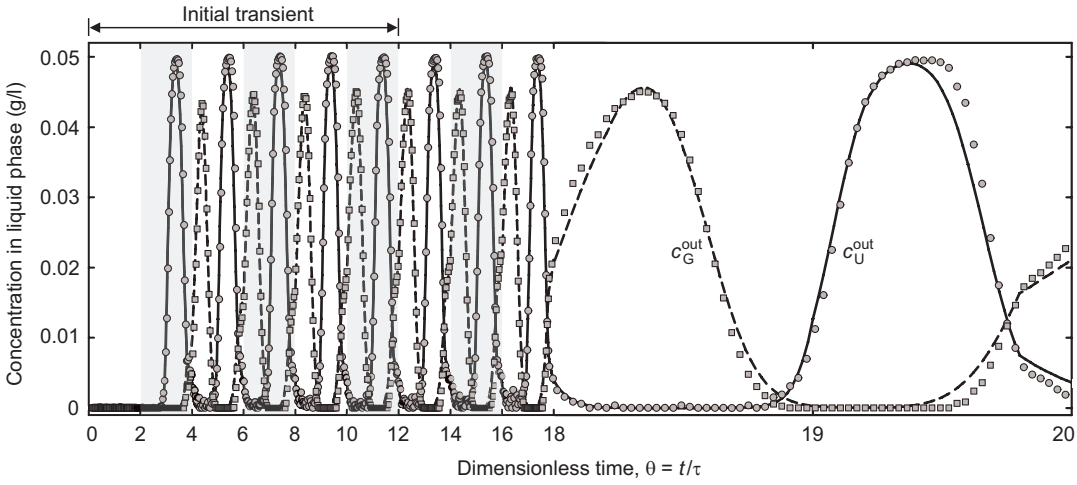

Figure 6.5: Solute concentration profiles at the outlet of column 1, measured over 10 cycles, for the optimized scheme listed in Table 6.2. Symbols denote experimental data (□, guanosine; ○, uridine), whereas lines represent the solution of the dynamic process model for the chromatographic parameters given in Table 6.3. For visual clarity, only 1/20th of the UV measurements are plotted for the first 9 cycles and 1/15th for the 10th cycle.

results are reported in Fig. 6.6, showing good agreement between the experimental and simulation data, although the experimental concentration profile of the more-retained nucleoside lags somewhat behind the simulation curve. Furthermore, and probably more significantly, the experimental purities, $P_X = 98.8\%$ and $P_R = 98.5\%$, are now within the desired specification.

6.7 Discussion

Figure 6.7 shows the movement of the internal concentration profiles within the two-column loop over half of the cycle, together with the positioning of the active inlet/outlet ports. The lower part of the Figure includes a graphical representation of the flow-rate modulation. To save space, only half the cycle is shown; the second half is identical but with the two columns exchanged.

The cycle can be viewed as an open-loop 1/0/1/0 column configuration with

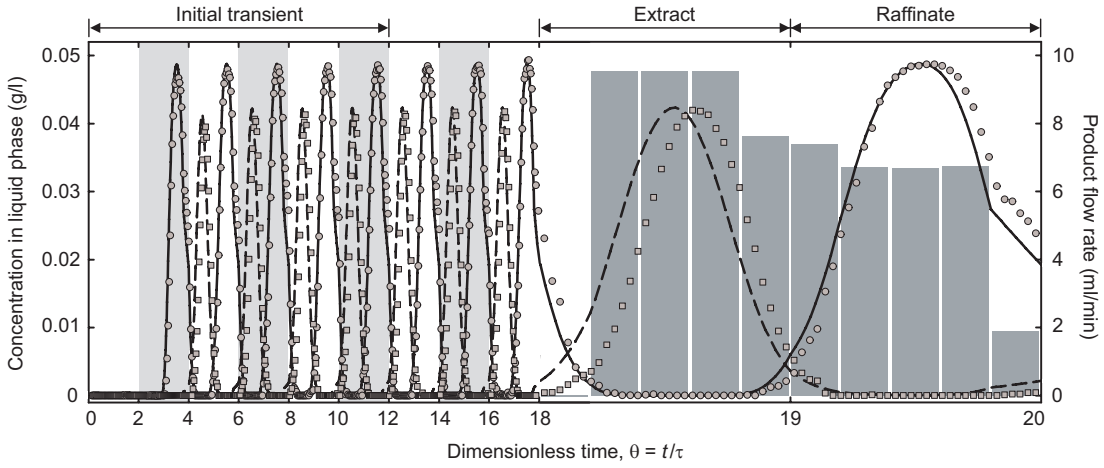

Figure 6.6: Solute concentration profiles at the outlet of column 1, measured over 10 cycles, for the optimized scheme listed in Table 6.3. Symbols denote experimental data (□, guanosine; ○, uridine), whereas lines represent the solution of the dynamic process model. The shaded bars represent the piecewise-constant flow rate modulation of the extract and raffinate streams. For visual clarity, only 1/20th of the UV measurements are plotted for the first 9 cycles and 1/15th for the 10th cycle.

partial feed and selective product withdrawal. There is no adsorbent allocated to zones II and IV. During the first step of the cycle, column 1 plays the role of zone I of a classical SMB, whereas column 2 plays the role of zone III; the recirculation pump located downstream of column 1 provides the flow rate for zone II, whereas the other internal pump gives the flow rate for zone IV. During the second step of the cycle, the two columns exchange zones as well as the two internal recirculation pumps. The more-strongly adsorbed nucleoside is recovered in pure form from the column which is being partially regenerated with fresh eluent. At the end of the step the leading band of the less-retained nucleoside touches the end of the column and is ready to be collected over the next step. The other column, on the other hand, is partially fed with fresh feedstock during 2/5th of the step.

An important aspect is that our two-column process is not a scheme where one can define a specific port configuration like in any typical SMB process. Due to our generalized approach based on flow modulation steps, one do not restrain

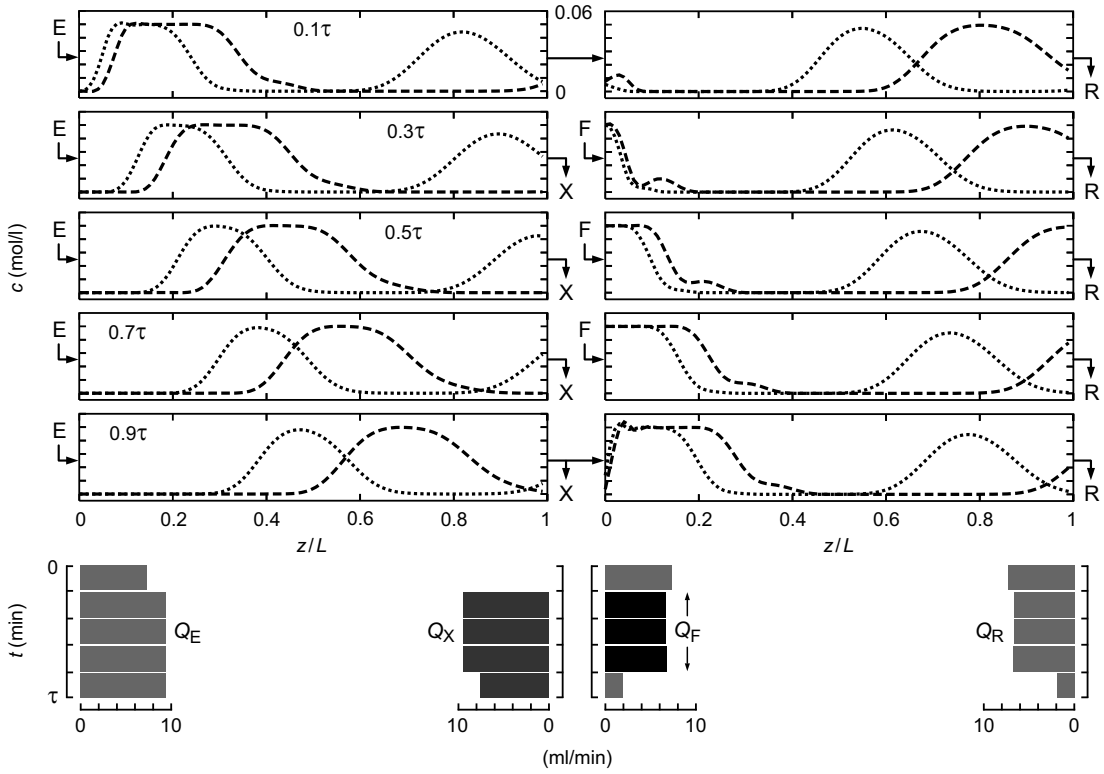

Figure 6.7: Positioning of the inlet/outlet ports, internal concentration profiles, and flow rates, over the first step of the cycle for the optimized scheme listed in Table 6.3. The plotted data are the steady periodic solution of the process model. The second step of the cycle is identical, but the two columns are exchanged. Symbols E, X, F, R, denote eluent, extract, feed, and raffinate, respectively.

our process into a rigid configuration, instead the configuration changes accordingly to the nature of the desired separation. Logically, for a more restrained separation the moving solutes will need a higher residence time in the system for the complete separation to occur. To evaluate the difficulty of a chromatographic separation, usually the value of selectivity $\alpha = K_2/K_1$ is used, where the separation is empirically classified as *hard* for $\alpha = 1.1$, *moderate* for α around 1.5 and *easy* for $\alpha = 4$ [27]. However this simple parameter does not always represent properly the real separation difficulty as in the case of small values of K_i, a better definition is [28]:

$$\alpha'_{21} = \frac{1 + \beta K_2}{1 + \beta K_1} \tag{6.7}$$

In our separation test case $\alpha'_{21} = 1.47$, which is considered a *moderate* difficult separation. One can evaluate the effectiveness of our process from a *easy* to a *hard* separation (i.e from a high to a low selectivity) by decreasing the value of α'_{21}, this means that the difference between the Henry constants K_i of both solutes is tending to zero. The general idea is to fix the value for the more retained

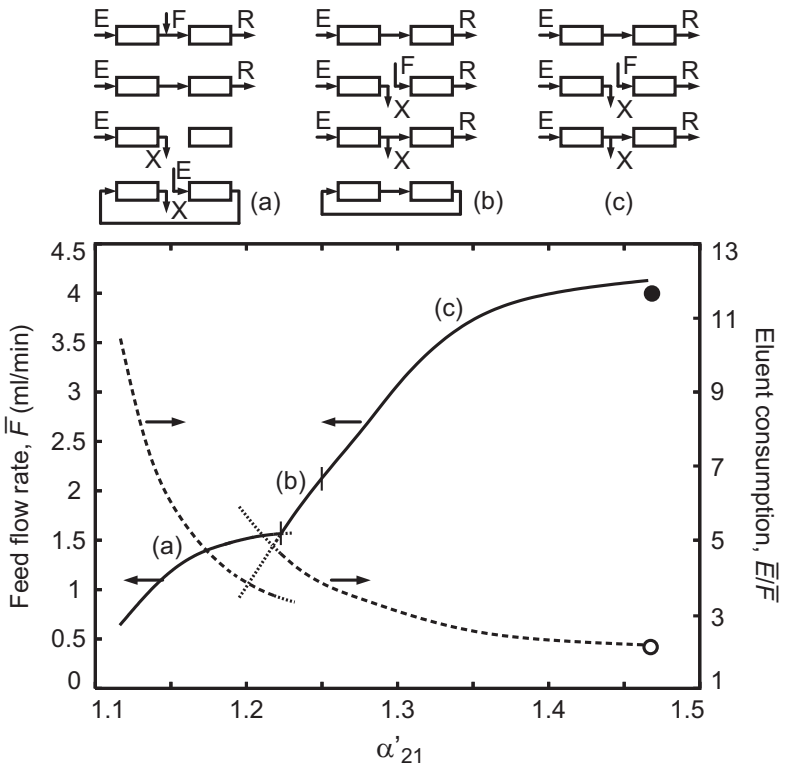

Figure 6.8: Optimal operating curves of the two-columns SMB process with 5 subdivisions step flowrate modulation for a range of lower selectivity separations than our experimental case. The dashed line represents the eluent consumption and the solid line feed throughput. The curves were drawn for product purity $\geq 98\%$ and $Q_{\max} = \infty$. On the top the influence of the separation selectivity on the process scheme. The closed circle identifies the feed throughput and the open circle the eluent consumption for the experimental cycle defined in Table 6.3.

compound and progressively increasing the Henry constant of the less retained solute to analyze how the process scheme changes accordingly to the productivity $\bar{F}$ and eluent consumption $\bar{E}/\bar{F}$. Figure 6.8 represents the optimal operating curves for a two-column process with 5 piecewise-constant steps flowrate modulation ($n_{\mathrm{Q}} = 5$) for a separation with a lower selectivity than our experimental case $\alpha'_{21} \leq 1.47$. The dashed line represents the eluent consumption $\bar{E}/\bar{F}$ and the solid line the Productivity $\bar{F}$. To obtain these curves the $Q_{\max}$ restriction was relaxed so one can represent absolute optimal operating curves in terms of Productivity and consumption. As expected, when the separation is progressively becoming more *hard*, i.e. α'_{21} is approaching 1.0, it is followed by a drastic decrease in feed throughput and a opposite increase on eluent consumption. Figure 6.8 shows that in terms of selectivity the operating curves can be divided into three different zones, denoted by (a), (b) and (c). Each zone correspond to a change on the configuration of the two-column scheme, represented in the schematic diagrams at the top of Fig. 6.8. Zone (c) correspond to the area where one can find our experimental run which represents, as stated before, an open loop configuration with three major steps. This scheme is the best till a $\alpha'_{21} = 1.25$, however as the separation starts to become more *hard*, the solutes need to recycle more in the system in order to achieve complete separation, creating an additional fourth step of a complete closed loop recycle in the process scheme, represented by zone (b). Continuing on decreasing the selectivity for values lower then 1.22 take us to zone (a) where the separation is becoming even more *hard*, here the configuration changes to a complete different four step open loop scheme. Curiously, a closed loop recycle step is no longer needed, but instead a step where one of the columns is frozen (i.e. there is no stream going in or out of the column) appears, this means that the separation is so constraint that one can not use all available stationary phase at the same time to enhance the separation, consequentially having a low productivity and a high eluent consumption.

In the more general case, optimal design of an SMB process is a two-objective optimization problem where productivity is maximized ($f_{\mathrm{obj},1} = \max \overline{F}$) and eluent consumption is minimized ($f_{\mathrm{obj},2} = \min \overline{E}$), subject to the same product quality requirements and operating restrictions as in the single-objective case. The solution to this problem can be expressed as a Pareto curve. The adopted

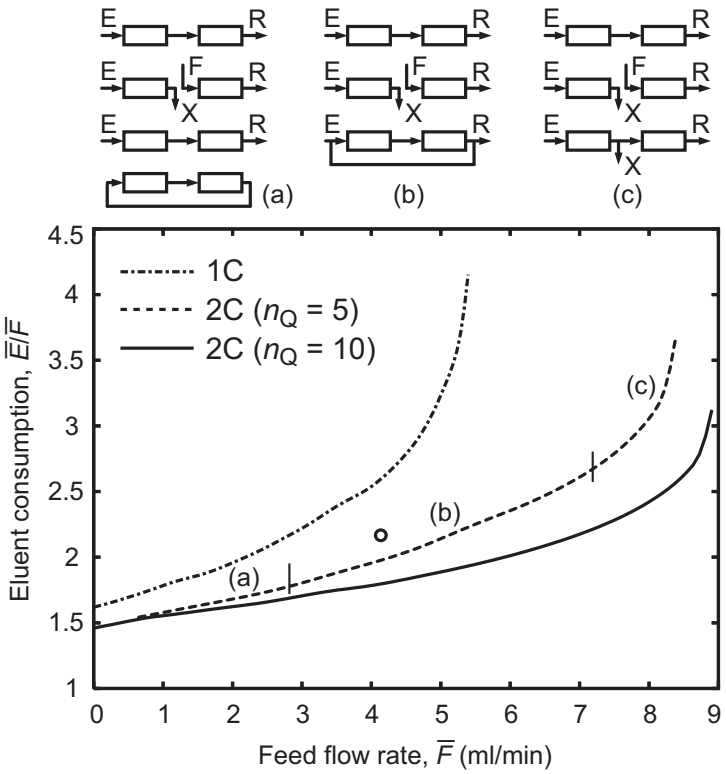

Figure 6.9: Comparison of the two-column SMB process (2C) with conventional single-column batch chromatography with ideal recycling (1C) with respect to feed throughput and eluent consumption for a product purity $\geq 98\%$. The open circle identifies the experimental cycle defined in Table 6.3. n_Q denotes the number of subdivisions per step allocated for the piecewise-constant modulation of the flow rates.

procedure for generating such Pareto curve is to convert the objective function for eluent consumption ($f_{obj,2}$) into an inequality constraint,

$$\overline{E} \leq E_{max}, \tag{6.8}$$

and then to carry out a series of single-objective optimizations, in which $\overline{F}$ is maximized for progressively larger values of E_{max}.

Pareto curves are used in Figure 6.9 to compare the two-column (2C) process against conventional single-column (1C) batch chromatography with ideal

recycling, with respect to feed throughput and eluent consumption for a product purity $\geq 98\%$.

The single-column batch process is an idealized version of the steady-state recycling (SSR) technique [29, 30], in which not only the time delay but also the extra-column dispersion originated by the injection loop are absent [31]. It thus represents the ideal performance that can be obtained by implementing a recycling strategy with a single column. For this process, one column with length $L = 2 \times 6$ cm has been assumed, so that the amount of stationary phase is the same as that employed in the two-column process.

Figure 6.9 includes two distinct Pareto curves for the two-column process, each corresponding to a different value of n_{Q}: the dashed line was obtained for a flow-rate modulation with five piecewise-constant subdivisions per step ($n_{\mathrm{Q}} = 5$), whereas the solid line was obtained for $n_{\mathrm{Q}} = 10$. To assess the full effectiveness of the proposed process, the restriction on the maximum allowable flow rates was removed; this is equivalent to solving the NLP problem for $Q_{\max} = \infty$. This is the reason why the experimental cycle of Fig. 6.6 does not lie on the Pareto curve for $n_{\mathrm{Q}} = 5$, but above it; the flow-rate constraints imposed by the HPLC pumps increase somewhat the eluent consumption of the experimental cycle with respect to that of an identical system but without flow-rate limitations.

The mathematical theory of Pareto multi-objective optimization is somewhat complex [32], but some basic definitions and properties are easily explained for the special case of a dual-objective. In the present case, each Pareto curve represents the opposing objectives of maximizing the feed throughput and minimizing the solvent consumption for a given number of columns and operating scheme. Any point above the Pareto curve has worse performance than the points constituting the Pareto curve, because there is always one element of the Pareto set which has a lower solvent consumption for the same productivity. The points located below the Pareto curve are not feasible because the purity requirements are not fulfilled. When moving along the Pareto curve, each point is nondominant with respect to the others. The choice of a particular point in the Pareto curve over all other points requires additional considerations about the problem, such as the overall separation cost and profit functions.

Note that the Pareto curve exists only in a finite domain of the F-vs-E/F plane, and that the extent of the domain enclosing a given Pareto curve is a measure of versatility of the corresponding operating scheme. Given that the maximum allowable flow rate constraints were removed from the NLP problem, the extent of the domain enclosing each Pareto curve is determined solely by the band broadening in the system.

Figure 6.9 shows that the two-column process performs significantly better than single-column batch chromatography with recycle for the same amount of stationary phase. In one hand, the feasible region of feed throughput spanned by the two-column process is nearly twice as large as that attained by the single-column process. On the other hand, the two-column process always requires less solvent consumption than the batch process for the same productivity, and the difference becomes more pronounced with increasing feed throughput. Increasing the number of subdivisions per step for piecewise-constant time-variable operation, from five to ten, reduces the solvent requirement, but this is only significant for high feed flow rates. Higher values of n_{Q} provide more degrees of freedom for more efficiently cutting the fractions with only partial separation of the band profiles. Alternatively, less subdivisions per step could be employed if their individual lengths were also optimized.

The schematic diagrams at the top of Fig. 6.9 show the major configuration changes in the two-column scheme as it adapts to different productivity specifications or solvent usages. The discussion, however, is more apparent when the changes are correlated in terms of solvent consumption. The schematic diagrams show that, to meet an increasingly stringent solvent requirement, the cycle relies progressively on a more extensive recycling strategy. In the upper end of the productivity region the system operates in an open-loop configuration and a lot of solvent is "wasted". One should keep in mind, however, that this is the only way to attain such high productivity values.

This new two column PowerFeed process showed to be a future promising continuous chromatographic separation process for its setup simplicity and low cost relatively to a classical SMB unit. Because the system only uses two columns, pressure drops problems are minimized and the inherent experimental variabilities derived from the high number of columns packing are reduced. One have also

demonstrate that this process maintains a level of productivity close to a typical 4-column SMB.

6.8 Summary

In this chapter, one have presented a two-column SMB process for binary separation, which relies on a flexible node design, robust pump configuration, and optimized flow-rate modulation. The system was successfully implemented experimentally and tested on the linear separation of two nucleosides by reversed phase.

The two-column SMB process proved to be a simple, but more effective, alternative to single-column batch chromatography with recycling. In one hand, the region of feed throughput attained by the two-column process is much larger than that of the batch process. On the other hand, the two-column process always requires considerably less solvent than the batch process for the same productivity.

The effectiveness of the proposed two-column system was assessed through exploratory simulations for different difficulties of separation and desorbent-to-feed ratios. The optimal port configuration is tightly coupled to the flow-rate modulation, and changes whenever the difficulty of separation or the process specifications change. The same principle can be applied for ternary separation by adding one more withdrawal port to the node design of Fig. 5.2(c).

References

[1] P. Adam, R. Nicoud, M. Bailly, O. Ludemann-Hombourger, Process and device for separation with variable-length, US Patent 6 136 198 (2000). 111

[2] O. Ludemann-Hombourger, R. Nicoud, M. Bailly, The varicol process - a new multicolumn continuous chromatographic process, Separation Science and Technology 35 (2000) 1829–1862. 111

[3] A. Toumi, F. Hanisch, S. Engell, Optimal operation of continuous chromatographic processes: Mathematical optimization of the varicol process, Industrial and Engineering Chemistry Research 41 (2002) 4328–4337. 111

[4] H. Schramm, M. Kaspereit, A. Kienle, A. Seidel-Morgenstern, Improving simulated moving bed processes by cyclic modulation of the feed concentration, Chemical Engineering Technology 25 (2002) 1151–1155. 111

[5] H. Schramm, M. Kaspereit, A. Kienle, A. Seidel-Morgenstern, Improved operation of simulated moving bed processes through cyclic modulation of feed flow and feed concentration, Chemical Engineering Science 58 (2003) 5217–5227. 111

[6] M. Kearney, K. Hieb, Time variable simulated moving bed process, US Patent 5102553 (1992). 111

[7] E. Kloppenburg, E. Gilles, A new concept for operating simulated moving-bed processes, Chemical Engineering Technology 22 (1999) 813–817. 111

[8] Z. Zhang, M. Mazzotti, M. Morbidelli, Powerfeed operation of simulated moving bed units: changing flow-rates during the switching interval, Journal of Chromatography A 1006 (2003) 87–99. 111

[9] Z. Zhang, M. Morbidelli, M. Mazzotti, Experimental assessment of powerfeed chromatography, AIChE Journal 50 (2004) 625–632. 111

[10] Y. Zang, P. Wankat, Smb operation strategy-partial feed, Industrial and Engineering Chemistry Research 41 (2002) 2504–2511. 111

[11] T. Jensen, T. Reijns, H. Billiet, L. van der Wielen, Novel simulated moving-bed method for reduced solvent consumption, Journal of Chromatography A 873 (2000) 149–162. 111

[12] D. Antos, A. Seidel-Morgenstern, Two-step solvent gradients in simulated moving bed chromatography. numerical study for linear equilibria, Journal of Chromatography A 944 (2002) 77–91. 111

[13] S. Abel, M. Mazzotti, M. Morbidelli, Solvent gradient operation of simulated moving beds i. linear isotherms, Journal of Chromatography A 944 (2002) 23–39. 111

[14] W. Jin, P. Wankat, Two-zone smb process for binary separation, Industrial and Engineering Chemistry Research 44 (2005) 1565–1575. 112

[15] M. Eusébio, Development of an universal interface for monitoring and control of chemical and biochemical processes, Ph.D. thesis, Universidade Nova de Lisboa (2006). 113

[16] Y. Kawajiri, L. Biegler, Nonlinear programming superstructure for optimal dynamic operations of simulated moving bed processes, Industrial and Engineering Chemistry Research 45 (2006) 8503–8513. 113, 116

[17] J. Mota, J. Araújo, Single-column simulated-moving-bed process with recycle lag, AIChE Journal 51 (2005) 1641–1653. 116

[18] J. Araújo, R. Rodrigues, J. Mota, Use of single-column models for efficient computation of the periodic state of a simulated moving-bed process, Industrial and Engineering Chemistry Research 45 (2006) 5314–5325. 116

[19] J. Araújo, R. Rodrigues, J. Mota, Optimal design and operation of a certain class of asynchronous simulated moving bed processes, Journal of Chromatography A 1132 (2006) 76–89. 116

[20] J. Mota, E. Saatdjian, D. Tondeur, A. Rodrigues, On the numerical solution of partial differential equations with two spatial scales, Computers & Chemical Engineering 21 (1997) 387–397. 116

[21] Y. Kawajiri, L. Biegler, Optimization strategies for simulated moving bed and powerfeed processes, AIChE Journal 52 (2006) 1343–1350. 116

[22] R. Fourer, D. Gay, B. Kernighan, AMPL - a Modeling Language for Mathematical Programming, 2nd Edition, Brooks/Cole Thomson Learning, 2003. 116, 117

[23] A. Wächter, L. Biegler, On the implementation of an interior-point filter line-search algorithm for large-scale nonlinear programming, Mathematical Programming 106 (2005) 25–57. 116, 117

[24] J. Mota, I. Esteves, M. Eusébio, Synchronous and asynchronous smb processes for gas separation, AIChE Journal 53 (2007) 1192–1203. 116

[25] S. Abel, G. Erdem, M. Amanullah, M. Morari, M. Mazzotti, M. Morbidelli, Optimizing control of simulated moving bedsexperimental implementation, Journal of Chromatography A 1092 (2005) 2–16. 117

[26] G. Guiochon, S. Golshan-Shirazi, A. Katti, Fundamentals of Preparative and Nonlinear Chromatography, Academic Press, 1994. 118

[27] P. Wankat, Simulated moving bed cascades for ternary separations, Industrial and Engineering Chemistry Research 40 (2001) 6185–6193. 125

[28] J. Hur, P. Wankat, Two-zone smb/chromatography for center-cut separation from ternary mixtures: Linear isotherm systems, Industrial and Engineering Chemistry Research 45 (2006) 1426–1433. 125

[29] C. M. Grill, Closed-loop recycling with periodic intra-profile injection: a new binary preparative chromatographic technique, Journal of Chromatography A 796 (1998) 101–113. 129

[30] C. M. Grill, L. Miller, Separation of a racemic pharmaceutical intermediate using closed-loop steady state recycling, Journal of Chromatography A 827 (1998) 359371. 129

[31] I. Quinones, C. Grill, L. Miller, G. Guiochon, Modeling of separations by closed-loop steady-state recycling chromatography of a racemic pharmaceutical intermediate, Journal of Chromatography A 867 (2000) 1–21. 129

[32] K. Deb, Multi-objective Optimization Using Evolutionary Algorithms, Wiley, 2001. 129

7

Two-Column SMB - making the process simpler and more efficient

7.1 Brief introduction

Chromatography has been used in the pharmaceutical and fine chemistry industries for several decades for the analysis and separation/purification of a wide range of products. Excluding some recent SMB applications, these industries mainly use batch column chromatography and are somewhat sceptical about changing to continuous chromatography since it may represent a big step from an economical and operational point of view. Additionally, in pharmaceutical and fine chemistry the annual volume of processed products is low when compared to petrochemical or sugar industries, which makes room for simple and efficient small-scale SMB units.

Although the 2-column SMB process presented in the previous chapter represents an improvement over batch chromatography, it still faces the typical drawbacks of an SMB process when compared to batch or SSR chromatography. Mainly, the SMB major drawback is its high investment/maintenance cost and complexity (it is also not straightforward to apply it for center-cut separations and gradient elution); on the other hand, batch and SSR chromatography

do not achieve a high productivity/yield and low solvent consumption when compared to the SMB [1], but have the advantage of being simple processes with a low capital investment [2]. Based on this idea, the logical choice is to develop a process that combines the best of the two worlds: low complexity, but with high productivity and low solvent consumption.

In the previously formulated 2-column process, we have downsized the SMB process in number of columns but not as much in the amount of ancillary equipment (especially the total number of pumps); the process cycle is still somewhat complex. In the present chapter, a simplification of the two-column SMB system for binary separation is introduced. The system can now be viewed not as a simplification of an SMB scheme but as an evolution of the batch or recycle chromatography process in a way that combines their low complexity with the high productivity and low solvent consumption of the countercurrent SMB system. Furthermore, the process can be further enhanced with a closed-loop recycle step which can be useful specially for low selectivity separations.

7.2 Simplified two-column process

The developed unit is similar to the one described in chapter 6; however, in order to simplify the setup, we have reduced the number of pumps to just 2 pumps: the eluent pump and the feed pump. As a consequence of using only two pumps, we get a node configuration like the one presented in Figure 5.2(b). As shown in Figure 7.1, the possible seven port configurations introduced in Figure 6.1 are reduced to only five potential candidates. As demonstrated in Fig. 7.1, because of the absence of the node pumps, it becomes impossible to perform partial withdrawal, making it impossible to achieve configurations e) and g) (shaded off in Fig. 6.1 for visual clearance). With reference to the same figure, it must be also pointed out that the port configurations b) and c), which represent a frozen bed step, are also not considered here since we are working with the limiting case of 2 columns and a high efficient use of stationary phase is required, which is not the case for these two steps; also, and because we are defining an open-loop operation, step a) cannot be applied simultaneously to the two process nodes.

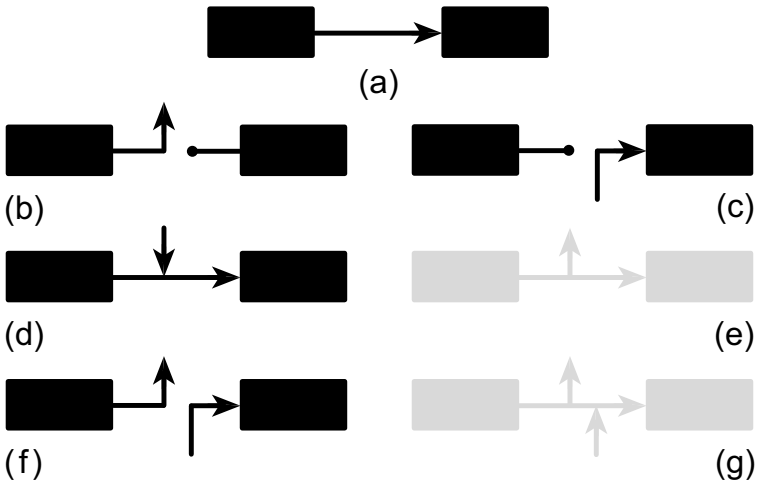

Figure 7.1: Flow diagram for the different types of port configuration that can be implemented with the proposed node design: (a) complete direction of flow to the next column, (b) downstream frozen bed, (c) upstream frozen bed, (d) flow addition to circulating stream, (f) complete withdrawal and flow injection on the same node. Partial withdrawal steps (e) and (g) are not allowed since they require the use of internal node pumps.

A schematic diagram of the proposed setup is shown in Fig. 5.5(a). The system uses only two inlet pumps for supplying feed and eluent and 10 two-way valves to control the port switching.

7.2.1 Cycle design

As in the previously developed two-column SMB, the cycle is equally divided into two steps of equal length, τ, where τ is equivalent to the switching interval of a standard SMB. At the end of each τ time units the inlet/outlet ports are switched and the columns reverse roles. Additionally, the switching interval τ is also divided into a given number n_{Q} of subintervals of different length. Again, the adopted formulation does not track the port switching over the cycle but the status of the two-way valves is inferred from the piecewise-constant flow-rate modulation profiles over each step. At each step of the flow-rate modulation, the following basic restrictions are employed:

$$0 \leq E_j \leq Q_{\max}, \quad X_j \geq 0, \quad 0 \leq F_j \leq Q_{\max}, \quad R_j \geq 0, \tag{7.1}$$

$$0 \leq Q_j \leq Q_{\max}, \tag{7.2}$$

where $Q_{\max}$ is the capacity of the installed pumps. Eq. 7.2 represents an hypothetical pressure drop restriction, however is this case $Q_{\max}$ is limited by the capacity of the installed pumps.

Additionally, due to the suppression of the node pumps and in order to only allow the possible port configurations represented in Fig. 7.1, some more restrictions have to be implemented:

$$Q_j - X_j - R_j = 0 \quad \text{or} \quad X_j = R_j = 0 \tag{7.3}$$

these restrictions represent the conditions where there is total withdrawal of the outlet stream of column j or no product collection. On the other hand, if we only enforce these conditions then a possible result would be a total recycle step i.e. the two nodes may have a port configuration like the one exemplified in Fig. 7.1(a); this situation represents in practise the need for an extra recycle pump (which must be inserted into the process loop) like in the scheme of Fig. 5.5(c). However, for the developed simplified scheme we want to limit the practical scheme to only the eluent and feed pumps. In order to achieve that an additional condition must be employed:

$$\sum_{j=1}^{N} X_j + R_j > 0 \tag{7.4}$$

which ensures that there is always at least one active withdrawal stream for each step.

Constraints to product purity and recovery still apply (Equations 6.3 and 6.4) and the same single-column model described in Figure 6.2 is employed with

the previously described additional constraints. Single feed pump and a single eluent pump conditions (Eq. 6.6) are also active and the objective function, f_{obj}, is likewise the maximization of the feed throughput (productivity):

$$f_{\text{obj}} = \max \overline{F}, \quad \overline{F} = \int_0^N F_j \, d\theta, \tag{7.5}$$

where $\theta = t/\tau$ is a dimensionless time coordinate and $\overline{F}$ is the average feed flow rate per cycle.

Similar to the previous chapter, the resulting optimization problem is formulated by a single-column model that replicates the cyclic steady state of the two-column unit [3, 4], with a full-discretization in both space and time for the cyclic steady state. The resulting nonlinear programming problem obtained after discretization is devised in AMPL [5] and solved using IPOPT 3.2.3 [6] as in a previous work [7]. The initial transient zone of the process is obtained via a gProms (PSE, London, UK) code (see Fig. 6.3).

7.2.2 Process definition

After some parametric studies, a specific process cycle scheme was defined. The process cycle consists of three subdivisions τ_n, of variable length, of the switching interval ($nQ = 3$). The duration of each step is set to nonuniform (opposite to the cycle in the previous chapter) as long as their sum equals the switching time:

$$\sum_{n=1}^{nQ} \tau_n = \tau \tag{7.6}$$

As described in Figure 7.2, the first step represents an elution step with collection of product (extract or raffinate), eluent is added to the first column with a complete recycle of the stream to the next column and total withdrawal of the outlet in column 2; the scheme remains the same for all the steps but in the second period there is the addition of the feed mixture to the 2nd column. During the next switching interval the process undergoes the same schematic but with all lines moved forward by one column in the direction of fluid flow, like in a classical SMB process. The product line (P) represented in Fig. 7.2 denotes either

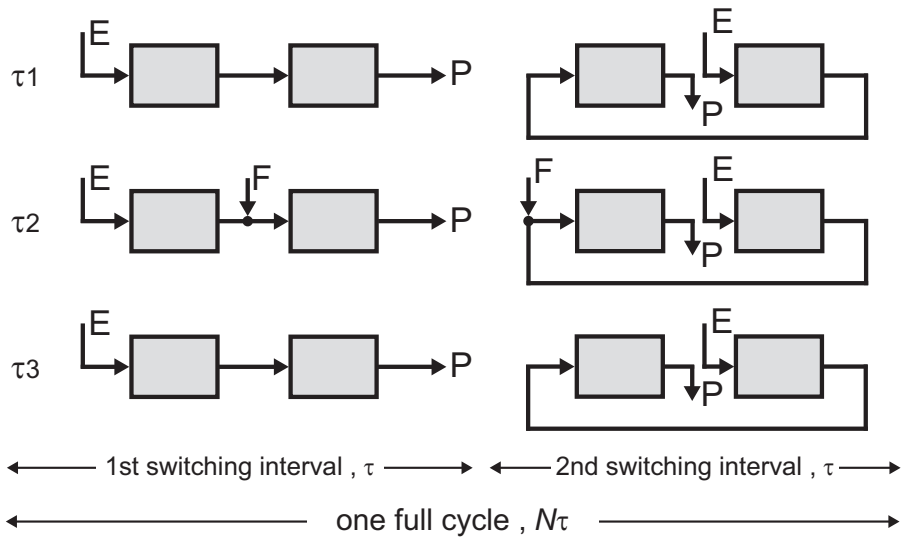

Figure 7.2: Simplified two-column SMB process cycle. Each switching interval is divided into three different steps of variable length (as long as $\sum \tau_n = \tau$, for $n = 1, \ldots, nQ$) which represent two elution steps and one feeding step; in the next switching interval the scheme repeats but staggered one column ahead in the direction of the fluid flow (like in the classical SMB process). Notice that E denotes for the eluent line, F for the feed and P represents the product outlet stream which can denote for the extract or raffinate depending on the separation nature.

the raffinate or extract streams, which are left open for process optimization, but logically (in the case of a binary separation) two of them are for collection of the same product and the third for the other one.

Moreover, notice that this simple cycle resembles the batch chromatographic scheme: one feed step and two elution steps for collecting each product of the binary mixture. However, it adds the extra addition of the simulated counter-current movement of the SMB scheme which, as we will see next in this chapter, will greatly enhance the process efficiency.

Mathematically speaking, in order to enforce the suggested scheme, several conditions must be imposed:

$$E_{j=2}(\theta) = 0, \qquad \text{for } \theta \leq 1 \tag{7.7}$$
$$E_{j=1}(\theta) = 0, \qquad \text{for } \theta > 1 \tag{7.8}$$

which expresses that there is no eluent addition into column 2 during the first switching interval and in column 1 during the second switch time.

$$F_{j=1}(\theta) = 0, \qquad \text{for } \theta \leq 1 \tag{7.9}$$
$$F_{j=2}(\theta) = 0, \qquad \text{for } \theta > 1 \tag{7.10}$$

which imposes no feed addition into column 1 for the first switching interval and in column 2 for the second switch time. Furthermore, since there is no withdrawal in column 1 for the first τ nor in column 2 for the second swith time:

$$P_{j=1}(\theta) = 0, \qquad \text{for } \theta \leq 1 \tag{7.11}$$
$$P_{j=2}(\theta) = 0, \qquad \text{for } \theta > 1 \tag{7.12}$$

for P being extract plus raffinate.

Additionally, besides having downsized the process to only two columns and two pumps, for extra simplicity the eluent flowrate is also kept constant for the whole cycle. In practice, this implies the employment of a condition to ensure that the eluent flowrates are always constant from step to step:

$$E_1^n = \overline{E} = \int_0^N E_j \, d\theta, \qquad \text{for } n = 1, \ldots, nQ \tag{7.13}$$

where $\overline{E}$ is the average eluent flow rate per cycle.

Also, due to the nonuniform step duration and in order to maintain the setup feasible from the experimental point of view, a minimum step length $\tau_{\min}$ is defined:

$$\tau_n \geq \tau_{\min} \qquad \text{for } n = 1, \ldots, nQ \tag{7.14}$$

As a summary, we propose a simple open-loop simulated countercurrent chromatographic process which employs only 2 columns and 2 pumps. Each process switching interval is divided into three different steps and the flowrates, the duration of each step/switching interval and the outlet lines are obtained by process optimization.

7.2.3 Experimental validation

In order to experimentally validate the feasibility of the proposed process, the linear separation of the two nucleosides uridine and guanosine on reversed-phase stationary phase is considered . The mobile phase is maintained isocratic at a composition of 5% (v/v) ethanol in water [8] and the system temperature is now set constant at 30°C; the feed concentration c_F is 0.059 for uridine and 0.05 for guanosine. The columns are the ones described in Table 6.1 and the detection system using multi-wavelength USB4000 UV detector is equal to the one described in previous chapters.

Table 7.1: Adsorption parameters and cycle parameters for the simplified two-column process. The parameter values for the NLP problem ($f_{\text{obj}} = \max \overline{F}$) are: $n_{\text{Q}} = 3$, $Q_{\max} = 9.5$ ml/min, $P_{\text{R}}^{\min} = P_{\text{X}}^{\min} = 0.99$ and $\tau_{\min} = 0.167$ min.

$\epsilon = 0.318^a$	K	Pe	αL (s)	k (s^{-1})
Uridine (U)	1.275	744	0.108	1.809
Guanosine (G)	1.9	640	0.163	0.973
τ (min)		τ_1 (min)	τ_2 (min)	τ_3 (min)
6.245		0.362	3.356	2.527
Step	E	F	X	R
1	6.086	0.000	6.086	0.000
2	6.086	3.414	9.500	0.000
3	6.086	0.000	0.000	6.086
Average	6.086	1.835	5.458	2.463

Flow rates are expressed in ml/min. [a]Average of the two columns.

To characterize the adsorption column dynamics an equilibrium dispersed plug-flow model [9] was employed (see chapters 2 and 4). The initial chromatographic parameters were determined by pulse analysis at several flowrates (similarly to the preceding chapters); the method used to accommodate the extra column dead volume effects was different from the previous chapter: a process cycle using the initial adsorption parameters was reproduced experimentally and, instead of fitting the data by means of an adjustable ϵ value, the adjusted values were the Henry constants K_i. This procedure was found to be more suitable since it gives more accuracy to the fitted concentration profiles.

The obtained values (with the dead volume effect lumped into the Henry constants K_i) are listed in the top of Table 7.1. The optimal cycle for the two-column process was determined by solving the design problem with these chromatographic parameters, subject to minimal extract and raffinate purity requirements, $P_{\mathrm{X}}^{\mathrm{min}} = P_{\mathrm{R}}^{\mathrm{min}} = 99\%$ and Q_{max} was again fixed at 9.5 ml/min. The optimized operating parameters are listed in the bottom rows of Table 7.1.

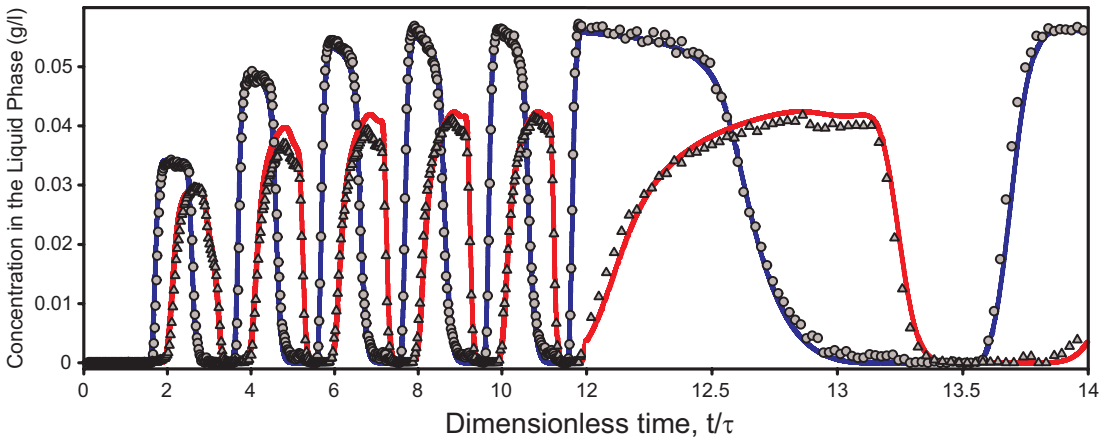

Figure 7.3: Solute concentration profiles at the outlet of column 1 for the chromatographic parameters given in Table 7.1. Symbols denote experimental data (∘, uridine; △, guanosine), whereas lines represent the solution of the dynamic process model (blue for uridine and red for guanosine). For visual clarity, only 1/30th of the UV measurements are plotted for the first 6 cycles and 1/15th for the 7th cycle.

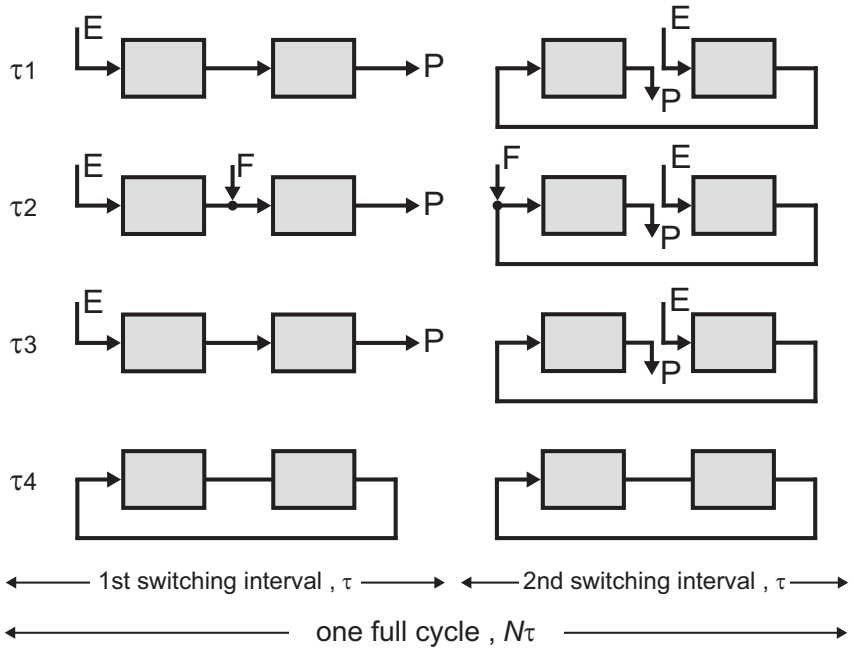

Figure 7.4: Schematic diagram of the simplified two-column SMB process with recycle step. Each switching interval is divided into four different steps of variable length (as long as $\sum \tau_n = \tau$, for $n = 1, \ldots, nQ$) which represent two elution steps, one feeding step and one recycle step; in the next switching interval the scheme repeats but staggered one column ahead in the direction of the fluid flow (like in the classical SMB process). Notice that E denotes for the eluent line, F for the feed and P represents the product outlet stream which can denote for the extract or raffinate depending on the separation nature.

The optimized SMB scheme was reproduced experimentally over 7 operating cycles. As one can see in Figure 7.3, the process quickly reaches the CSS regime in only 5 to 6 cycles. Fig. 7.3 compares the experimental concentration profiles at the outlet of column 1, measured during the 7th cycle, with those predicted by process simulation. The results reported in Fig. 7.3 show an excellent agreement between the experimental and simulation data.

7.3 Enhancing the process

Due to the various simplifications made to the process scheme, there are some inherent limitations which will increase solvent consumption and decrease productivity specially if we compare it with setups with more columns. With the objective of enhancing the scheme to achieve an higher efficiency while maintaining a simple process cycle, an extra step τ_4 was added to the scheme. As one can see in Figure 7.4, the additional interval τ_4 consists of a recycle step with no addition to nor withdrawal of material from the columns.

In practise, this extra step requires an extra process pump placed inside the process loop as shown in Fig. 5.5(c). The third process pump introduces extra complexity and is a drawback from the economical point of view; however, depending on the nature of the separation it can represent a positive economical balance (specially in low selectivity cases).

These new pump/step implicates the elimination of Eq. 7.4 from the NLP to allow an operating step during which there are no inlet nor outlet lines; this means that the two nodes have a port configuration like the one shown in Fig. 7.1(a).

7.3.1 Experimental validation

Employing the same nucleoside binary separation, the chromatographic parameters were again fitted since the presence of the inner-loop pump implicates additional dead volume. The optimal cycle for the process was determined by solving the design problem with the newly fitted chromatographic parameters, again subject to the same conditions: minimal extract and raffinate purity requirements, $P_{\mathrm{X}}^{\mathrm{min}} = P_{\mathrm{R}}^{\mathrm{min}} = 99\%$ and Q_{max} fixed at 9.5 ml/min. The optimized operating parameters are listed in the bottom rows of Table 7.2.

The optimized scheme was reproduced experimentally over 10 operating cycles. As one can see in Figure 7.5, the process reaches the CSS condition in around 7 to 8 cycles. Fig. 7.5 compares the experimental concentration profiles at the outlet of column 1, measured during the 10th cycle, with those predicted by process simulation. The results reported in Fig. 7.5 show an excellent agreement between the experimental and simulation data.

Table 7.2: Adsorption parameters and cycle parameters for the simplified two-column process with recycle step. The parameter values for the NLP problem ($f_{\text{obj}} = \max \overline{F}$) are: $n_{\text{Q}} = 3$, $Q_{\max} = 9.5$ ml/min, $P_{\text{R}}^{\min} = P_{\text{X}}^{\min} = 0.99$ and $\tau_{\min} = 0.167$ min.

$\epsilon = 0.318^a$		K	Pe	αL (s)	k (s^{-1})
Uridine (U)		1.434	744	0.108	1.708
Guanosine (G)		2.03	440	0.163	0.934
τ (min)		τ_1 (min)	τ_2 (min)	τ_3 (min)	τ_4 (min)
6.611		0.167	3.200	2.617	0.627
Step	E	F	X	R	Q_{recycle}
1	5.934	0.000	5.934	0.000	0.000
2	5.934	3.566	9.500	0.000	0.000
3	5.934	0.000	0.000	5.934	0.000
4	0.000	0.000	0.000	0.000	9.500
Average	5.371	1.727	4.749	2.349	-

Flow rates are expressed in ml/min. [a]Average of the two columns.

7.4 Discussion

Considering the first two-column process proposed in this chapter, Figure 7.6 shows the internal concentration profiles inside the two-column loop over the duration of a switching interval (half of a cycle since a complete cycle is $N\tau$) and the corresponding position of the inlet and outlet ports. Only half of the cycle is shown, since for the other half the columns undergo the same concentration profiles and port scheme but with their position exchanged.

As explained before, the cycle can be viewed as a simplified version of an open-loop simulated moving bed process with port switching and flowrate modulation. However, due to the simplicity of the scheme, it can be regarded as an evolution of the batch chromatography process. This process cannot be looked at as a four zone SMB scheme but as a complete autonomous scheme where the chromatographic simulated countercurrent behavior is exploited to the maximum.

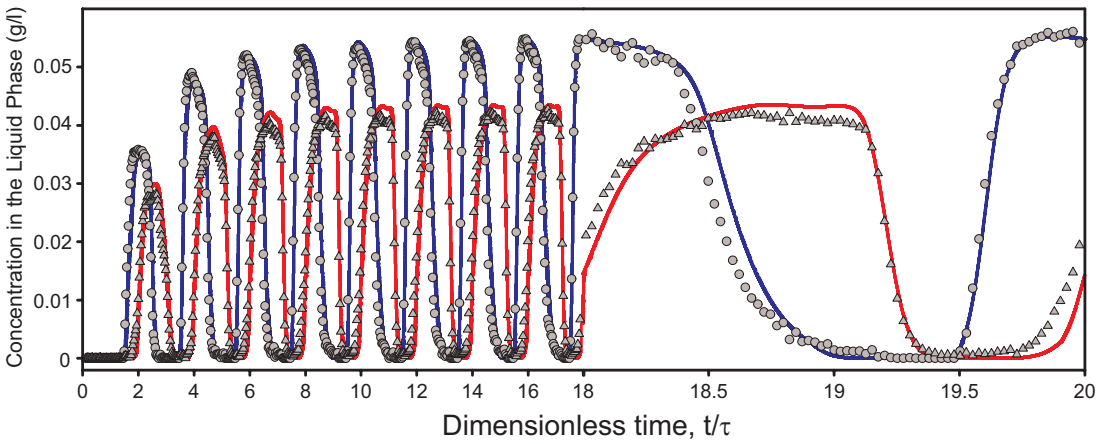

Figure 7.5: Solute concentration profiles at the outlet of column 1 for the chromatographic parameters given in Table 7.2. Symbols denote experimental data (○, uridine; △, guanosine), whereas lines represent the solution of the dynamic process model (blue for uridine and red for guanosine). For visual clarity, only 1/30th of the UV measurements are plotted for the first 9 cycles and 1/15th for the 10th cycle.

The concentration profiles plotted in Fig. 7.6 show that, as in batch mode, this process consists of constant elution with a periodic feed mixture injection and a selective withdrawal of the two components of the feed mixture. Moreover, the process can be manipulated according to the separation nature by allowing the flowrates, durations each step and the outlet lines to be nonfixed parameters in a way to accommodate the separation needs.

On the other hand, if one takes a look at the axial concentration profiles presented in Fig. 7.6 it is clear that around 0.3τ to 0.5τ the collection of extract is mostly constituted of pure eluent, this fact suggests a possibility of improvement in terms of eluent consumption. The more straightforward improvement is to recycle this fraction of the extract stream into the eluent reservoir; however, although feasible, this solution can have contamination problems since in practice it is difficult to ensure that the stream is completely solute-free from cycle to cycle. Another solution is to use the stream itself to replace the eluent stream; the eluent flow is used mainly as a drag force in order to move the solutes through

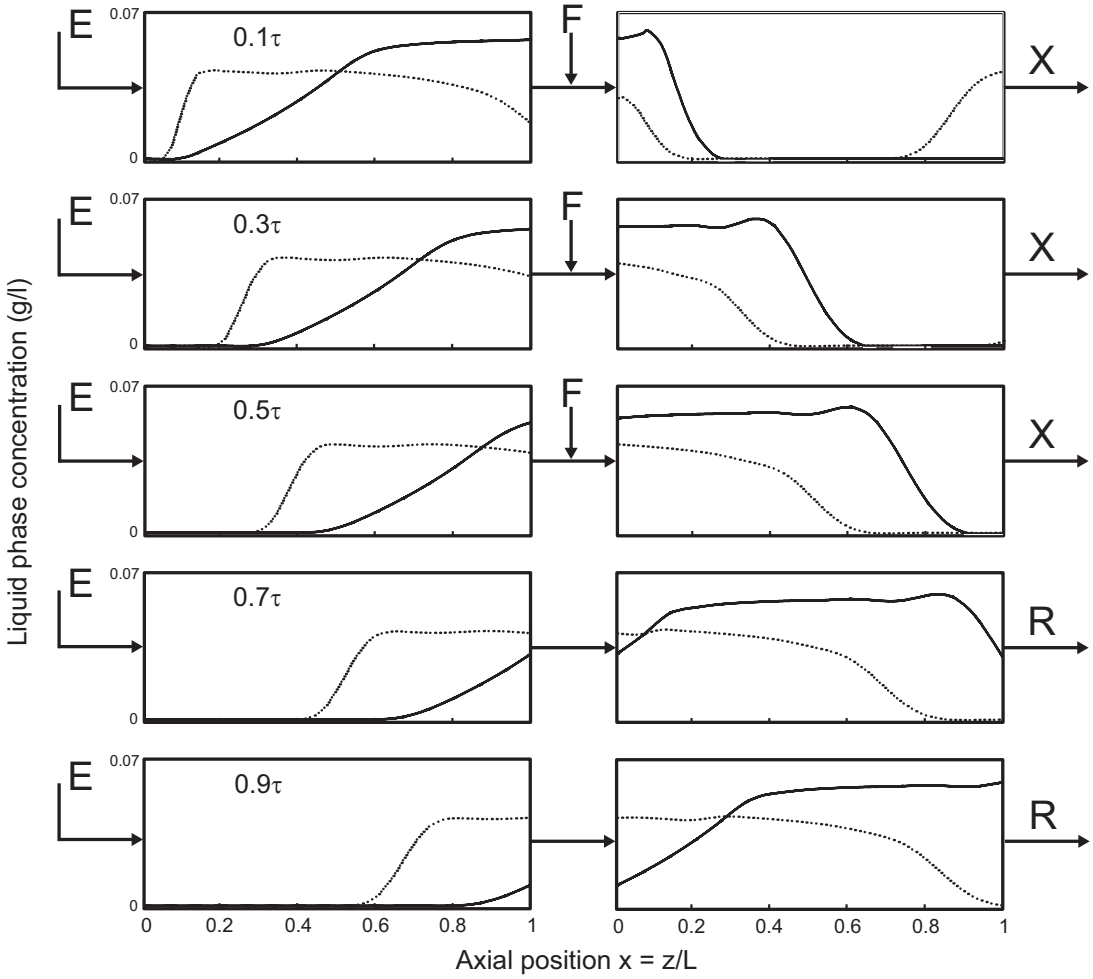

Figure 7.6: Axial concentration profiles at CSS and inlet/outlet lines positions over one switching interval for the simplified two-column scheme listed in Table 7.1. In the second switch the columns undergo the same cycle but with their position exchanged. The full line denotes the less retained component (uridine) and the dotted line the more retained one (guanosine); E, F, X and R refers to the eluent, feed, extract and raffinate lines respectively.

the solid phase. However, by means of an extra pump one can create a recycle step where there is no addition or collection and the outlet stream from one column is completely recycled to the next column. This possibility is exploited in the second process presented in this chapter.

Figure 7.7 represents the internal concentration profiles inside the two-column loop for a switching interval and the corresponding position of the inlet and outlet ports for this new scheme with a recycle step. It is clear from Fig. 7.7 that the extract line is more concentrated relatively to the scheme without recycle step, this fact is also proved if one compare the optimized cycles of Tables 7.1 and 7.2 where we can see that in this scheme the productivity $\overline{F}$ is marginally reduced by around 6% due to the presence of extra dead volume (the presence of the pump inside the process loop inserts more dead volume into the system). However, eluent consumption $\overline{E}$ is reduced by 13%, which reduces the extract flowrate by 15%.

In order to compare the effectiveness of these two proposed schemes, a set of Pareto curves was computed. As described before, the Pareto curve expresses the relation between two objective functions, in this case eluent consumption $\overline{E}/\overline{F}$ and productivity $\overline{F}$; logically, the best process is the one which maximizes $\overline{F}$ and minimizes $\overline{E}$. In all pareto curves, and in order to obtain a fair comparison, the set of adsorption parameters was at the values listed in the top of Table 7.1 and for all the described processes the total amount of stationary phase was maintained constant.

Figure 7.8 shows the pareto curves of the simplified two-column process for the cases of nonuniform and uniform eluent flowrate profiles. The construction of these set of curves is distinguished by a simple fact: in the case of the uniform eluent the restriction from Eq. 7.13 is set active in the NLP problem and is relaxed for the nonuniform solution. As seen in Fig. 7.8, for the case of constant eluent flowrate one can achieve the same productivity $\overline{F}$ (except for the highest flowrates) with a slight increase on eluent consumption $\overline{E}/\overline{F}$; this result is expected since we are applying an extra restriction (Eq. 7.13) which narrows the dimension of the solution space. However, this uniform eluent solution can present some extra advantages from the practical point of view since it simplifies the eluent pump control software and specially decreases the mechanical erosion of the pump.

Figure 7.9 displays the pareto curves for the proposed simplified two-column, batch, SSR and classical 4-column SMB processes. As shown in Fig. 7.9, one can obtain a much higher productivity in the two-column process and still maintain a

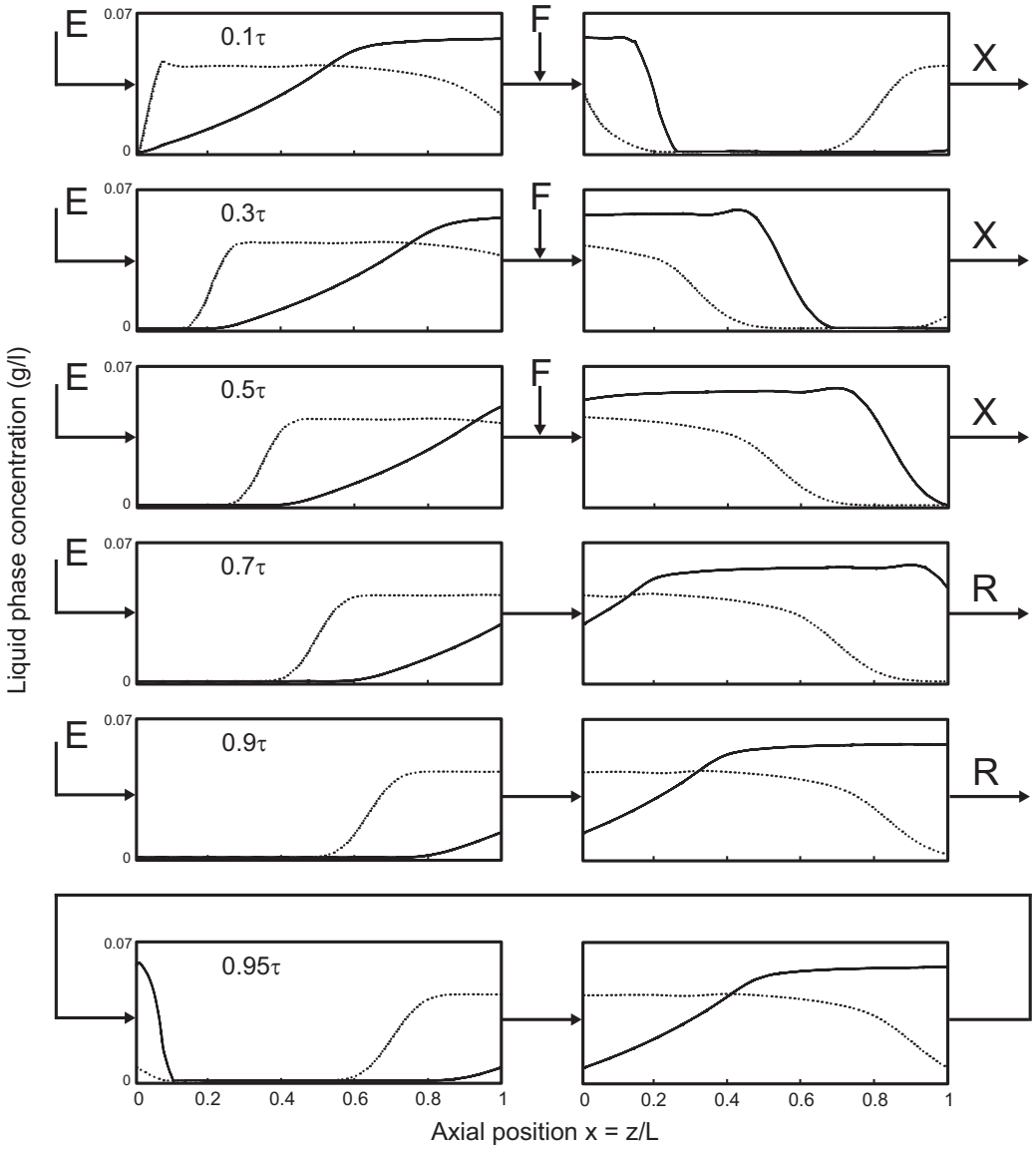

Figure 7.7: Axial concentration profiles at CSS and inlet/outlet lines positions over one switching interval for the simplified two-column scheme with recycle step listed in Table 7.2. In the second switch the columns undergo the same cycle but with their position exchanged. The full line denotes the less retained component (uridine) and the dotted line the more retained one (guanosine); E, F, X and R refers to the eluent, feed, extract and raffinate lines respectively.

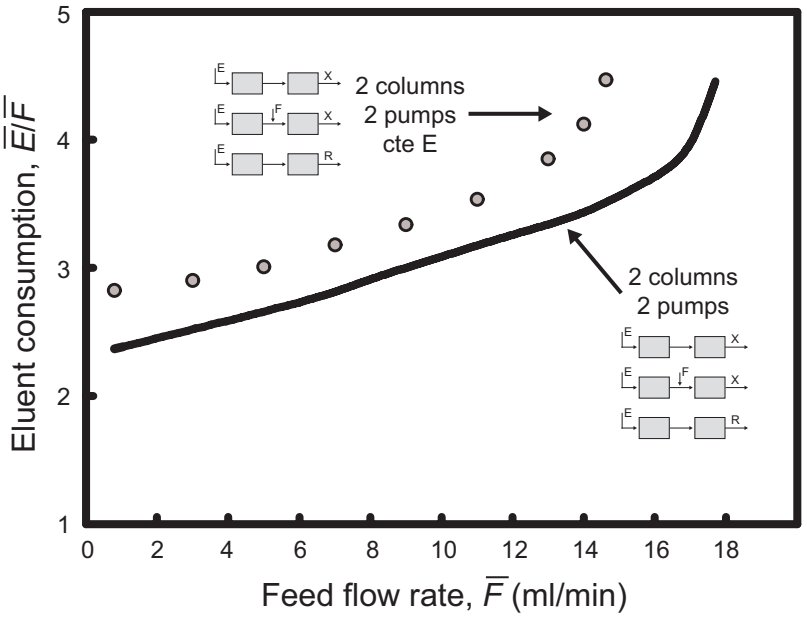

Figure 7.8: Optimal operating curves of the simplified two-column SMB process for our separation test case. Comparison between the constant and nonuniform eluent flowrate option. The full line represents the simplified two-column process with a nonuniform eluent flowrate behavior and the symbols ∘ the particular case of constant eluent flowrate condition (Eq. 7.13 is active).

relatively low eluent consumption; this fact represents a significant breakthrough since we are operating with the same amount of stationary phase and marginally the same equipment as for the single-column schemes. Generalizing, if we start with the simplest batch process we can improve it by merely adding a recycle step creating the known recycle chromatography process. Furthermore, with the simple splitting of the batch process into two columns the process is significantly improved when compared to single-column chromatography with recycle, simply due to the application of the simulated countercurrent chromatography; furthermore, even if we take as comparison another countercurrent process like the 4-column classical SMB system, which is a more complex and more equipment demanding scheme, the two-column presents a fairly good performance with only a small increase on eluent consumption for low throughput but it can achieve a much higher productivity. It is then evident that, for the same amount of

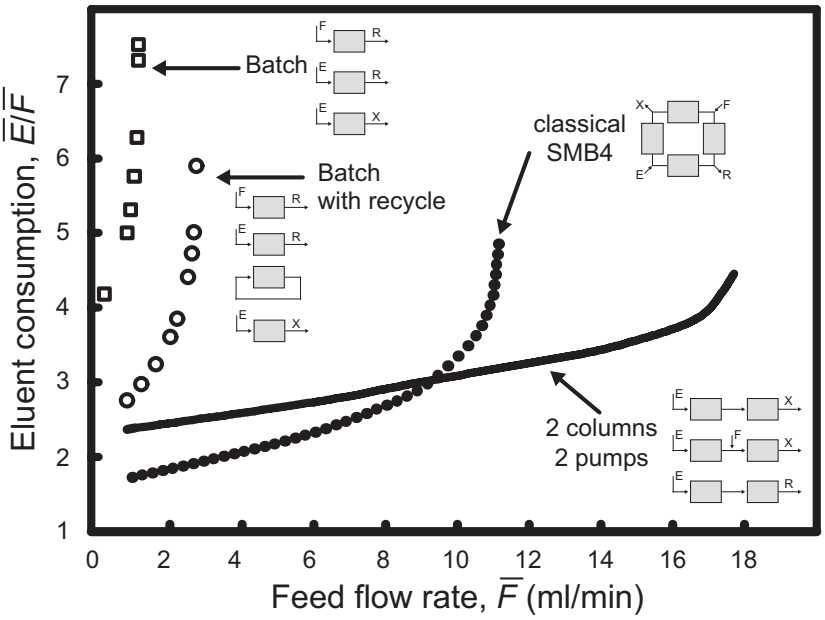

Figure 7.9: Optimal operating curves of the simplified two-column SMB process for our separation test case. Comparison between the simplified two-column, batch, batch with recycle and the classical 4-column SMB processes. For all processes the total amount of stationary phase is kept constant; denote that the full line represents the simplified two-column process, the symbols □ and ○ the batch with recycle and batch processes respectively and the dotted line the classical 4-column SMB process.

stationary phase, the two-column process reveals an extremely high performance both in productivity and in eluent consumption when compared to the simplest single-column processes or to a more complex process like the classical 4-column SMB.

Figure 7.10 show the optimal operating curves for the two-column SMB process, with and without recycle step; the analysis of this figure shows that the simple addition of a recycle step improves the scheme mainly in terms of eluent consumption. However, for better comparison these operating curves are built using the adsorption parameters listed at the top of Table 7.1. In the case of the process with a recycle step, we are not taking into account the extra dead volume introduced into the process by the presence of the extra inner-loop pump. Nev-

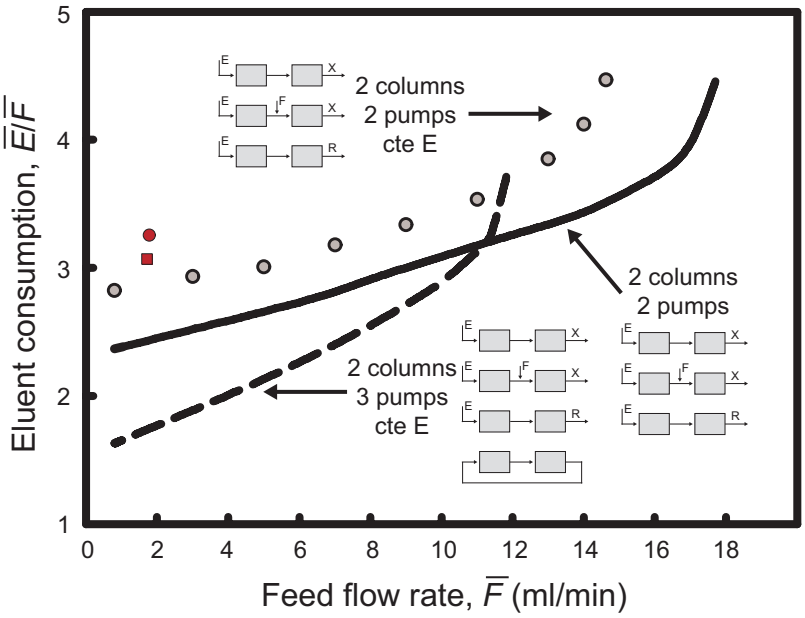

Figure 7.10: Optimal operating curves of the simplified two-column SMB process with and without recycle step for our separation test case. Note that the full line represents the simplified two-column process with nonuniform eluent flowrate, the gray symbols ∘ the same process with constant eluent flowrate and the dashed line the two-column process with a recycle step. The two red symbols ∘ and □ are the experimentally reproduced process from Tables 7.1 and 7.2 respectively.

ertheless, from the two optimized and experimentally reproduced schemes one can fairly conclude that this has only a negative effect on the productivity (with a decrease of around 6%) but still has a significant impact on decreasing eluent consumption; furthermore, the operating curve for the two-column scheme with recycle step represented in Fig. 7.10 is also obtained for a process with constant eluent policy. If we further compare it to the corresponding two-column process with uniform eluent (gray symbols ∘ in Fig. 7.10), the eluent consumption reduction is even more evident. The two symbols in red represent the two experimental points from Tables 7.1 and 7.2, which have a performance outside the pareto lines due to the $Q_{\max}$ restriction (Eq. 7.2).

The first simplified process presented in this chapter can be viewed as an evolution of batch chromatography, and the one with recycle step an enhancement of

the batch with recycle chromatography process. These new two-column processes are promising because of their simplicity and low cost relatively to the classical SMB unit, and high productivity and low solvent consumption when compared to batch or SSR chromatography. The system only uses two columns and two or three pumps, and it comprises a simplified operating scheme and uniform flowrate procedure. A version similar to the scheme (without recycle step) is already being commercialized by NOVASEP for SFC applications [10].

7.5 Summary

In this chapter, we have presented two simplified versions of a two-column SMB process for binary separation, which relies on a downgrade of the process complexity relatively to the system presented in the previous chapter. Both schemes were successfully implemented in practice for the linear separation of two nucleosides by reversed phase.

These new processes rely on a simplified 3-step open-loop scheme with constant eluent addition; an extra enhancement to this process was done by the simple addition of a recycle step into the scheme; these enhancement proved to be very efficient, mainly on the decrease of eluent consumption, and it could be a good alternative for very low selectivity separations since they are more eluent demanding.

Both two-column processes proved to be more efficient relatively to single-column batch chromatography processes and to a classical 4-column SMB. It is clear that for high-valued separations/purifications like the ones in the pharmaceutical, fine chemistry or biotechnology industries, these new schemes can provide a very promising alternative chromatographic process, specially to single-column systems, since the level of complexity and equipment is identical and the level of productivity is increased several times.

References

[1] J. Strube, S. Haumreisser, H. Schmidt-Traub, M. Schulte, R. Ditz, Comparison of batch elution and continuous simulated moving bed chromatography, Organic Process Research & Development 2 (1998) 305–319. 136

[2] L. Miller, C. Grill, T. Yan, O. Dapremont, M. Juza, Batch and simulated moving bed chromatographic resolution of a pharmaceutical racemate, Journal of Chromatography A 1006 (2003) 267–280. 136

[3] J. Mota, J. Araújo, Single-column simulated-moving-bed process with recycle lag, AIChE Journal 51 (2005) 1641–1653. 139

[4] J. Araújo, R. Rodrigues, J. Mota, Use of single-column models for efficient computation of the periodic state of a simulated moving-bed process, Industrial and Engineering Chemistry Research 45 (2006) 5314–5325. 139

[5] R. Fourer, D. Gay, B. Kernighan, AMPL - a Modeling Language for Mathematical Programming, 2nd Edition, Brooks/Cole Thomson Learning, 2003. 139

[6] A. Wächter, L. Biegler, On the implementation of an interior-point filter line-search algorithm for large-scale nonlinear programming, Mathematical Programming 106 (2005) 25–57. 139

[7] J. Mota, I. Esteves, M. Eusébio, Synchronous and asynchronous smb processes for gas separation, AIChE Journal 53 (2007) 1192–1203. 139

[8] S. Abel, G. Erdem, M. Amanullah, M. Morari, M. Mazzotti, M. Morbidelli, Optimizing control of simulated moving bedsexperimental implementation, Journal of Chromatography A 1092 (2005) 2–16. 142

[9] G. Guiochon, S. Golshan-Shirazi, A. Katti, Fundamentals of Preparative and Nonlinear Chromatography, Academic Press, 1994. 143

[10] E. Valery, O. Ludemann-Hombourger, Method and device for separating fractions of a mixture, WO Patent 2007/012750 (2007). 154

8

Robust Design of an SMB process

8.1 Brief introduction

The practical implementation of a simulated moving bed process, as most chemical processes, is subject to variations and/or fluctuations which are inherent to every experimental implementation. For an SMB, those uncertainties can derive from variations on process parameters such as the isotherm parameters, band broadening, extra-column volumes and packing reproducibility, or from fluctuations on the imposed pump flowrates and temperature stability. Those uncertainties are even more evident in production-scale operation.

Although there have been previous studies on the effect of variations in operating and system parameters on SMB performance, only a few of them have addressed the problems of handling parameter uncertainty and robustness of operation. Storti et al. [1] and Mazzotti et al. [2] were the first to introduce the concept of robustness in optimal SMB design in the framework of their triangle theory. These authors have shown that the further the operating point is from the boundaries of the complete separation region in the four dimensional (4-D) space whose coordinates are the m_j flow rate ratios, the more robust the operating conditions are.

More recently, Mun et al. [3] have produced a comprehensive study of how SMB performance is affected by variations in operating and system parameters. Practically every conceivable source of disturbance was taken into consideration and a robust pump configuration for minimizing the effects of pump output deviations was proposed. The authors also extended their standing-wave design method [4, 5] to handle robust design. They have shown that even when the worst parameter deviations occur, the desired yield and purity can still be achieved.

In this chapter we address the issue of robustness in SMB operation, and present a general procedure for robust SMB design under operating uncertainty based on a worst-case scenario. The approach will be applied to the previously developed two-column SMB scheme presented in chapter 7. The issue of robustness is particularly important for for processes with a small number of columns, because they provide further gains at the expense of additional complexity making them more sensible to operating disturbances.

8.2 Robust process design

Looking at an SMB operation, it is clear that the main sources of uncertainty can be separated into two groups: the flowrates and the packing and isotherm parameters. It is then assumed that these parameters are subject to an error, or uncertainty, defined by a maximum relative deviation δ, from their nominal values. For the flowrates, the deviation δ_k is defined as:

$$(1 - \delta_k)\ Q_k^* \leq Q_k \leq (1 + \delta_k)\ Q_k^* \tag{8.1}$$

where Q_k^* is the design variable and k stands for the pump index, e.g. $k = E$ (eluent) and $k = F$ (feed) for the case of the simplified two-column process.

On the other hand, considering the equilibrium dispersed plug-flow column model, all the packing and isotherm parameters can be lumped together into a single variable V_{ij}:

$$V_{ij} = [\epsilon_j + (1 - \epsilon_j)\ K_i]\ (L_j A) \tag{8.2}$$

where i is the solute index and j the column index. The corresponding deviation variable δ_j is:

$$(1-\delta_j)\ V_{ij}^* \leq V_{ij} \leq (1+\delta_j)\ V_{ij}^* \tag{8.3}$$

Consequently, the chromatography model becomes:

$$\frac{\partial c_{ij}}{\partial \theta} = \frac{\tau Q_j}{V_{ij}} \left(\frac{h_{ij}}{2} \frac{\partial^2 c_{ij}}{\partial x^2} - \frac{\partial c_{ij}}{\partial x} \right) \tag{8.4}$$

where $\theta = t/\tau$ and $x = z/L$ are the dimensionless temporal and axial coordinates respectively, c is the concentration in the liquid phase and h is the dimensionless plate height.

Notice that in the absence of uncertainty ($\delta_k = \delta_j = 0$), the nonlinear programm problem yields the solution to the nominal design problem discussed in previous chapters.

The optimal solution of the design problem, when subject to the uncertainties given by Equations 8.1 and 8.3, are obtained from its robust counterpart: Q_k^* and V_{ij}^*, which simultaneously obey the imposed flowrate and purity restrictions:

$$\begin{array}{l} Q_k \leq Q_{\max} \\ P_R(\tau, V_{ij}, Q_k) \geq P_{\mathrm{R}}^{\min} \\ P_X(\tau, V_{ij}, Q_k) \geq P_{\mathrm{X}}^{\min} \end{array} \quad \left\{ \begin{array}{lll} \forall\ Q_k & \text{in} & [(1-\delta_k)Q_k^*, (1+\delta_k)Q_k^*] \\ \forall\ V_{ij} & \text{in} & [(1-\delta_j)V_{ij}^*, (1+\delta_j)V_{ij}^*] \end{array} \right. \tag{8.5}$$

There is an increase in complexity while moving from the nominal problem to its robust counterpart, because the latter works simultaneously with more than one instance of the chromatographic model. However, the problem remains computationally tractable if the right solution approach and optimization solver are employed [6].

The previously described compact representation of the two-column process is employed as a convenient framework for an efficient solution method for the nominal optimization problem and its robust counterpart. Part of the solution strategy relies on the direct calculation of the steady periodic solution (see Fig 6.3). A

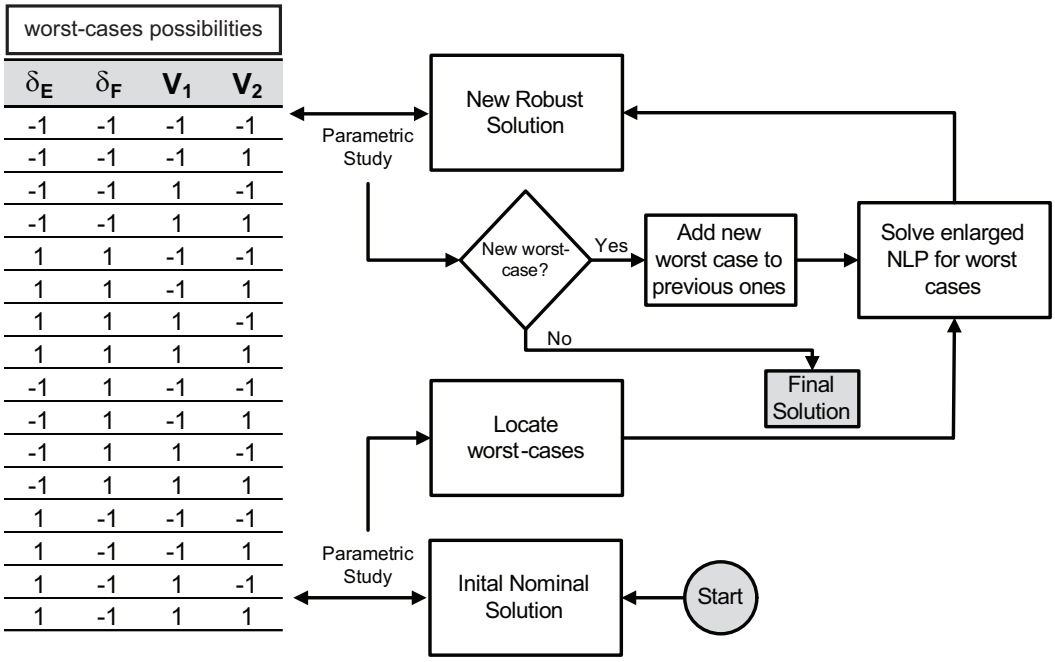

Figure 8.1: Decision flowchart for the worst-case disturbances. From the initial nominal solution a parametric study decides which disturbances most affect the purities; a new enlarger NLP is now solved considering the selected cases and a new nominal solution is obtained, this solution is tested for new worst-cases until one reaches the desired robust result.

full-discretization method is applied in which the time coordinate is discretized over a full cycle and a periodic condition is directly imposed. As reported before, the nonlinear programming problem obtained after discretization is formulated in AMPL [7] and solved using IPOPT [8].

8.2.1 Worst-Case method

In order to simplify the robust counterpart of the NLP, a worst-case method was applied. As one can see in Figure 8.1, the method relies on a parametric search to choose, among all the possible disturbance combinations, only the ones that mostly affect the controlled variable: the purity of the extract and raffinate streams.

The method is very straightforward. Starting from the initial nominal solution ($\delta_k = \delta_j = 0$) a parametric study is performed to analyze the effect that each possible disturbance will have on the purity; from this study only the disturbances that mostly effect the purities are chosen (usually 2 or 3) for the formulation of the robust counterpart of the NLP. The enlarged NLP is solved and a new nominal solution is obtained which fulfils the purity requirements for the previously chosen worst-case disturbances. However, in order to ensure that the solution is the global worst-case solution, a new parametric study is employed. This new parametric study will show wether the solution is already the robust solution or if there is the need to add a new worst-case constraint to the enlarged NLP; this methodology is employed until no more new worst-cases are obtained and consequently the robust solution is achieved.

It should be pointed out that this simple and direct approach represents a direct measure of all possible process disturbances and their affect in the system performance. It also presents a simplified way of designing a robust scheme with a real and independent manipulation of the process variables in order to overcome the inherent practical disturbances and/or fluctuations.

8.3 Experimental validation

For the case of the previously developed simplified two-column process (see Fig. 7.2), our main sources of uncertainty are the feed and eluent flowrates ($k = E, F$) and of course the packing properties and the isotherm parameters (porosity ϵ and Henry constants K_i). The assigned relative uncertainty (δ_k and δ_j) were set to a maximum of 1% in our design procedure.

The linear separation of uridine and guanosine on reversed phase SOURCE 30RPC (GE Healthcare Amersham Biosciences, Uppsala, Sweden) is again chosen as the test case. The mobile phase is 5%(v/v) ethanol in water [9]. Column characterization and adsorption parameters are listed in the top of Table 7.1. The temperature is fixed at 30°C and the feed concentration is 0.057 for uridine and 0.05 to guanosine.

Three different sets of robust operating condition were determined. In the first case δ_k and δ_j are set to 1% and the nominal solution is experimentally employed.

Table 8.1: Adsorption parameters and cycle parameters for the robust solution of the simplified two-column process with $\delta_k = \delta_j = 1\%$. The parameter values for the NLP problem ($f_{\text{obj}} = \max \overline{F}$) are: $n_{\text{Q}} = 3$, $Q_{\max} = 9.5$ ml/min, $P_{\text{R}}^{\min} = P_{\text{X}}^{\min} = 0.99$ and $\tau_{\min} = 0.167$ min.

Adsorption parameters				
$\epsilon = 0.318^a$	K	Pe	αL (s)	k (s^{-1})
Uridine (U)	1.275	744	0.108	1.809
Guanosine (G)	1.9	640	0.163	0.973
Switching intervals				
τ (min)		τ_1 (min)	τ_2 (min)	τ_3 (min)
6.087		0.527	3.229	2.331
Worst-cases				
	δ_E	δ_F	δ_1 (i)	δ_2 (i)
	+1	+1	-1	-1
	-1	+1	+1	+1
Robust Solution				
Step	E	F	X	R
1	6.360	0.000	6.360	0.000
2	6.360	3.140	9.500	0.000
3	6.360	0.000	0.000	6.360
Average	6.360	1.665	5.590	2.435

Flow rates are expressed in ml/min. [a]Average of the two columns.

Next, only the relative uncertainty for the flowrates is activated ($\delta_k = 1\%$) and no safety margin is used for the packing and adsorption parameters; this means that $\delta_j = 0$, however in the experimental run a disturbance into the flowrates is imposed (0.5% increase on Feed and 0.5% decrease on Eluent flowrates). In the third run, a nonzero relative uncertainty is only imposed on the packing and adsorption parameters and no margin is set to the flowrates, which means that $\delta_k = 0$ and $\delta_j = 1\%$. In this case for the experimental run an increase of 1°C is imposed on the system to add a disturbance to V_{ij}.

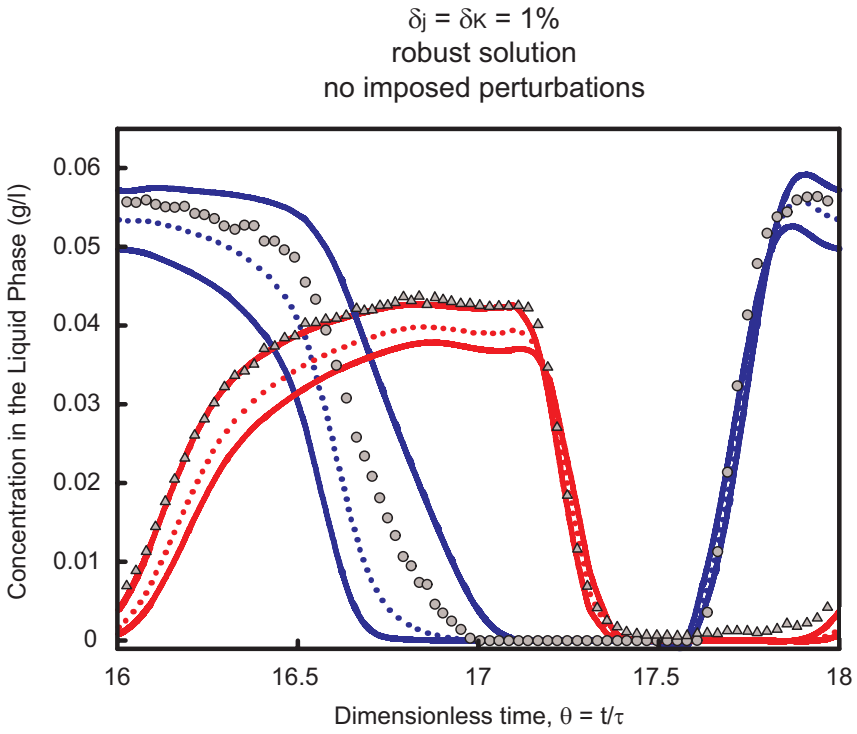

Figure 8.2: Solute concentration profiles at the outlet of column 1 for the parameters given in Table 8.1 during the 9th process cycle. Symbols denote experimental data (∘, uridine; △, guanosine), whereas lines represent the worst-case scenario (blue for uridine and red for guanosine). The dotted lines symbolize the nominal solution, again blue for uridine and red for guanosine. For visual clarity, only 1/15th of the UV measurements are plotted.

Because the used experimental setup is the same as for the previous chapter, the column characterization and adsorption parameters listed are the same represented in the top of Table 7.1 and repeated in Table 8.1 as a reminder.

As one can see in Table 8.1, the optimized robust solution for $\delta_k = \delta_j = 1\%$ presented two worst-cases. The solution was implemented in practice over 9 cycles (one cycle corresponds to $N\tau$) which was enough to reach CSS condition. The concentration measured at the outlet of column 1 over the 9th process cycle can be viewed in Figure 8.2.

Afterwards, a new enlarged NLP solution with $\delta_k = 1\%$ and $\delta_j = 0$ was con-

Table 8.2: Cycle parameters for the robust solution of the simplified two-column process with $\delta_k = 1\%$ and $\delta_j = 0$. The parameter values for the NLP problem ($f_{\text{obj}} = \max \overline{F}$) are: $n_{\text{Q}} = 3$, $Q_{\max} = 9.5$ ml/min, $P_{\text{R}}^{\min} = P_{\text{X}}^{\min} = 0.99$ and $\tau_{\min} = 0.167$ min.

Switching intervals				
τ (min)		τ_1 (min)	τ_2 (min)	τ_3 (min)
6.167		0.447	3.297	2.423
Worst-cases				
	δ_E	δ_F	δ_1 (i)	δ_2 (i)
	-1	+1	0	0
	+1	+1	0	0
Robust Solution				
Step	E	F	X	R
1	6.224	0.000	6.224	0.000
2	6.224	3.276	9.500	0.000
3	6.224	0.000	0.000	6.224
Average	6.224	1.751	5.530	2.445

Flow rates are expressed in ml/min.

sidered. This option results in a solution that only accommodates for fluctuations in the flowrates and not in the packing and isotherm parameters. The optimized robust solution is presented in Table 8.2. It also presents two worst-cases hypothesis.

Starting from the 9th cycle of the previous solution, six more complete cycles were ran but with process parameters set to the ones shown in the bottom of Table 8.2. This time one imposed a perturbation into the system which consisted of increasing the feed and decreasing the eluent flowrates by 0.5% (one of the worst-cases). The concentration measured at the outlet of column 1 over the 15th process cycle can be viewed in the bottom graphic of Figure 8.3.

For the third run, we have implemented the opposite of run 2, that is, we have kept $\delta_k = 0$ and set δ_j to 1%. In this case we only take into account disturbances

Table 8.3: Cycle parameters for the robust solution of the simplified two-column process with $\delta_k = 0$ and $\delta_j = 1\%$. The parameter values for the NLP problem ($f_{\text{obj}} = \max \overline{F}$) are: $n_{\text{Q}} = 3$, $Q_{\max} = 9.5$ ml/min, $P_{\text{R}}^{\min} = P_{\text{X}}^{\min} = 0.99$ and $\tau_{\min} = 0.167$ min.

Switching intervals				
τ (min)		τ_1 (min)	τ_2 (min)	τ_3 (min)
6.179		0.436	3.286	2.457
Worst-cases				
	δ_E	δ_F	δ_1 (i)	δ_2 (i)
	0	0	-1	-1
	0	0	+1	+1
	0	0	+1	-1
Robust Solution				
Step	E	F	X	R
1	6.200	0.000	6.200	0.000
2	6.200	3.300	9.500	0.000
3	6.200	0.000	0.000	6.200
Average	6.200	1.755	5.490	2.465

Flow rates are expressed in ml/min.

in the packing and isotherm parameters and not in the flowrates. The optimized robust solution is presented in Table 8.3. This time it delivers three worst-case vertices.

In order to experimentally implement this third robust solution, the same procedure as for run 2 was made: 9 cycles with the parameters from Table 8.1 were ran and then six more cycles were reproduced but with the process parameters set to the ones shown in the bottom of Table 8.3. The imposed perturbation into the system was an increase of 1°C on the temperature. The concentration measured at the outlet of column 1 over the 15th process cycle can be viewed in the top graphic of Figure 8.3.

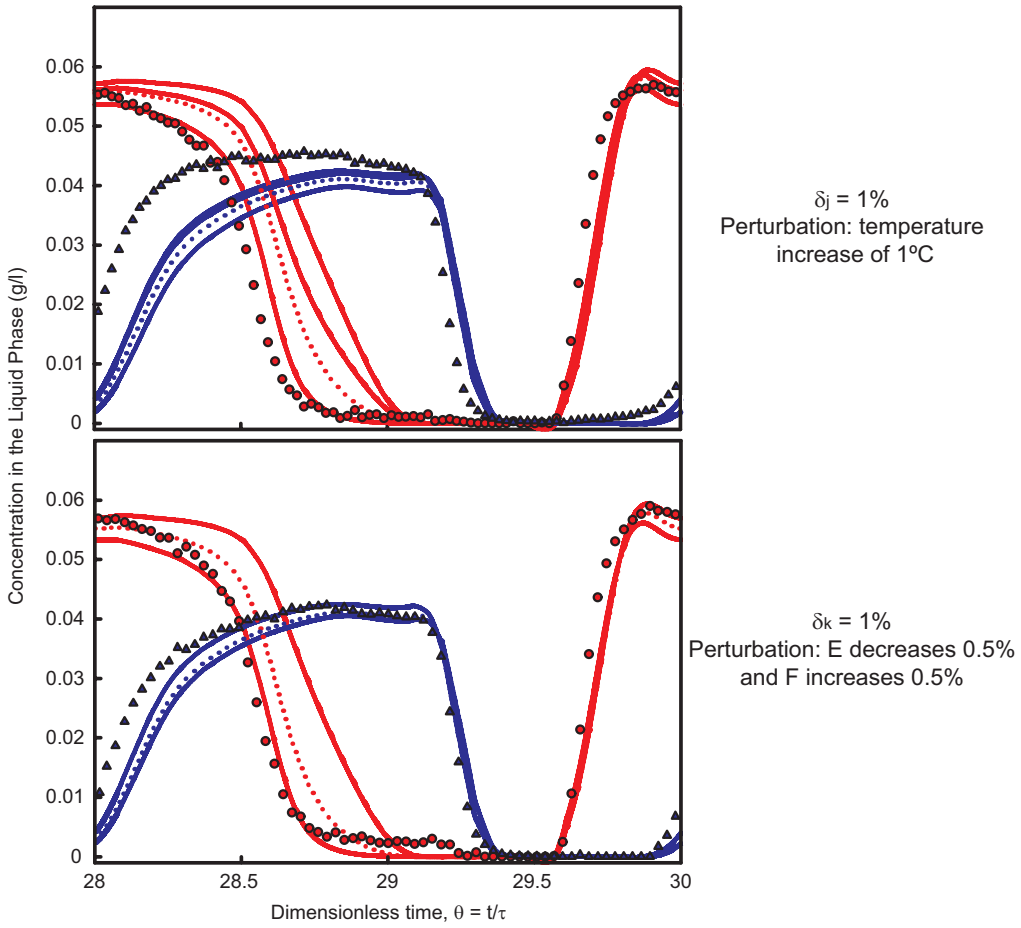

Figure 8.3: Solute concentration profiles at the outlet of column 1 for the parameters given in Tables 8.2 and 8.3 during the 15th process cycle. Symbols denote experimental data (∘, uridine; △, guanosine), whereas lines represent the worst-case scenario (blue for uridine and red for guanosine). The dotted lines symbolize the nominal solution, again blue for uridine and red for guanosine. The bottom graphic represents the case of a 0.5% perturbation in eluent and feed flowrates and the top graphic the disturbance of an increase of 1% in temperature. For visual clarity, only 1/15th of the UV measurements are plotted.

8.4 Discussion

After the design of a simplified two-column process with minimum equipment demand and high performance achievement (see chapter 7), we have developed a

robust approach analysis for process design that takes the experimental parameter uncertainty/fluctuation in account in order to create a safety operating margin that still fulfils process requirements. The approach considers relative deviation parameters δ_k and δ_j which correspond to flowrates (pumps) and packing and isotherm uncertainties, respectively.

To demonstrate the effectiveness of the proposed robust approach a set of three experimental runs were made. The model system was the linear binary separation of two nucleosides in a reversed phase stationary phase. In the first run the set of relative deviation parameters were set both to 1%. The resulting enlarged NLP was solved using the worst-case method. In this case, the resulting worst-case hypothesis correspond to a simultaneously increase on the flowrates and a decrease on V_{ij} or an increase on V_{ij} and in the feed flowrate with a decrease on eluent flowrate.

The obtained robust result, as seen in the bottom of Table 8.1, is identical to the previously nonrobust solution (see Table 7.1), however an increase on eluent consumption (around 5%) and a 10% decrease on feed throughput is obtained. This fact was expected since we are imposing further restrictions into the NLP and narrowing our solution domain. For instance, in the framework of the triangle theory, our approach is equivalent to moving our operating point further away from the maximum throughput vertice to the interior of the operating area. However, and despite this downgrade on process performance, the system becomes more immune to process uncertainties and/or fluctuations that usually occur in every practical implementation.

The obtained robust solution was ran for over 9 complete cycles, which was found enough to reach the CSS. The measured concentration, at the outlet of column 1, for the 9th cycle is shown in Fig. 8.2. In Fig. 8.2 one has represented the experimental points (symbols), the profiles for the two worst-case scenarios (lines) and the doted lines are the imposed nominal solution (the solution with no experimental uncertainties). As one can see from Fig. 8.2, our experimental cycle still meets the process requirements, mainly in terms of purity, since the experimental profile is well limited by the worst-case curves. However, it should be pointed out that the real safety margin is bigger then the one delimited by

the worst-case profiles since all the other possible disturbances (besides the two worst-case hypotheses) are not considered in the graphic of Fig. 8.2.

Next, a new robust solution that only considers a deviation parameter for the flowrates was calculated. In this case δ_k was set to 1% and no deviation parameter was used for the packing and isotherm parameters ($\delta_j = 0$). This solution was developed in order to be able to more clearly see the separate influence of each of the deviation parameters and, afterwards employ some experimental perturbations to test our approach in practice.

The second optimized robust solution is presented in Table 8.2. It also presents two worst-case hypothesis, which are the increase on the feed and the decrease or increase on the eluent flowrates. It is curious to see that the worst-case always correspond to the event where the feed flowrate is higher than its set-point; from this one can conclude, and with surprise, that in terms of flowrates the worst process perturbation is the increase of the feed throughput.

This robust solution was reproduced experimentally in our practical setup right after the previously 9 experimental cycles and for 6 operating cycles. However, an extra perturbation was imposed: increase on feed and decrease on eluent flowrate by 0.5%. The measured profiles at the outlet of column 1 are presented in the bottom graphic of Figure 8.3. The graphic shows that the process still fulfills the purity requirements even with the imposed perturbation; this can be easily observed by the fact that the profiles cutting zones are bellow the demand for the purity specifications which means the if we plot all the possible disturbances, and not only the worst-cases, all experimental points should fall inside the safety margin.

The third optimized robust solution is presented in Table 8.3 and it represents the opposite case relatively to the second robust solution: δ_k is set to zero and $\delta_j = 1\%$. This is the particular case where we only adjusted a safety margin for the packing and isotherm parameters. It presents three worst-case vertices, which are the simultaneously increase or decrease of V_{ij} or the increase of V_i in one column and the decrease in the other, which means all the possible cases. From this one can conclude that this perturbation is independent of the column number.

This robust solution was experimentally reproduced over 6 cycles (the same procedure as for the second robust solution) but with an increase of 1°C in the setup temperature as a perturbation. The imposed disturbance will affect the value of K_i (increase) and consequently the value of V_{ij}. The experimental profiles can be viewed in the top graphic of Fig. 8.3. The result show a slightly decrease of the raffinate purity which could mean that the 1°C increase on temperature represent a bigger disturbance than 1% in the value of V_{ij}. However, one can state that the presence of the robust factor, even if only for the packing and isotherm parameters, helped to attenuate a big part of the imposed perturbation.

It should be pointed out again that these last two robust designs also deliver a increase on eluent consumption and a decrease on feed throughput when compared to the nonrobust solution of Table 7.1. As mentioned before, this can be described as the *cost of robustness*.

The present results suggest that the developed robust approach may be a direct and straightforward solution to account for the inherent practical implementation uncertainties that occur in these very sensible processes.

8.5 Summary

A general procedure for robust design of SMB processes under flow rate uncertainty was developed which accounts for fluctuations in the flowrates and in the packing and isotherm parameters. A worst-case method was employed in order to estimate the most hazardous disturbance that could be applied to the process in terms of raffinate and extract purities, and the nominal problem is replaced by a worst case problem. The resulting enlarged NLP problem chooses the best solution only among candidate solutions that are robust feasible, that is, remain feasible for perturbations from the worst-case uncertainty set.

The proposed procedure was successfully employed to find three different robust operating conditions for the linear separation of two nucleosides in the previously developed simplified two-column scheme. The pros and cons of running each scheme under nominal and robust operating conditions were discussed. Regardless of the operating mode, robustness is achieved at the expense of a higher eluent consumption and/or lower feed throughput.

The three robust solutions were effectively implemented in practice and shown to successfully immunize the operation against disturbances because they create a safe operating space where the purity requirements are always fulfilled.

References

[1] G. Storti, M. Mazzotti, M. Morbidelli, A. Carrà, Robust design of binary countercurrent adsorption separation processes, AIChE Journal 39 (1993) 471–492. 156

[2] M. Mazzotti, G. Storti, M. Morbidelli, Optimal operation of simulated moving bed units for nonlinear chromatographic separations, Journal of Chromatography A 769 (1997) 3–24. 156

[3] S. Mun, Y. Xie, N.-H. Wang, Robust pinched-wave design of a size-exclusion simulated moving-bed process for insulin purification, Industrial and Engineering Chemistry Research 42 (2003) 3129–3143. 157

[4] Z. Ma, N.-H. Wang, Standing wave analysis of smb chromatography: Linear systems., AIChE Journal 43 (1997) 2488. 157

[5] B. Hritzko, Y. Xie, R. Wooley, N.-H. Wang, Standing wave design of tandem smb for linear multicomponent systems., AIChE Journal 48 (2002) 2769. 157

[6] J. Mota, J. Araújo, R. Rodrigues, Optimal design of simulated moving-bed processes under flow rate uncertainty, AIChE Journal 53 (2002) 2630–2642. 158

[7] R. Fourer, D. Gay, B. Kernighan, AMPL - a Modeling Language for Mathematical Programming, 2nd Edition, Brooks/Cole Thomson Learning, 2003. 159

[8] A. Wächter, L. Biegler, On the implementation of an interior-point filter line-search algorithm for large-scale nonlinear programming, Mathematical Programming 106 (2005) 25–57. 159

[9] S. Abel, G. Erdem, M. Amanullah, M. Morari, M. Mazzotti, M. Morbidelli, Optimizing control of simulated moving bedsexperimental implementation, Journal of Chromatography A 1092 (2005) 2–16. 160

9
Conclusions and Future Work

In this thesis we have exploited several SMB-based techniques both experimentally and theoretically.

A numerical design procedure to directly compute the cyclic steady behavior of the process was used as modeling procedure. A full discretization scheme, in both time and space, is applied in order to define the nonlinear programming problem. The resulting NLP is formulated in AMPL and solved using an interior-point solver. Later, the solution is obtained in gProms to determine the initial transient and to check the accuracy of the full discretized approach.

An experimental setup and procedure to reproduce the periodic state of multicolumn countercurrent chromatography with just one column was developed. The feasibility of the proposed system has been demonstrated with success on the separation of two nucleosides using six different process configurations. We investigated the performance of Varicol and PowerFeed processes, and their combination into a single hybrid scheme, both experimentally and by numerical simulation. The PowerFeed scheme always outperformed the classical SMB process and Varicol operating mode, both in productivity and eluent consumption. It was also shown that the Varicol scheme allows for the operation of three-column processes, which both the classical SMB and PowerFeed schemes cannot handle, and that its combination with PowerFeed in a single hybrid scheme can turn a three-column unit into a very competitive alternative.

In order to experimentally evaluate all the proposed schemes, a versatile lab-scale unit was built to reproduce the compact SMB setups. The equipment description and the problematic of creating an effective and versatile small-scale unit is discussed.

A SMB setup using only two-columns and based on piecewise-constant flowrate modulation is proposed. The setup was successfully implemented both numerically and experimentally. The results have proven the effectiveness of the presented scheme for the binary separation of two nucleosides in a reversed-phase stationary phase. Emphasis was given to the versatility of the approach as a nonrigid operating scheme that varies according to the nature of the chromatographic separation. Potentialities of this new unit were illustrated comparing it to setups using the same amount of stationary phase. The two-column SMB process demonstrated to be a real alternative to single-column batch chromatography with recycling.

Furthermore, we have presented and demonstrated experimentally and theoretically a simplified version of the developed two-column SMB process for binary separation. This new unit couples the simplicity of the batch system with the high performance of the continuous process. It has a minimum equipment requirement, since it uses only two pumps, nevertheless it proved that it can outperform equivalent schemes that use two times more columns.

These new processes rely on a simplified 3-step open-loop strategy with constant eluent addition procedure. Moreover, the addition of an extra recycle pump was exploited and implemented in practice, proving to be an efficient way to decrease the eluent consumption, making it a good alternative for low-selectivity separations.

A general procedure for robust design of SMB processes under uncertainty was developed which accounts for fluctuations in the flowrates and in the packing and isotherm parameters. A worst-case method was employed in order to estimate the most hazardous disturbance that could be inflicted to the process in terms of raffinate and extract purities. The proposed procedure was successfully employed to find three different robust operating conditions for the linear separation of two nucleosides by the previously developed simplified two-column scheme. The

robust issue is very important, specially at production scale, and calls for further developments.

The developed tools and schemes have proved to be powerful instruments at the research level and specially for low level of production scale, such as the pharmaceutical and biotechnology industries. In this framework, further developments should be investigated. The application of gradient elution profiles in the developed two-column schemes is a possibility not yet exploited and could lead to an important process in the biotechnology world; the evolution of the process from binary separation to a center-cut behavior can also be an important path for further developments.

Another interesting subject, besides the further development of the proposed robust approach, is the creation of a online automation procedure tool for optimum process control with minimum process information, in order to fully enhance the economic potential of the SMB technology and create a *user-friendly* process.

As we have seen, the continuous chromatography world, as well as all other scientific areas of research, is far from being a changeless field and still presents a large room for further developments. As *Albert Einstein* said: *The important thing is not to stop questioning. Curiosity has its own reason for existing.*

A

Extra-column Dead Volume

In an SMB unit the extra-column dead volume due to the tubing and connections between the columns must be properly accounted in order to find the right operating conditions. This fact is particulary important in this case of a small-scale unit since the extra-column dead volume may be similar to the column volume itself.

In the case of a single chromatographic column, it is broadly known that extra-column volume leads to an extra-column band broadening of the peaks, which affects the column efficiency and the separation performance. However, in this case of a small unit, the dead volume has also another and more important effect: additional retention time.

Regarding the case of a binary system characterized by a linear adsorption isotherm $q_i = K_i c_i$, for the injection of a dilute pulse of an adsorbed component i into a chromatographic column, the residence time of a molecule is the result

of two contributions: the retention time in the chromatographic column and in the extra-column volume.

The retention time in the chromatographic system $t_{R,i}$ becomes:

$$t_{R,i} = t_0^*(1+\beta K_i) + t_D \tag{A.1}$$

$$t_0^* = \frac{V\epsilon}{Q} \tag{A.2}$$

$$t_D = \frac{V_D}{Q} \tag{A.3}$$

where t_0^* is the column residence time for a nonadsorbing component (excluding extra volume influences), t_D the residence time for the extracolumn dead volume, V_D the dead volume (considered equal for every column in the case of a multicolumn system), $V = AL$ the column volume and Q the flowrate.

It is clear that the extra volume will increase the retention time of component i. A possible solution to mathematically describe this extra volume influence is to lump this retention time increase into the Henry constant K_i, i.e. by increasing its value.

However, this problem could have another approach. If we consider the case of a pulse of a nonadsorbing component (Blue Dextran in the case of SOURCE 30RPC) into a chromatographic column, the porosity of the stationary phase is:

$$\epsilon = \frac{t_0^*\, Q}{V} \tag{A.4}$$

With the presence of dead volume, the retention time t_0 becomes:

$$t_0 = t_0^* + t_D \tag{A.5}$$

$$\epsilon_D = \frac{t_0\, Q}{V} \tag{A.6}$$

Consequently, if we considerer the extra volume influence in the t_0 value, then Eq. A.1 is simplified to:

$$t_{R,i} = t_0(1 + \beta K_i) \tag{A.7}$$

In this case, the porosity in the presence of dead volume ϵ_D is bigger then the porosity without the extra volume ϵ:

$$\begin{aligned} \epsilon_D &> \epsilon \\ 1 - \epsilon_D &< 1 - \epsilon \\ \frac{1 - \epsilon_D}{\epsilon_D} &< \frac{1 - \epsilon}{\epsilon} \\ \beta_D &< \beta \end{aligned} \tag{A.8}$$

where $\beta_D = (1 - \epsilon_D)/\epsilon_D$.

It is then clear that another possible solution to fit the extra-column influence into the model is to either increase the value of ϵ or decrease the value of β.